SCIENTIFIC AND TECHNICAL JOURNAL

ISSN 1608-5043 (Print)

GEORESOURCES

www.geors.ru

V. 20. Is. 2. 2018

GEORESURSY GEORESOURCES. SCIENTIFIC AND TECHNICAL JOURNAL

SCIENTIFIC AND TECHNICAL JOURNAL
GEORESURSY
www.geors.ru
e-mail: mail@geors.ru

ISSN 1608-5043 (Print)
ISSN 1608-5078 (Online)
V. 20. Is. 2. 2018

Key title: «Georesursy». Parallel title: «Georesources»

Publisher: Georesursy LLC
Editorial and Publisher's address: 10-1 Mayakovsky St., Kazan, 420012, Russian Federation
Phone: +7 843 2390530, e-mail: mail@geors.ru

Georesursy (Georesources) is a peer-reviewed scientific and technical journal published since 1999

The journal is included/indexed in:
- **Emerging Sources Citation Index (ESCI);**
- **CAS (Chemical Abstracts Service) databases;**
- **GeoRef database;**
- **EBSCOhost™ databases;**
- **Ulrich's Periodicals Directory.**

The full-text e-versions of the articles are available on: **www.geors.ru**

Registered by the Federal Service for Supervision of Communications and Mass Media No. PI FS77-38832

The Journal is issued 4 times a year. Circulation: 1000 copies.
Issue date: 30.06.2018

First cover created by Freepik

Table of Contents

ORIGINAL RESEARCH ARTICLE

DOI: https://doi.org/10.18599/grs.2018.2.58-66

The Unified Scale of Natural Waters

V.F. Nikolaev[1], L.E. Foss[2], B.F. Sulaiman[1], A.B. Agybay[1], A.Kh. Timirgalieva[1], R.B. Sultanova[1]*

[1]*Kazan National Research Technological University, Kazan, Russian Federation*

[2]*Arbuzov Institute of Organic and Physical Chemistry, FRC Kazan Scientific Center of RAS, Kazan, Russian Federation*

Abstract. The article presents a continual scale of natural waters based on the characteristics of a vector, constructed on the superimposed cationic and anionic Gibbs triangles. We made a stylized hydrochemical clock-type dial based on the compression data of a six-component ionic composition of waters. To ensure successful communication of hydrochemists, exchanging information, we suggest characterize the mineral composition of waters by the direction of the vector, expressed in units (minutes) of the hydrochemical clock-type dial. The article presents equations for digitizing natural waters and for color visualization on hydrogeochemical maps of their mineral composition using Red/Green/Blue and Hue/Saturation/Value models. The analysis of the changes occurring in the natural water composition on maps in time enables us to visually establish hydrodynamic connections between ocean currents, water-bearing horizons, oil reservoirs, producing and injecting wells without using tracers. We provide examples of how the six-component composition of the natural waters of lakes, rivers, seas and oceans transforms into indicators of the hydrochemical clock-type dial and the corresponding color tones. The use of the color mapping method to analyze the World Ocean processes, associated with the Arctic ice thawing and changes in the waters composition of ocean currents, will allow us to take a fresh look at the global processes of climate change.

Keywords: natural waters, ground waters, seawaters, ocean currents, reservoir waters, water classification, cationic composition, anionic composition, analytical chemistry, physical chemistry, mineralization, geochemical map, Gibbs-Roseboom triangle, Maxwell triangle, hydrogeochemistry, HSV (HSB) color model, RGB model, horizontal hydrogeochemical zoning, vertical hydrogeochemical zoning, oil and gas field, data compression

Recommended citation: Nikolaev V.F., Foss L.E., Sulaiman B.F., Agybay A.B., Timirgalieva A.Kh., Sultanova R.B. (2018). The Unified Scale of Natural Waters. *Georesursy = Georesources*, 20(2), pp. 58-66. DOI: https://doi.org/10.18599/grs.2018.2.58-66

The diversity of the natural waters composition in six basic ionic components significantly complicates their typification and limits the possibility of "coloring" them in color mapping. In order to partially bypass this obstacle, the waters, marked on the hydrochemical map, are divided into color groups by means of cluster analysis (Narany et al., 2014). The shortcoming of these methods, such as partitioning of waters in the well-known Palmer and Sulin classifications (Palmer, 1911; Sulin, 1946; Collins, 1975; Samarina, 1977; Sulin, 1948), is the discrete character of the boundaries of natural water types, which is incompatible with the continual scales of HSV (HSB) and RGB (Ibraheem et al., 2012; Meskaldji et al., 2009) color models. It is impossible to use the known methods to visualize the six-component composition of natural waters on the Gibbs ionic triangles and to employ the variations of these methods (Žaporozec, 1972) to color hydrogeochemical maps. To date, regional hydrogeochemical maps have been based on the data with one single parameter, for example: total mineralization (*Total Dissolved Solids – TDS*), or the content of chloride ion, sulfate ion or calcium ion (Fraser, 2003). As a result of such mapping, we lose a significant part of the information about the six-component composition of water. Another way of representing natural waters on hydrochemical maps is to draw circular diagrams at the geographical sampling points, the sectoral areas of which reflect the content of the six major ionic components using an equivalent-percent, while the total mineralization of the waters is reflected by the radius of the diagram (Hem, 1985; Dinka et al., 2015). A visual analysis of such maps is also complicated, failing to provide a visual representation of the mineral components migration in water streams.

We used the procedure of data compression by means of a six-component ionic composition represented by points on the cationic (Ca^{2+}, Na^{+}/K^{+}, Mg^{2+}) and anionic (Cl^{-}, SO_4^{2-}, HCO_3^{-}) Gibbs triangles to create a scale of natural waters and their color visualization on hydrogeochemical maps. As shown by the analysis of the experimental data (Collins, 1975; Samarina,

* *Corresponding author: Lev E. Foss*
E-mail: iacw212@gmail.com

1977; Warner et al., 2012), the area of these triangles is extremely unevenly populated because of the low solubility of a number of salts (e.g, calcium sulfate $CaSO_4$, magnesium hydrogen carbonate $Mg(HCO_3)_2$, calcium hydrogen carbonate $Ca(HCO_3)_2$). Due to the low population in the center of ionic triangles, it is possible to use this point to create the scale of natural waters as a center of two auxiliary coordinate systems – Cartesian and polar. The procedure of compressing the data of the six-component water composition involves choosing the optimal way for combining the vertices of the cation and anion triangles, which provides good separation of location of soft water points or vectors (rivers, lakes) and highly mineralized natural waters (sea, ocean, oil-field waters).We did not consider the orientation variants of the anionic triangle with respect to the cationic triangle by rotation to an angle multiple of π/3 (like the six-pointed star of David) because of the possibility of complete mutual compensation of the cation and anion vectors upon their summation.

Having analyzed the compositions of lake, river, sea and ocean waters, given in article (Samarina, 1977), as well as the compositions of the reservoir waters of oil fields (Dresel et al., 2010; Khisamov et al., 2009), we determined that Mg^{2+}/Cl^-, Ca^{2+}/HCO_3^- и $(Na^+/K^+)/SO_4^{2-}$ was the preferred combination of the vertices of the cation and anion triangles. For better perception of the hydrochemical scale, the latter was presented in the form of a regular clock-type dial with sixty divisions and a minute hand, varying in length. The choice of the method for combining the superimposed ionic triangle with the scale of a clock-type dial was made to provide the position of the slightly water-insoluble $Mg(HCO_3)_2$ salt at the beginning of the circular scale (at $\tau_S = 0'$), and position $CaCl_2$ salts with maximum solubility at the end of the scale (at $\tau_S = 60'$). In addition, it was desirable that the remaining salts of natural waters should also be located on the hydrochemical clock-type dial when moving from $\tau_S = 0'$ clockwise in accordance with their increasing solubility in water. The orientation, shown in Figure 1, meets this requirement.

Figure 1 shows that practically all the salts (with the exception of $Ca(HCO_3)_2$) are located on the hydrochemical clock-type dial in accordance with their increasing solubility in water (Kaltofen et al., 1966; Lide, 2006).

The position of a certain sample of natural water on the scale of the hydrochemical clock-type dial can easily be graphically determined by marking the data of cation and anion composition on the superimposed triangle (Figure 1), plotting cationic and anionic vectors, their graphical summation and determining the magnitude τ_S on the hydrochemical scale. Further, we describe in detail the algorithm for computer processing of the hydrochemical information. The following sequence

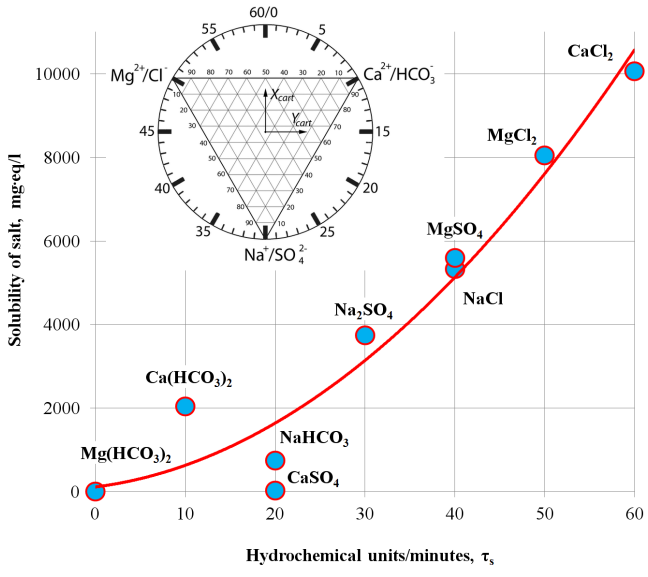

Figure 1. The relationship of solubility of the main individual salt components of natural waters with their position τ_S on the hydrochemical clock-type dial

of coordinate transformations is performed using the chosen mutual orientation of the ionic triangles and the hydrochemical clock-type dial (Figure 1):

$$(X_{GIBBS}; Y_{GIBBS}) \rightarrow (X_{CART}; Y_{CART}) \rightarrow (\varphi; \rho) \rightarrow$$
$$\rightarrow (\varphi'; \rho) \rightarrow (\tau; \rho), \quad (1)$$

where X_{GIBBS} and Y_{GIBBS} are data from a six-component analysis of a certain sample of natural water, meq% (Table 1), X_{CART} and Y_{CART} are the coordinates of the water composition point in the auxiliary Cartesian coordinate system (Figure 1), $\varphi(-180^o<\varphi<+180^o)$ and ρ are the polar coordinates of the radius-vector radiating from the center of the ionic triangle to the point (X_{CART}; Y_{CART}), $\varphi'(0^o<\varphi'<360^o)$ and ρ – are the polar coordinates of the radius-vector with shifted polar angle via clockwise to 180º ($\varphi'=\varphi+180^o$), τ and ρ are the polar coordinates of the radius-vector on the hydrochemical dial scale ($\tau=\varphi'/6$, $0\le\tau\le60$ *min*). Below, we provide specific equations for the transformation of coordinates.

$$X_{GIBBS} = \frac{X_{GIBBS}(Ca^{2+}) + X_{GIBBS}(HCO_3^-)}{2}, \quad (2)$$

$$Y_{GIBBS} = \frac{Y_{GIBBS}(Na^{+}) + Y_{GIBBS}(SO_4^{2-})}{2}. \quad (3)$$

We no longer need the third coordinate $Z_{GIBBS} = [Z_{GIBBS}(Mg^{2+}) + Z_{GIBBS}(Cl^-)]/2$, because by the normalization condition it is uniquely determined by the two used coordinates $Z_{GIBBS} = 100 - X_{GIBBS} - Y_{GIBBS}$.

The coordinates of the superimposed Gibbs triangle (X_{GIBBS}; Y_{GIBBS}) are converted into Cartesian coordinates (X_{CART}; Y_{CART}) using the Eq. (4), (5). The directions of the axes are shown in Figure1.

$$X_{cart} = (100 - Y_{GIBBS}) \cdot \cos\left(\frac{\pi}{6}\right) - 100 \cdot \sin\left(\frac{\pi}{3}\right) + \frac{50}{tg\left(\frac{\pi}{3}\right)}, \quad (4)$$

$$Y_{cart} = (2 \cdot X_{GIBBS} + Y_{GIBBS} - 100) \cdot \cos\left(\frac{\pi}{3}\right). \quad (5)$$

We calculated the direction of the natural water radius-vector in scale units of the hydrochemical clock-type dial by the equation:

$$\tau = 30 \cdot \left(\left(1 - sign\left(30 \cdot \frac{atan2(Xcart;Ycart)}{\pi} - \right.\right.\right.$$
$$\left.\left.\left. - 0.00001\right)\right) + \frac{atan2(Xcart;Ycart)}{\pi}\right), \quad (6)$$

and the length of the normalized radius of the vector is calculated according to the equation:

$$\rho = \sqrt{Xcart^2 + Ycart^2}. \quad (7)$$

Table 1 presents a calculation of the mineral composition characteristics of 21 natural waters. Since after compressing, the data of the six-component composition have been normalized by Eq. (2) and (3), then ρ_S, calculated from Eq. (7) in Table 1, is half the value of ρ_S shown in Figure 2. The given algorithm for calculating the direction and length of the natural waters radius-vector allows us to systematize all natural waters according to the direction τ_S and the length of the radius-vector ρ_S. The subscripts S, A and C at τ, ρ and ρ^{max} mean that the latter values refer to the salt composition of the water, to the anionic composition and to the cationic composition, respectively. By parameter τ_S river waters are located mainly in the range of 5 ÷ 18 units, while sea and ocean waters lie in the range of 35 ÷ 50 units (see τ_S in table 2). A useful addition to the characterization of the water composition is the value $\tau_S \cdot \rho_S / \rho_S^{max}$ which is a derivative from the obtained characteristics of the position of the mineral water composition vector on the hydrochemical clock-type dial, where ρ_S^{max} is the distance from the center of the clock-type dial to the edge of the ionic triangle for the particular direction τ, calculated from equation:

$$\rho^{max} = 50 \cdot \frac{tg\left(\frac{\pi}{6}\right)}{cos\left(\left(abs(abs(abs(\tau - 30) - 20) - 10)\right) \cdot \frac{\pi}{30}\right)}. \quad (8)$$

Using the value $\tau \cdot \rho / \rho^{max}$, we obtain an additional criterion for characterizing the water composition. According to this criterion, lake and river waters come within the range of $\tau_S \cdot \rho_S / \rho_S^{max} = 1 \div 10$, while sea and oceanic waters and reservoir waters of oil and gas fields are found in the range of $\tau_S \cdot \rho_S / \rho_S^{max} = 25 \div 40$.

Digitization of compression data on the composition of natural waters for hydrogeochemical mapping using HSV(HSB) and RGB models

HSV(HSB) color model

For color visualization of changes in the mineral composition of natural waters on the hydrogeochemical maps, we used the data compression procedure for the six-component composition described above and the HSV color model (Hue/Saturation/Value (or Brightness), in which the first position (Hue) changes within the range 0 ÷ 360°, while the second (Saturation) and the third (Value/Brightness) positions change within the interval 0 ÷ 100%. The previously determined characteristics of the vector $\bar{\rho}_S$ position on the hydrochemical clock-type dial and the position of Hue create a circular color scale from the red through yellow, green, blue to purple color. It is only natural that the position of the Hue should be related to the direction τ_S of the natural water total vector $\bar{\rho}_S = \bar{\rho}_C + \bar{\rho}_A$ on the hydrochemical clock-type dial (Figure 2). In the simplest case, if the waters marked on the map cover almost the entire scale of the hydrochemical clock-type dial $\tau_S = 0 \div 60'$, then the Hue value can be calculated as Hue = $6 \cdot \tau_S$. According to the HSV color model, the color circle, surrounding the hydrochemical clock-type dial, has a maximum in the red region of the spectrum (palette) at the point of Hue = 0/360° (τ_S = 0/60′). For the purpose of a more precise color separation, hydrochemical maps of low mineralized lacustrine and river waters lying, with exception of Nile and Yellow River, in the interval $\tau_S = 5 \div 18'$, and highly mineralized sea, oceanic and formation (underground) waters, it is desirable to perform a minute-wise rotation of the color circle by 10′ relative to the clock-type dial. This procedure allows us to color red to yellow all low mineralized and fresh waters of lakes and rivers in the warm part of the spectrum, as for highly mineralized sea, oceanic and reservoir waters, located in the sector $\tau_S = 35 \div 50'$,

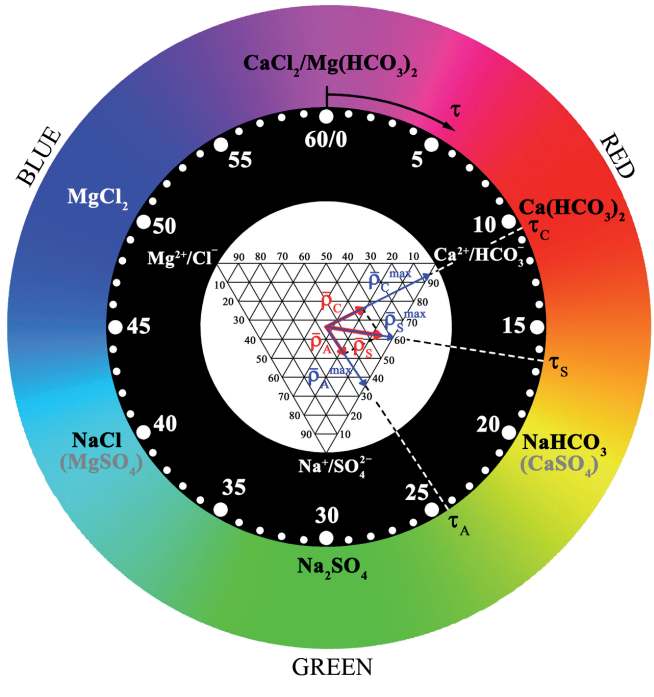

Figure 2. The hydrochemical clock-type dial (HSV model, Hue = 6·(τ$_S$ – 10)) with superimposed triangles of cationic and anionic composition and a graphic example of determining the characteristics of the hydrochemical vector for the water from the Thames River (UK) (Table 1)

we color them in cold colors from blue to purple. Analytically, this rotation of the color circle relative to the clock-type dial by 10′ is expressed by the equation:

$$Hue = 6 \cdot \left(\tau - 10 + 60 \cdot TRUNC\left(\frac{60-\tau}{50}\right)\right), \quad (9)$$

where TRUNC is the Microsoft Office Excel function. Equation (9) is used to form a column of colors (Table 2).

As will be shown below, such ten-minute shift of the colored circle relative to the clock-type dial ensures the similarity of the water color in the HSV (HSB) model to that of the RGB model (Maxwell triangle).

If the waters marked on the hydrogeochemical map have a narrow variation range τ_S, the color scale can be selected (Figure 3) by means of a linear transformation:

$$Hue = \frac{A \cdot (\tau_S - \tau_S^{min})}{(\tau_S^{max} - \tau_S^{min})} + B, \quad (10)$$

where A, B are constants selected from the range $(A + B) \leq 360$, τ_S is the direction of the water sample vector ρ_S on the hydrochemical clock-type dial, τ_S^{min}, τ_S^{max} are the minimum and maximum values of the directions of the water vectors. In order to ensure purity and saturation of colors, the position of the Saturation when forming a column of colors in Table 2 was equaled to the maximum value S = 100%, although other variants are possible. Another reason for not using all the three positions of the HSV (HSB) model is the difficulty of presenting a 3-dimensional decoding of the used color symbols on the plane of the map.

It is logical to connect the Value/Brightness position of the HSV (HSB) model with the distance of the water point to the center of the superimposed triangle ρ. However, the use of this parameter requires its preliminary normalization with respect to the maximum length of the radius-vector ρ_S^{max} for a given one τ_S, i.e. the value ρ_S/ρ_S^{max} that was used in the calculation of Eq. (11). We used the total mineralization of M_S (mEq/L or g/L) in the second variant (12) of calculating the parameter Value. To ensure the purity of the color (Table 2) and its recognizability at high brightness, we used only a narrow range of Value = 50 ÷ 80. There are three variants of equations (11)-(13) for calculating the magnitude of Value:

No*	Ca^{2+}	Na^+/K^+	Mg^{2+}	HCO_3^-	SO_4^{2+}	Cl^-	M	lnM	τ_C	ρ_C	ρ_C^{max}	$\frac{\rho_C}{\rho_C^{max}}$
	meq%			meq%			mEq/L					
1	44.07	14.97	40.95	52.53	27.62	19.85	14.3	2.661	0.9	16.0	29.0	0.551
2	26.68	29.35	43.98	75.77	10.29	13.94	8.2	2.103	10.2	23.2	56.0	0.414
3	54.66	21.92	23.43	67.10	16.16	16.73	2.7	1.006	9.6	18.5	54.0	0.343
4	91.04	6.64	2.33	86.81	4.37	8.82	12.0	2.487	10.4	50.0	53.8	0.930
5	75.73	13.33	10.94	64.78	18.19	17.03	13.3	2.587	10.3	36.7	54.7	0.672
6	64.05	15.95	20.00	89.58	9.40	1.02	2.5	0.905	9.3	26.7	51.2	0.521
7	73.49	14.33	12.18	71.19	18.11	10.69	10.1	2.311	10.3	34.8	54.8	0.635
8	34.53	46.49	18.98	67.97	15.35	16.68	2.6	0.956	24.3	13.8	32.0	0.431
9	44.94	30.27	24.79	50.91	40.63	8.46	12.4	2.518	12.5	10.4	40.6	0.256
10	54.30	24.11	21.59	34.23	46.79	18.98	16.0	2.770	10.7	18.2	51.6	0.352
11	3.80	88.68	7.51	59.39	0.33	40.28	321.7	5.773	30.4	48.0	54.1	0.886
12	3.93	44.41	51.66	4.12	91.77	4.11	942.9	6.849	41.4	25.7	29.2	0.882
13	8.69	62.88	28.43	0.64	29.36	70.00	431.5	6.067	33.5	27.4	37.1	0.739
14	3.43	79.62	16.95	0.28	10.59	89.14	1386.6	7.235	31.6	40.7	45.3	0.897
15	3.32	79.11	17.57	1.05	9.11	89.85	1401.1	7.245	31.7	40.3	44.7	0.900
16	4.04	78.34	17.62	1.04	9.28	89.68	600.9	6.398	31.6	39.6	45.0	0.879
17	3.35	78.73	17.92	0.38	9.28	90.34	1250.5	7.131	31.8	40.0	44.4	0.900
18	29.55	41.81	28.64	31.74	25.68	42.57	97.8	4.583	29.4	7.4	52.2	0.141
19	25.15	69.05	5.80	0.03	0.00	99.96	7014.2	8.856	27.1	32.4	39.2	0.826
20	13.07	32.41	54.53	0.17	0.06	99.76	12761.6	9.454	45.4	20.7	34.1	0.608
21	41.52	34.27	24.22	26.98	21.23	51.79	17.6	2.869	15.9	8.7	31.8	0.273

Table 1. A content of natural waters and characteristics of cationic component on dial.
**Numbers are the following water samples: 1) Southwestern Ontario's Breathing Well Region. Canada (Freckelton, 2012); 2) Volga river. Russia (Fraser, 2003); 3) Freshwater (typical ions) (Bortman et al., 2003); 4) Lambourn river, UK (Allen at al., 2010); 5) Seine river, France (Fraser, 2003); 6) Baikal Lake. Russia (Fraser, 2003); 7) Elbe river, Czech Republic (Ritter et al., 2011); 8) Severn river,UK (Shand et al., 2005); 9) Missouri river, USA (Criss et al., 2001); 10) Thames river basin, UK (Bearcock et al., 2010); 11) Yessentuki 17, mineral water, Russia (Samarina, 1977); 12) Hunyadi János, mineral water, Hungary (Halaj,2013); 13) Caspian Sea (Fraser, 2003); 14) Red Sea (Manheim et al., 2007); 15) Mediterranean sea (Demirel et al., 2006); 16) Black Sea (Schug, 2003); 17) Ocean (typical ions) (Bortman et al., 2003); 18) Nile river, Egypt (Hossam, 2010); 19) Pennsylvania brine water, USA (Dresel et al., 2010); 20) Dead Sea (Lopatina,2016); 21) Yellow river, China (Jing et al., 2014).*

No*	τ_A	ρ_A	ρ_A^{max}	$\frac{\rho_A}{\rho_A^{min}}$	τ_S	$\tau_{S\text{-}10}$	Hue	ρ_S	ρ_S^{max}	Value	$\frac{\rho_S}{\rho_S^{max}}$	$\tau_S \cdot \frac{\rho_S}{\rho_S^{max}}$	Color HSV
1	12.19	17.08	42.22	0.404	6.77	56.8	341	13.7	38.0	74	0.361	2.45	
2	14.53	20.70	34.36	0.602	7.26	57.3	344	21.4	42.1	76	0.508	6.21	
3	9.91	29.25	56.78	0.515	9.79	59.8	359	23.9	55.6	80	0.429	4.20	
4	9.54	46.37	53.37	0.869	9.99	60.0	360	48.1	57.7	74	0.835	8.34	
5	10.20	27.24	55.70	0.489	10.26	0.3	2	32.0	55.1	74	0.580	5.96	
6	10.82	48.89	50.43	0.969	10.27	0.3	2	37.7	55.0	80	0.685	7.03	
7	11.08	33.00	48.58	0.679	10.68	0.7	4	33.9	51.6	75	0.657	7.01	
8	9.79	30.00	55.61	0.539	13.81	3.8	23	16.8	36.2	80	0.465	6.42	
9	17.76	22.15	29.68	0.746	16.11	6.1	37	15.8	31.4	74	0.501	8.08	
10	24.47	13.93	32.34	0.431	16.45	6.5	39	12.1	31.0	73	0.391	6.44	
11	3.08	30.14	30.44	0.990	26.38	16.4	98	10.4	36.8	63	0.283	7.47	
12	30.00	50.61	57.72	0.877	33.60	23.6	142	32.4	36.8	59	0.879	29.54	
13	45.94	34.85	35.53	0.981	40.59	30.6	184	24.9	28.9	62	0.860	34.91	
14	48.99	48.60	49.01	0.992	41.38	31.4	188	27.6	29.2	58	0.944	39.08	
15	49.22	49.11	50.70	0.969	41.68	31.7	190	27.4	29.3	58	0.935	38.95	
16	49.20	48.98	50.55	0.969	41.74	31.7	190	27.1	29.4	61	0.924	38.56	
17	49.14	49.57	50.14	0.989	41.75	31.8	191	27.7	29.4	58	0.944	39.42	
18	53.46	8.56	37.28	0.229	43.63	33.6	202	2.5	31.1	67	0.081	3.52	
19	50.00	57.70	57.71	1.000	44.51	34.5	207	20.2	32.4	52	0.622	27.70	
20	50.01	57.53	57.64	0.998	48.80	38.8	233	38.2	47.7	50	0.801	39.11	
21	51.70	16.24	44.73	0.363	56.46	46.5	279	5.2	31.0	73	0.168	9.46	

Table 2. The positions of anionic and salt components of natural waters on dial.
**Denotation of water samples see Table 1*

$$Value(Brightness) = 80 - 30 \cdot \frac{\rho}{\rho^{max}}, \quad (11)$$

$$Value(Brightness) = 80 - 30 \cdot \frac{(M_{Si} - M_S^{min})}{(M_S^{max} - M_S^{min})}. \quad (12)$$

In the case of hydrochemical mapping when the waters differ significantly in total mineralization, we can use the logarithm of total mineralization lnM_s as in Eq. (13) instead of Eq. (12):

$$Value(Brightness) = 80 - 30 \cdot \frac{(lnM_{Si} - lnM_S^{min})}{(lnM_S^{max} - lnM_S^{min})}. \quad (13)$$

Table 2 shows examples of conversion of the natural waters composition into color (Hue is calculated by Eq. (9), Saturation = 100%, Value is calculated by Eq. (13)).

The approach, representing the mineral composition of waters with the values τ_S and ρ_S in the HSV model, is fully implemented in the construction of hydrogeochemical maps only in the case of the cationic or anionic components of the waters, if we replace τ_S with τ_C or τ_A, and ρ_S/ρ_S^{max} with ρ_C/ρ_C^{max} or ρ_A/ρ_A^{max}, respectively. The same relationships (4)-(9) are valid for the calculation of τ_C, ρ_C, ρ_C^{max}, τ_A, ρ_A, ρ_A^{max} parameters, only if $X_{GIBBS}(Ca^{2+})$, $Y_{GIBBS}(Na^+)$ and $X_{GIBBS}(HCO_3^-)$, $Y_{GIBBS}(SO_4^{2-})$ are used in equations (4) and (5) instead of X_{GIBBS} and Y_{GIBBS} for cations and anions respectively.

RGB color model. Combined Gibbs-Maxwell triangle

The RGB (Red / Green / Blue) is a second model, used for color visualization of various geological and hydrogeochemical characteristics of territories in mapping. The positions R, G and B vary in the range from 0 to 255 (Ibraheem et al., 2012). It is possible to transfer the coordinates of the superimposed cation-anion triangle of Gibbs composition to Maxwell's color triangle (14) due to the earlier compression of the data of the six-component water analysis by Eq. (2)-(3):

$$(X_{GIBBS}, Y_{GIBBS}) \rightarrow (x; y) \rightarrow (x; y; 1 - x - y) \rightarrow$$
$$\rightarrow (r; g; b) \xrightarrow{Maxwell} RGB. \quad (14)$$

The coordinates of the waters on the superimposed Gibbs triangle are equated with the coordinates of the Maxwell triangle (equations (15)-(17)) to achieve color visualization of the mineral composition of natural waters on hydrogeochemical maps:

$$x(Ca^{2+}/HCO_3^-) = \frac{X(Ca^{2+}/HCO_3^-)}{100} = r = \frac{R}{R+G+B}, \quad (15)$$

$$y(Na^+/SO_4^{2-}) = \frac{Y(Na^+/SO_4^{2-})}{100} = g = \frac{G}{R+G+B}, \quad (16)$$

$$z(Mg^{2+}/Cl^-) = \frac{Z(Mg^{2+}/Cl^-)}{100} = b = \frac{B}{R+G+B}, \quad (17)$$

where *r, g* and *b* are the color coordinates on the Maxwell triangle in the RGB model.

The examples of the transformation of the Gibbs coordinates for 21 natural waters into the Maxwell color RGB triangle are given in Table 3. The waters are arranged in Table 3 as τ_S grows. The hydrochemical clock-type dial shows that the color tones of river and lake waters are

No*	Gibbs triangle compressed coordinates			Coordinates of Maxwell triangle			Color
	$x(Ca^{2+}/HCO_3^-)$	$y(Na^+/SO_4^{2-})$	$z(Mg^{2+}/Cl^-)$	R	G	B	
1	0.483	0.213	0.304	255	112	160	
2	0.512	0.198	0.290	255	99	144	
3	0.609	0.190	0.201	255	80	84	
4	0.889	0.055	0.056	255	16	16	
5	0.703	0.158	0.140	255	57	51	
6	0.768	0.127	0.105	255	42	35	
7	0.723	0.162	0.114	255	57	40	
8	0.513	0.309	0.178	255	154	89	
9	0.479	0.355	0.166	255	189	88	
10	0.443	0.355	0.203	255	204	117	
11	0.316	0.445	0.239	181	255	137	
12	0.040	0.681	0.279	15	255	104	
13	0.047	0.461	0.492	24	239	255	
14	0.019	0.451	0.530	9	217	255	
15	0.022	0.441	0.537	10	209	255	
16	0.025	0.438	0.537	12	208	255	
17	0.019	0.440	0.541	9	207	255	
18	0.306	0.337	0.356	219	242	255	
19	0.126	0.345	0.529	61	166	255	
20	0.066	0.162	0.771	22	54	255	
21	0.342	0.277	0.380	230	186	255	

Table 3. Coordinates of natural waters on the Gibbs and Maxwell triangles.
**Denotation of water samples see Table 1*

characterized by either warm color or low color intensity (the River Nile in Egypt and the River Yellow in China) on the combined Gibbs-Maxwell triangle.

As shown above, the algorithms used for transferring the data of the six-component waters composition to color by means of the HSV and RGB models are fully applicable to the construction of individual hydrogeochemical maps only in the case of the cationic or anionic components.

A simplified example for color mapping of changes in mineral composition of reservoir waters of oil and gas field in Surfer program (Ozler, 2003)

We prepared color map using the Surfer software (Ozler, 2003). Figure 3 shows a schematic example of a hydrogeochemical chart based on the data on the six-component composition and total mineralization of the reservoir waters in oil and gas fields of Western Pennsylvania (Dresel et al., 2010). To create the map we used the well data with a virtually overlapping perforation depth range.

It shows the mineral composition of the reservoir waters. You can see that against the background of the main mineral component of NaCl, formation waters have a high content of calcium chloride $CaCl_2$ in the blue-colored area in contrast to other areas of the map, painted in red, yellow and green colors τ_S (NaCl)=40′ corresponds to the aqueous solution of pure sodium chloride while τ_S ($CaCl_2$)=60′ corresponds to the pure aqueous solution of calcium chloride. It should be noted that $MgCl_2$ at τ_S ($MgCl_2$) = 50′ is found on the hydrochemical scale τ_S between NaCl and $CaCl_2$; however, in this case, the displacement of the reservoir waters of the West Pennsylvania field is connected with an increase in the $CaCl_2$ content, which has τ_S ($CaCl_2$)=60′.

The proposed method of analyzing hydrochemical information about reservoir waters in oil fields will allow us, in certain cases, to reject tracer methods of determining hydrodynamic connections between strata and between producing and injection wells, since natural components of formation and injected waters can act as distinct tracers. The color similarity of waters on the hydrogeochemical map will also mean the similarity of their mineral composition, which in turn will indicate the presence of a hydrodynamic connection between water streams, horizons (strata) or wells. This method can be used in visual analyses of data both on horizontal (areal) and vertical (deep) hydrogeochemical zoning of oceanic and sea waters as well as waters of oil and gas fields. Color visualization of changes in the mineral composition of formation water can be carried out in the absence of data on the six-component analysis. It is sufficient to determine only its two characteristics – their refractive index n_D^{20} and density d^{20} (g/cm^3), and use the algorithm described in our article (Nikolaev et

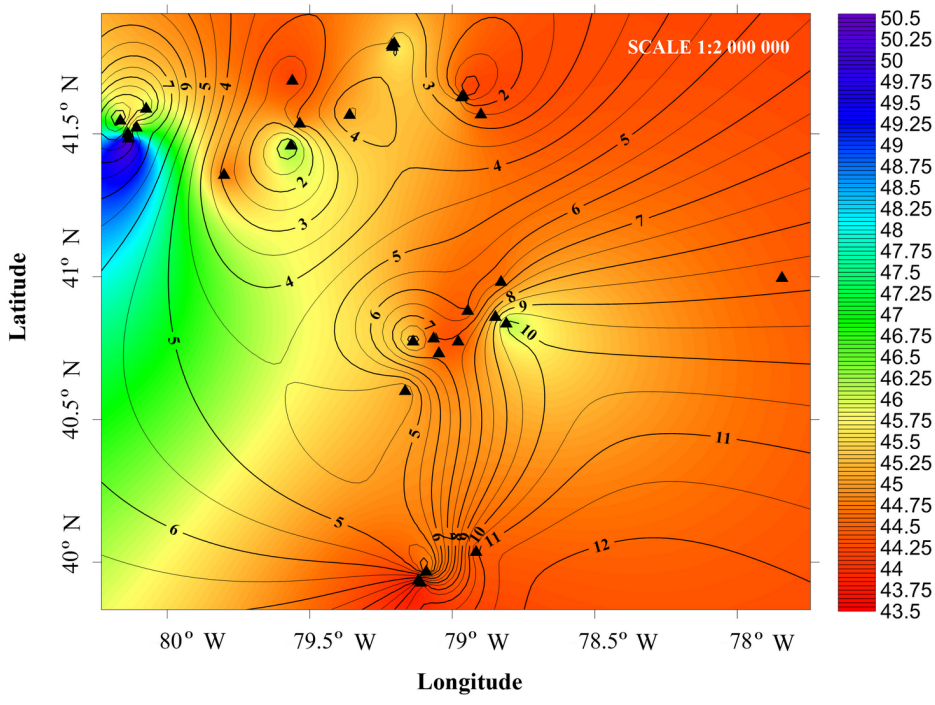

Figure 3. A schematic hydrogeochemical map of oil and gas province of Western Pennsylvania created with the SURFER software package and with the use of the values τ_S (color) and the logarithms of total mineralization lnM (M, mEq/L) (isolines)

al., 2016). To select the color (tone), we should use the identification polar angle φ_{IPA}, and the polar radius ρ as a measure of total mineralization (Nikolaev et al., 2018).

The described method of compression and digitization of analytical information can be used in color visualization of various mass transfer processes, as it groups individual components of a multicomponent system in accordance with some unifying property and presents a real multicomponent system of a composition changing in space and time as a form of a pseudo-ternary system, like the one used in analyzing light petroleum products and motor fuels (Nikolaev, 2015; Nikolaev, 2012). On the color petrogeochemical maps of oil fields, the change in the content of oils can be visualized by compressing the 4-component oil composition data, determined by the SARA analysis (ASTM D4124-09), up to a 3-component composition by allocating a saturated hydrocarbon group, an aromatic hydrocarbon group and a combined group of resins and asphaltenes.

Conclusion

We propose a continual circular hydrochemical scale (clock-type dial) of natural waters τ_S, based on the compression of data on their six-component ionic composition. A conventional agreement on a uniform method for compressing data on a six-component composition of natural waters, and a method for displaying it on a hydrochemical clock-type dial adopted by the International Association of Hydrogeologists (Hydrology) will facilitate the communication of hydrologists and hydrochemists in exchanging information.

The hydrochemical clock-type dial as a showing part of the device can be placed on the navigational instrument panel of sea and river vessels when used in developing a rapid method for determining the six-component composition of natural waters in the future.

Owing to the continuity of the hydrochemical scale, the results of digitizing the mineral composition of waters are well compatible with the HSV and RGB color models widely used in geochemical mapping. We demonstrate the effectiveness of combining the Gibbs ionic composition triangle and Maxwell's color triangle into a single Gibbs-Maxwell triangle in the case of using the RGB model.

By implementing the method of color visualization of the water mineral composition we can optimize the development of oil and gas fields. We can also conduct retrospective analyses of large volumes of hydrogeochemical and petroleum geochemical information, accumulated in laboratories of oil companies throughout the years of development and operation of oilfields. Of special interest is the information on the changes in hydrodynamic interactions between oil reservoirs, water horizons, producing and injection wells. In order to better visualize hydrodynamic connections between the injection and production wells, waters can be used instead of injecting tracers. These waters differ from natural reservoir waters either in their mineral composition or in their total mineralization. However, their mutual compatibility is required.

References

Allen D.J., Darling W.G., Gooddy D.C., Lapworth D.J., Newell A.J., Williams A.T., Allen D., Abesser C. (2010). Interaction between groundwater, the hyporheic zone and a Chalk stream: a case study from the River Lambourn. UK. *Hydrogeology*, 18, pp.1125-1141.

Bortman M., Brimblecombe P., Cunningham M.A., Cunningham W.P., Freedman W. (2003). Environmental Encyclopedia. Gale, Farmington Hills.

Bearcock J.M., Smedley P.L. (2010). Baseline groundwater chemistry: the Palaeogene of the Thames Basin. British Geological Survey Open Report, OR/10/057. http://nora.nerc.ac.uk/12600/1/OR10057.pdf

Collins A.G. (1975). Developments in Petroleum Science. Vol. I. *Geochemistry of Oilfield Waters*, Elsevier Science, New York, 496 p.

Criss R.E., Davidson M.L., Kopp J.W. (2001). Nonpoint sources in the lower Missouri River. *Am. Water Works Assoc*., 93, pp. 112-122.

Dinka M.O., Loiskandl W., Ndambuki J.M. (2015). Hydrochemical characterization of various surface water and groundwater resources available in Matahara areas, Fantalle Woreda of Oromiya region. *Journal of Hydrology: Regional Studies*, 3, pp. 444-456.

Dresel P.E., Rose A.W. (2010). Chemistry and Origin of Oil and Gas Well Brines in western Pennsylvania, Open-File Oil and Gas Report 10-01.0. Pennsylvania geological survey. http://www.fwspubs.org/doi/suppl/10.3996/052013-JFWM-033/suppl_file/patnodereference+s3.pdf

Demirel Z., Güler C. (2006). Hydrogeochemical evolution of groundwater in a Mediterranean coastal aquifer, Mersin-Erdemli basin (Turkey). *Environ Geol.*, 49, pp. 477-487.

Fraser A.S., Ongley E.D., Meybeck M, Hodgson K. (2003). The Annotated Digital Atlas of Global Water Quality, Global environment monitoring system freshwater quality programme, National Water Research Institute. http://colinmayfield.com/biology447/modules/module1/gems/intro.html

Freckelton C.N. (2013). A Physical and Geochemical Characterization of Southwestern Ontario's Breathing Well Region. The University of Western Ontario. https://ir.lib.uwo.ca/cgi/viewcontent.cgi?article=2407&context=etd

Hem J.D. (1985). Study and Interpretation of the Chemical Characteristics of Natural Waters. U.S. Geological Survey Water, United States government printing office, Wasington, 263 p.

Halaj E., Wachowicz-pyzik A. (2013). Examples of applications of geothermal waters for refraction, heating and bottling in selected regions of Hungary. *Geol, Geoph & Environ*, 39, pp. 21-32.

Hossam H.E. (2010). Potentialities of Water Resources Pollution of the Nile River Delta, Egypt. *The Open Hydrology J*., 4, pp. 1-13.

Ibraheem N.A., Hasan M.M., Khan R.Z. (2012). Understanding Color Models: A Review. *Journal of Sci. and Tech*., 2, pp. 265-275.

Jing L., Fadong L., Qiang L., Shuai S., Yan Zh., Guangshuai Z. (2014). Impacts of Yellow River Irrigation Practices on Trace Metals in Surface Water: A Case Study of the Henan-Liaocheng Irrigation Area, China. *Human and Ecolog Risk Assessment: An Inter J.*, 20, pp. 1042-1057.

Kaltofen R., Opitz R., Schumann K., Ziemann J. (1966). Tabellenbuch Chemie. VEB Deutscher Verlag für Grundstoffindustrie, Leipzig, 485 p.

Khisamov R.S., Gabdullin T.G., Farhullin R.G. (2009). Control over the development of oil and gas fields. Idel-Press, Kazan, 408 p. (In Russ.)

Lide D.R. (2006). Concentrative Properties of Aqueous Solutions: Density, Refractive Index, Freezing Point Depression, and Viscosity, in CRC Handbook of Chemistry and Physics. Taylor and Francis. http://www.hbcpnetbase.com

Lopatina A.B. (2016). The chemical composition of the Dead Sea (Israel). *Sci Bull*., 7, pp. 215-221. (In Russ.)

Meskaldji Kh., Boucherkha S., Chikhi S. (2009). Color Quantization and its Impact on Color Histogram Based Image Retrieval. CEUR-WS Publisher. http://ceur-ws.org/Vol-547/60.pdf

Manheim F.T., Waterman L.S., Woo C.C., Sayles F.L. (2007). Deep Sea Drilling Project DSDP Volume XXIII. Interstitial Water Studies on Small Core Samples, Leg 23 (Red Sea). http://www.deepseadrilling.org/23/volume/dsdp23_35.pdf

Narany T.S., Ramli M.R., Aris A.Z., Sulaiman W.A., Juahir H., Fakharian K. (2014). Identification of the hydrogeochemical processes in groundwater using classic integrated geochemical methods and geostatistical techniques, in Amol-Babol Plain, Iran. *The Sci World J*., 2014. pp. 1-15.

Nikolaev V.F., Timirgalieva A.Kh., Barskaya E.E., Egorov A.V., Khanova D.R., Sultanova R.B., Romanov G.V. (2016). Hydrogeochemistry: natural waters in full view. *Bulletin of Kazan Technological University*, 19, pp. 5-10. (In Russ.)

Nikolaev V.F., Tabrisov I.I., Penkovsky A.I., Sultanova R.B. (2015). Express method for total content assessment of aromatic hydrocarbons and oxygen in finished gasolines by refractometry and densimetry. *Fuel*, 142, pp. 94-101.

Nikolaev V.F. (2012). Rapid methods for testing composite products of oilfield chemistry and motor fuels. Kazan, KNRTU, 124 p. (In Russ.)

Nikolaev V.F., Bulygin D.V. (2018). Express Method to Evaluate Mineral Composition of Injected and Associated Water at the Oil Fields. *Oil. Gaz. Novations*, No.4, pp. 48-52.

Ozler H.M. (2003). Hydrochemistry and salt-water intrusion in the Van aquifer, east Turkey. *Environmental Geology*, 43. pp. 759-775.

Palmer C.C. (1911). The geochemical interpretation of water analysis. Government printing office, Washington, 31 p.

Ritter D.J. (2011). First Order Analysis of Nitrate Loading in the Upper Elbe River Basin, Czech Republic. Brigham Young University BYU Scholars Archive. http://scholarsarchive.byu.edu/cgi/viewcontent.cgi?article=3871&context=etd

Samarina V.S. (1977). Hydrogeochemistry. Leningrad, Leningrad State Univ-ty, 360 p. (In Russ.)

Sulin V.A. (1946). Waters of Petroleum Formations in the System of Nature Waters. Moscow, Gostoptekhizdat, 95 p. (In Russ.)

Sulin V.A. (1948). Conditions of formation, the basis of classification and composition of natural waters. Part 1. Moscow, USSR Academy of Sciences, 105 p. (In Russ.).

Shand P., Abesser C., Farr G., Wilton N., Lapworth D.J., Gooddy D.C., Haria A., Hargreaves R. (2005). Baseline Report Series: 17. The Ordovician and Silurian meta-sedimentary aquifers of central and south-west Wales. British Geological Survey. http://nora.nerc.ac.uk/3550/1/CR05034N.pdf

Schug D.M. (2003). Deep Sea Drilling Project DSDP Volume XXIII Interstitial Waters of Black Sea Cores. http://www.deepseadrilling.org/42_2/volume/dsdp42pt2_23.pdf

Warner N.R., Jackson R.B., Darrah T.H., Osborn S.G., Down A., Zhao K., White A., Vengosh A. (2012). Geochemical evidence for possible natural migration of Marcellus Formation brine to shallow aquifers in Pennsylvania *Proceed in Nat. Acad. of Sci.*, 109, pp. 11961-11966.

Žaporozec A. (1972). Graphical Interpretation of Water-Quality Data. *Ground Water*, 10, pp. 32-43.

About the Authors

Vyacheslav F. Nikolaev – DSc (Chemistry), Professor, Department of Technology of Basic Organic and Petrochemical Synthesis

Kazan National Research Technological University
68 Karl Marx str., Kazan, 420015, Russian Federation

Lev E. Foss – PhD, Junior researcher of Oil Chemistry and Geochemistry Laboratory

Arbuzov Institute of Organic and Physical Chemistry, FRC Kazan Scientific Center of the Russian Academy of Sciences

8 Arbuzov str., Kazan, 420088, Russian Federation
E-mail: iacw212@gmail.com

Bassel .F. Sulaiman – PhD Student, Department of Technology of Basic Organic and Petrochemical Synthesis

Kazan National Research Technological University
68 Karl Marx str., Kazan, 420015, Russian Federation

Asel B. Agybay – Master, Department of Technology of Basic Organic and Petrochemical Synthesis

Kazan National Research Technological University
68 Karl Marx str., Kazan, 420015, Russian Federation

Alina Kh. Timirgalieva – Master, Department of Technology of Basic Organic and Petrochemical Synthesis

Kazan National Research Technological University
68 Karl Marx str., Kazan, 420015, Russian Federation

Rasimya B. Sultanova – PhD (Chemistry), Associate professor, Department of Technology of Basic Organic and Petrochemical Synthesis
Kazan National Research Technological University
68 Karl Marx str., Kazan, 420015, Russian Federation

Manuscript received 8 February 2018;
Accepted 23 May 2018;
Published 30 June 2018

ORIGINAL RESEARCH ARTICLE

DOI: https://doi.org/10.18599/grs.2018.2.67-80

A new approach to the prospects of the oil and gas bearing of deep-seated Jurassic deposits in the Western Siberia

S.A. Punanova, V.L. Shuster
Oil and Gas Research Institute of the Russian Academy of Sciences, Moscow, Russia

Abstract. Complexly constructed low-permeability reservoirs are still poorly understood. This slows down the development of oil and gas resources of the Jurassic and deeply submerged pre-Jurassic deposits of the West Siberian oil and gas basin. There is also no consensus among the geological community on the prospects of these deposits from the perspective of the oil generation in them and subsequent emigration. There are many questions on the structure and oil and gas content of the deposits of the Bazhenov formation, whose oil resources amount to tens of billions of tons. The problems of oil and gas content and mapping of heterogeneous structure of massive rocks, including the basement formations, are considered in the article. In addition, the prospects of the oil and gas potential of the Jurassic and pre-Jurassic deposits of the northern regions of Western Siberia with geological and geochemical data were estimated. The revealed zones of highly transformed organic matter in the sediments of the Bazhenov formation and a number of other facts allow us to re-argue the prospects of the oil and gas bearing of the underlying deposits.

Keywords: pre-Jurassic deposits, reservoir rocks, oil and gas potential prospects, Bazhenov formation, hydrocarbons, oil, West Siberian oil and gas basin, microelements, vanadium, vanadylporphyrins

Recommended citation: Punanova S.A., Shuster V.L. (2018). A new approach to the prospects of the oil and gas bearing of deep-seated Jurassic deposits in the Western Siberia. *Georesursy = Georesources,* 20(2), pp. 67-80. DOI: https://doi.org/10.18599/grs.2018.2.67-80

Introduction

Currently, in the north of the Western Siberian oil and gas basin, over 220 prospecting and exploration wells have been drilled that have revealed Mesozoic terrigenous deposits in the stratigraphic range from the Upper Jurassic to the Triassic at depths of 2000 to 4000 m and more. All of them are located in Nadym-Pursky, Pur-Tazovsky and Gydansky oil and gas bearing areas. Significant progress in studying the structure and oil and gas potential of the deep horizons of the north of Western Siberia has been identified with regional and areal seismic surveys, drilling and exploration of super deep wells – SG-6 and SG-7, as a result of which a certain factual material has been accumulated (Khakhaev et al., 2008; Bochkarev et al., 2000; Skorobogatov, 2017; etc.).

However, the development of oil and gas resources in the Jurassic and especially in deeply buried pre-Jurassic deposits in Western Siberia is currently slowing down due to their insufficient knowledge and the difficulty in interpreting the results obtained. This particularly applies to geochemical and paleogeothermal estimates of the prospects for subsoil productivity at great depths exceeding 4.0-4.5 km. Among geologists, there is no unambiguous assessment of the prospects of oil and gas bearing deposits of great depths, significantly revised in the process of submerging them, from the point of view of identifying reservoirs. There remains much unexplored in the features of the structure and the oil and gas generation of the Bazhenov formation of the Titonian-Lower Berriasian age.

In the present article, we detail some of the concepts developed earlier by us, we consider in more depth the geochemical aspect of the oil and gas content of deep-lying sediments. In addition, data on the content of trace elements (ME), in particular vanadium (V), and metal-porphyrin complexes (MPC)-vanadylporphyrins (V_p) in OM of rocks from the Bazhenov formation and oils were used to evaluate their thermal transformation. We suggest a new angle of view to consider the geological structure of dense deposits of monolithic strata, their oil and gas content. A new perspective on the problem of the prospects of deposits under study has to be developed.

Low-permeability reservoir rocks

Necessary and sufficient conditions (geological factors) for the formation of oil and gas fields for deep horizons remain the same as for the formation of

* *Corresponding author: Svetlana A. Punanova*
E-mail: punanova@mail.ru

hydrocarbon (HC) accumulations in the Upper Jurassic-Cretaceous rock complex. They are the presence of a trap, reservoir rocks, fluids, favorable geochemical and hydrogeological characteristics of the section. However, the characteristics of these factors are changing (sometimes drastically) and, accordingly, the assessment of oil and gas prospects, the choice of directions and objects of geological exploration.

The reason for the significant, sometimes fundamental difference in the geological conditions of the Upper (Jurassic-Cretaceous) from the Lower Pre-Jurassic (Triassic-Paleozoic-basement) floor is, firstly, the substantial compaction of rocks at great depths under the influence of hydrostatic pressure, that leads to a change in the structure and texture of the rocks, the rupture of the seams and, in general, to a change in the structure. Increased tectonic activity at great depths, as compared to depths of 3-4 km, also causes a significant difference in the structure of reservoir rocks and fluid rocks. Secondly, the lithological composition of the rocks varies: from predominantly terrigenous and carbonate rocks in the upper floor, to the same but compacted rocks, as well as to effusive-terrigenous, effusive and crystalline (igneous) and metamorphic rocks (in the lower). As a result, the permeability decreases with depth, the character of voidness changes: from the porous type it transforms into a fractured-porous, fractured-cavern and at the same time its values are significantly reduced. The length of the seams varies considerably, they are broken into fragments, which can be easily traced in seismic sections: at the depth of the in-phase axis they are often broken. In deep horizons it is often difficult to relate the correlation of strata along the wells to seismic materials.

For a number of deposits, an extreme heterogeneity of the structure of deep-lying productive strata has been established, in particular, a chaotic distribution in the section of reservoir rocks and inflow zones. So, we (Shuster, 2003), on the well-studied Vietnamese oil field White Tiger in the basement, revealed an extremely uneven distribution of the reservoir rocks both in the area and in the section (based on GIS, 3D seismic data and the results of thermohydrodynamic studies). Moreover, when testing 500-800 m intervals of the open trunk in the wells, the main part of the oil inflow is fixed (according to the results of thermohydrodynamic studies in 20 wells) in 20-40 meter intervals. And, if in the Central arch of the White Tiger field, oil-saturated reservoir rocks lie immediately from the basement surface, then in the North arch the first reservoir rocks were found in a section at a depth of 500-600 m from the surface. The heterogeneity of the structure is also evidenced by a sharp difference in the filtration-capacity properties (reservoir properties) of reservoir rocks and, as a consequence, the values of oil rates. So, the received inflows of oil from wells, as a generalized index of the reservoir properties of rocks, in the basement deposits differ by three orders: from the first units to 2000 tons/day. These factors are difficult to explain from the standpoint of classical physics. The deposit is classified as massive.

The same picture in the structure of the basement is observed on two exploratory areas of Western Siberia: Ust-Balyksky and Severo-Danilovsky. At the Ust-Balyksky field, reservoir rocks identified by the seismic survey method using scattered waves are concentrated in the eastern part of the basement, and at the Severo-Danilovsky fields the reservoirs are detected directly below the basement surface, but are extremely unevenly distributed over the area. Not taking into account the complex heterogeneous structure of the basement, perhaps, is the reason that in Western Siberia large oil and gas reserves have not yet discovered in these deposits.

It is possible to consider hydrocarbon deposits in massive dense rocks from the position of the model of the "geophysical environment", nonlinear, hierarchically heterogeneous, energetically saturated and active (Nikolaev, 1991), i.e. from the position of transition to a new understanding of the properties of rocks, which requires serious additional research and confirmation.

A sharp heterogeneity is established in the structure of the Bazhenov formation of Western Siberia: a change in its lithological composition both in area and in section, the variability of alternation in the section of reservoir rocks and intervals of oil tributaries. The lack of reliable technologies for mapping the structure of the Bazhenov formation, along with technological problems, does not allow full-scale development of the resources and oil reserves of this unique stratum, a length of 1 million km, a width of 200 km.

Numerous studies have established that the voidness of dense massive rocks is confined, mainly, to fractured and fractured-cavern reservoirs, which are the centers of accumulation of oil (gas). We (Shuster, 2003) was suggested that the formation of zones of unconsolidated fractured rocks in the basement formations occurs under the influence of static and dynamic internal and external stresses, with a relatively rapid decrease in pressure and temperature accompanied by a pulse of released energy, which is the primary cause of destruction. In the Bazhenov formation, fracturing ("decompression") is created artificially, by hydraulic fracturing.

Today, seismic exploration technologies using scattered waves have been developed that allow the sections and zones of development of reservoir rocks-potential oil and gas deposits-to be identified in the section of massive strata in prospective exploration areas even before the drilling stage. It should also be noted

that the role of fluidisation for oil (gas) deposits in the basement formations can be played not only by regional but also by zonal and local fluidicides. Moreover, it can be not only clay or carbonate strata, but also effusive and crystalline rocks.

In the north of the Tyumen region, where deposits in the Cretaceous and Upper Jurassic fields, unique for the reserves of hydrocarbons, have been discovered, there has been a trend to reduce the increase in gas reserves in these deposits. Drilling was previously carried out only to a depth of 3-4 km with the thickness of the sedimentary cover according to geophysical data up to 9-11 km. Therefore, for today, the agenda is the question of a detailed study of the prospects for oil and gas potential of the Lower Middle Jurassic and pre-Jurassic sediments (the lower floor), including in the giant fields of the north of Western Siberia. According to a number of scientists (V.S. Bochkarev, A.M. Brekhuntsov, N.P. Zapivalov, I.A. Kleshchev, A.E. Kontorovich, I.A. Plesovskikh, V.A. Skorobogatov, V.S. Shein, V.L. Shuster, and others), the basal layers of the Middle and Lower Jurassic, sedimentary deposits of the Triassic and Paleozoic, the formation of the weathering crust and the zone of decompaction of the basement are referred to new promising objects.

Assessment of oil and gas potential prospects of Jurassic and pre-Jurassic deposits

The geochemical aspect of the prospects assessment of the oil and gas potential of the Jurassic and deep-lying pre-Jurassic deposits of Western Siberia is extremely important. Our studies on the composition of bitumen from Bazhenov deposits of the Western Siberian oil and gas basin not only clarified the features of the OM of the formation itself, but also provided additional information for assessing the possible generation capacity of pre-Jurassic and Paleozoic deposits from new positions.

Geochemical details of the genetic features of organic matter from the Bazhenov formation

The relevance of the study and the increased interest in the sediments of the Bazhenov formation is quite natural and is associated with its well-known uniqueness (oil resources) and the need to clarify the prospects for the oil and gas potential of the formation in most of the basin. The deposits of the Bazhenov formation, which are widely developed within the Western Siberian oil and gas basin, have been fairly well studied and described by OA. Arefiev et al.; V.I. Goncharov; M.V. Dakhnova et al.; A.E. Kontorovich et al.; D.V. Nemova et al.; I.I. Nesterov and I.N. Ushatinsky; G.S. Pevnevoy, etc. However, a relatively high degree of study of the formation did not lead to unambiguous judgments about the origin of the hydrocarbon series in it and the regularities of their spatial location. So one part of the researchers believes that the oil of the Bazhenov formation is syngenetic with its rocks (Lopatin, Emets, 1999; Kontorovich, Kostyreva, 2015; etc.). Other authors consider the oil in the formation to be epigenetic or mixed due to their secondary arrival from the underlying deposits in areas of high fracturing (Skorobogatov, 2017; Soboleva, 2017; etc.). The existence of different views on the source of oil has further increased the scientific and practical interest in the problem of the oil and gas potential of the Bazhenov formation, in particular, the geochemical aspects of the origin of hydrocarbons in them. The deposits of the formation are mainly black bituminous argillites with an admixture of siliceous and carbonate material, considerably enriched in Corg (up to 10-15% per rock) and chloroform extracted bitumen (CEB) (up to 2% per rock). A.E. Kontorovich et al. (2014) characterize these rocks as "carbonate-clay-kerogen-siliceous". To the outskirts of the sedimentation basin, an admixture of sandy material appears in the clays, and their bituminous content is significantly reduced.

Let us dwell in more detail on the features of the diagnostics of oil-producing sequences of the Bazhenov deposits, using the ME criteria for the genetic relationships "oil-scattered OM". A search in the section of the sedimentary strata of the oil source formations and their diagnostics is a necessary stage in assessing the prospects of the petroleum potential of sedimentary basins. The similarity of oils and syngenetic CEB rocks to the distribution of ME can be indicative of the participation of these strata in the processes of oil formation. Undoubtedly, the biogenic nature of most ME of oils provides a complete basis for such a correlation. For a more reasonable judgment on the presence in the sedimentary section of the oil deposits, it is necessary to clearly separate the bituminous components into syngenetic and epigenetic components.

The syngenetic bitumen from rocks with high organic carbon (C_{org}) and low bitumen content ($\beta = CBA/C_{org}$,%) is usually characterized by a high content of V, Ni, Co, Mo and other MEs associated with asphalt-resinous components, so-called "heavy". The concentrations of these ME can be two orders of magnitude higher than in oils or epibitumoids. The concentration of ME, associated with oil hydrocarbon components, the so-called "mobile" – Fe, Au, Pb, Cu, etc., in these bitumen is lower than the concentration of "heavy". The distribution of ME in epigenetic bitumen reflects their migratory nature, sometimes contaminated, they are more mobile, they have relatively lower concentrations of "heavy" MEs (in the same order as in oils) compared to syngenetic bitumen (Punanova, 2017; Punanova, Chakhmakhchev, 1992).

The study of the composition of the bitumen Bazhenov formatiion (by the method of atomic adsorption) and metal-porphyrin complexes (on the

Specord device) by the area of distribution, carried out by the authors, showed its considerable heterogeneity (Chakhmakhchev, Punanova, 1992; Punanova, 2017). As can be seen in Fig. 1, the content of V_p in the OM of rocks in the basin varies from their total absence to very high values. Thus, the CEB of rocks in the western regions is characterized by the absence or small values of the V_p content. The central regions (Surgutsky, Nizhne-Vartovsky, Aleksandrovsky swells and some areas to the north of them) are distinguished by substantial enrichment of the CEB with porphyrins. The peculiarity of the presented scheme is the zone of anomalously small values of V_p in the CEB, marked on the map by color, which has a northeasterly strike and covers areas of the areas of Salymsky, Kamenny, Dekabrsky, Verkhne-Lyaminsky, Vyngayakhinsky, Tarasovsky, etc. Spreading

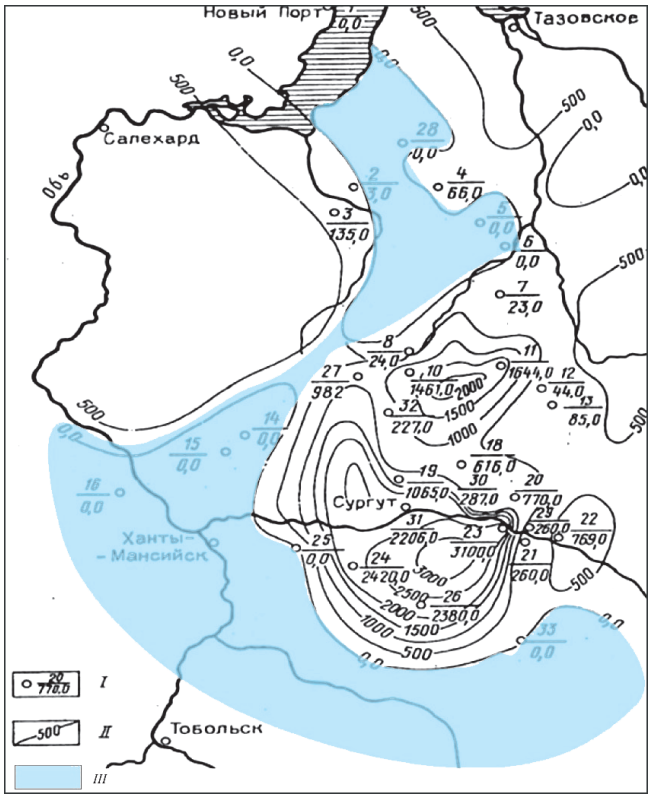

Fig. 1. Distribution scheme of the content of vanadium porphyrins (Vp) in OM from the Bazhenov Formation of Western Siberia (Chakhmakhchev, Punanova, 1992; Punanova, 2017). I – the core extraction area (numerator) indicating the content of Vp ($n\times10^{-3}$%) in OM (denominator). The core sampling areas are as follows: 1 – Novoportovsky, 2 – Nadymsky, 3 – Khaginsky, 4 – Yamovsky, 5 – Gubkinsky, 6 – Tarasovsky, 7 – Vengayakhinsky, 8 – Itursky, 9 – Kollektivny, 11 – Vyngapurovsky, 12 – Tagrinsky, 13 – Northern Erkalsky, 14 – Verkhnelyaminsky, 15 – Dekabrsky, 16 – Kamenny, 18 – Pokachevsky, 19 – Fedorovsky, 20 – Samotlorsky, 21 – Sosninsky, 22 – Medvedevsky, 23 – Megionsky, 24 – Ust-Balyksky, 25 – Salymsky, 26 – Ugutsky, 27 – Soimlorsky, 28 – Mezhvezhy, 29 – Strezhevy, 31 – Surgutsky, 32 – Kholmogorsky, 33 – Matyushinsky; II – isolines of the content of Vp in the OM of rocks; III – zone of anomalously low contents of Vp.

on Gubkinsky-Tarasovsky areas, this zone continues north-west towards New Port.

Fig. 2 shows the distribution of the contents of V in the CEB rocks of the Bazhenov Formation of Western Siberia. Based on the values of this parameter, the entire basin area is significantly dissected. The V content in the CEB varies from 0.83×10^{-2}% (Ugutsky district) to 30×10^{-2}% in the western regions of the basin (Kamenny area, Khaginsky and Nadymsky districts). An anomalous zone of low contents of V, tracing from the south-western direction to the northeast, also shown on the map by color, is clearly traced. This zone repeats in its orientation the areas highlighted in Fig. 1 on the anomalously low content of V_p (Chakhmakhchev, Punanova, 1992; Punanova, 2017). As we know, we also noted earlier, in the conditions of high paleotemperatures, V_p are destroyed, forming pyrroles and short chains of hydrocarbons of different structures. In the catalytic conversion zones, oil and OM also lose a significant share of ME, in particular V (T.V. Karaseva, O.V. Serebrennikova, S.A. Punanova, et al.).

A detailed study at the regional level of the OM composition of the formation made it possible to distinguish two of its genetic varieties. The first one, slightly transformed, is characterized by low values (not

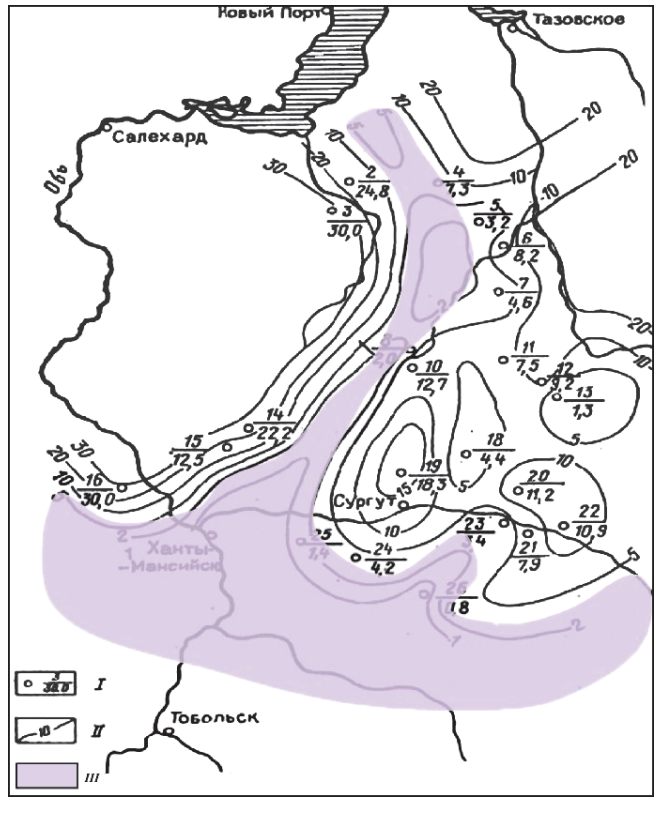

Fig. 2. Scheme of distribution of vanadium content in OM of the rocks from the Bazhenov Formation of Western Siberia (Chakhmakhchev, Punanova, 1992; Punanova, 2017). I – the core extraction area (numerator) with the content V ($n\times10^{-2}$%) in the OM (denominator), the core selection area – see Fig. 1; II – isolines of the content of V in the OM of rocks; III – zone of anomalously low contents of V.

more than 7-8%) of the bituminous coefficient (β) and relatively high values of the metamorphism coefficient k_i = (P+F)/(*n*-C_{17} + *n*-C_{18}) to 0,8, and also a relatively high concentration and diversity of different oxygen-containing structures with increased total aroma. This type of bitumen is developed in the deposits of the Latitudinal Ob Region. The second type of bitumen is characterized by increased β (up to 30%), low values of k_i (0.1-0.3), low relative concentration of oxygen-containing compounds and total aromaticity of CEB with respect to CH_2 groups of *n*-alkanes. In the CEB of this type, practically no porphyrins are found and vanadium concentrations are negligible. Such indicators, as noted earlier, are characteristic of high conversion stage of OM. This geochemical zone coincides with the zone of industrial oil content, and in the regional plan it was reflected in the form of a wide strip having a northeastern strike. It covers part of the Yugansky depression, the Koltogorsky trough, the Salym uplift and extends further to the northwest.

Thus, the revealed heterogeneity of OM rocks of the Bazhenov formation can be explained from our point of view by their different nature – syngenetic and epigenetic. Such dismemberment of bitumen in the oil and gas basin is a necessary condition for further comparison of OM of rocks and oil for detection in the section of oil source formations.

In order to compare the composition of the oils and OM of the rocks of the Bazhenov formation, the well No. 554 of the Salymsky field, which is part of the so-called Great Salym, was studied in detail. The layer Yu_0, confined to the clays of the Bazhenov Formation J_3v^1-K_1b^1, is oil-bearing in a considerable area. Well No. 554 is located within the oil-bearing contour on the central dome of the structure. Based on the results of the study of the rocks of the Bazhenov formation, a close similarity in the composition of oil in the formation and in the composition of the bitumen rocks was revealed. It was expressed in the absence of porphyrins, disproportionately low concentrations V, close to the quantitative distribution of ME and oxygen-containing groups. Due to the fact that the comparison of oils is likely to be carried out with epigenetic bitumen (in the oil-bearing contour), this similarity is not genetically developed and does not prove, but on the contrary it refutes the idea of the connection between the industrial oil bearing capacity of the formation and the generation capacity of its OM, and the revealed proximity – this is the result of contamination of OM rocks by naftides of other sources of generation.

The features of the formation, its shale nature and the frequent alternation of denser and less dense rocks – reservoirs and hydrocarbon producers, lead to difficulties in deciphering the actual oil-material interlayers in its structure. This uncertainty is caused by the fact that the methods of studying conventional hydrocarbon accumulations are not applicable to non-conventional objects, which are both oil source and oil-containing objects. Any movement of fluids within such strata results in a change in their composition, in particular, enrichment with more mobile components and depletion with resin-asphaltene components, to which ME and MPC are associated.

Based on these considerations, for a more correct interpretation of the results obtained, ie. to clarify the nature of the epigenetic bitumen and the role of the OM of rocks from the Bazhenov formation in the processes of oil formation, and, taking into account the noted difficulty in identifying the syngenetic component and sources of oil formation in the Bazhenov formation, we carried out experimental studies on the soft thermolysis (up to 300 °C) of deeply de-bituminous OM for the production of kerogen. The similarity of the ME composition of the released products (during thermolysis) to the trace element composition of oil of the formation will indicate the syngenetic nature of the OM of the enclosing rocks. In the case of reverse results, the idea of the secondary nature of oil relative to the rocks of the formation becomes more convincing, which is illustrated graphically (Fig. 3) (Chakhmakhchev, Punanova, 1992; Punanova, 2017): after heating, there is no similarity of ME between oils and syngenetic bitumen, like it was observed before heating. Thus, as a result of the analytical work carried out, it can be concluded that the similarity of oil and OM of rocks from the Bazhenov formation is not genetic, but manifests itself at the expense of secondary oil content. The bitumen obtained after heating (out of oil-bearing contour), as in the case of bitumen of the wells No. 554 (inside the oil-bearing contour), differs in ME composition from the oils of the Bazhenov formation of the Salymsky field: in V/Ni value, concentration series of the ME distribution, and also in magnitude of ME ratio. All this testifies to the epigenetic character of highly transformed bitumen, migrating probably from the lower high-heated horizons of the basin to higher and unrelated to the syngenetic, poorly catagenetically transformed bitumen of the Bazhenov deposits. The involvement of data on the bitumen characterization and hydrocarbon composition of rock formations also indicates the presence of highly transformed OM in abnormal zones (Chakhmakhchev, Punanova, 1992). The complex comparison of HC biomarkers and ME in the system "kerogen-bitumen-oil" made it possible to call into question of oil-generating role of OM of the Bazhenov formation within the boundaries of the Salymsky field.

Proceeding from this, it can be assumed that within the zones with anomalously low V_p and V contents or their complete absence in bitumen, a mixture of

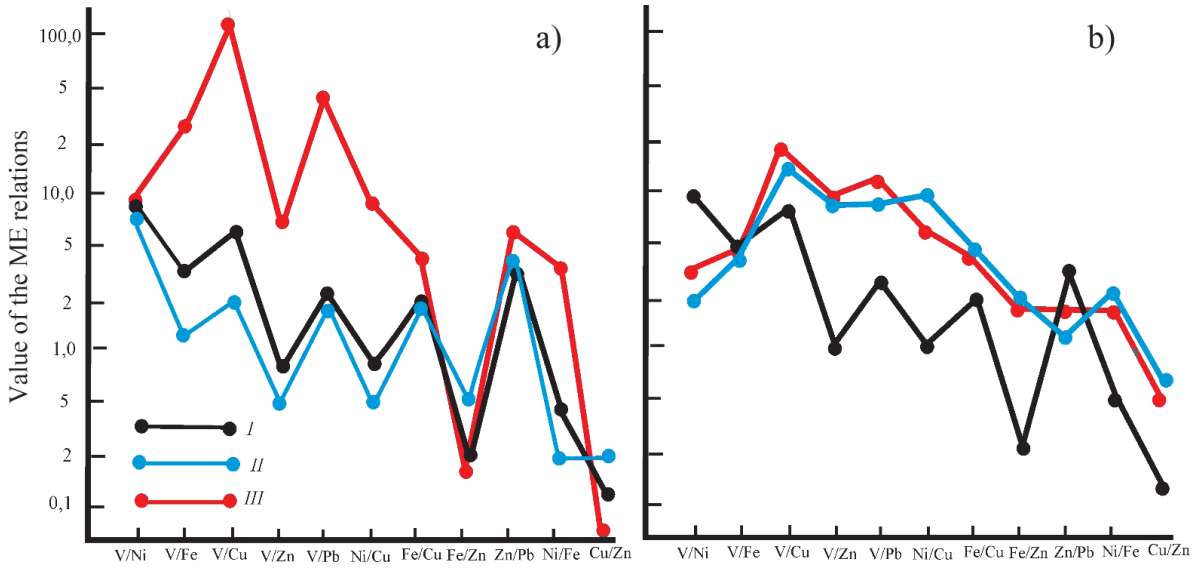

Fig. 3. Comparison of ME ratios in OM of rocks and oils before heating (a) and after heating (b) (Chakhmakhchev, Punanova, 1992; Punanova, 2017). Relations of the ME: I – in oils, II – in the CEB of rocks of the Bazhenov formation inside the oil-bearing contour, III – in the CEB of rocks of the Bazhenov formation outside the oil-bearing contour.

bitumen of the Bazhenov formation with bitumen formed in deeper horizons at higher paleotemperatures occurred. The Bazhenov formation is characterized by the transformation stages of end of MK_1-MK_2 ($R° = 0.45 – 0.85\%$), which corresponds to the second half of the main zone of oil formation (main zone of oil generation) (Kontorovich et al., 2014; Neruchev et al., 1986). These data confirm the possible flow of liquid hydrocarbons from the underlying deposits of the Jurassic (Vasyugan and Tyumen formations), the Triassic and the Paleozoic, capable of generating a high productivity of the entire Jurassic and underlying section. A zone extends through the Yugansky depression, the Koltogorsky basin, the Salymsky uplift and further north-west to the Yamal Peninsula. The territory of highly transformed OM corresponds to the spread of Triassic rifts, granitoid massifs and fluid-conducting faults in the basement (Kontorovich et al., 2008; Fomin, 2011). According to basin modeling (Stoupakova et al., 2015), Triassic rifting and subsequent development of the basin resulted in deep regional faults favorable for vertical fluid migration. According to the results of mathematical modeling (Shuster, Punanova, 2014) this zone practically coincides with the prospective oil-bearing zone of pre-Jurassic deposits and the existing oil bearing capacity of the Khanty-Mansi and Nyurol regions.

Some researchers have a different view on the genesis of oil in the Bazhenov formation, considering it a syngenetic OM of the formation itself, refuting the epigenetic or mixed nature of it. Thus, N.P. Fadeeva, A.V. Stoupakova et al. believe that in this region the deposits of the Bazhenov formation are in the oil window (mid-second half of the main zone of oil generation); the original OM is phytogenic, and can generate oil itself; and the bitumen that we take for epigenetic, are parautochthonous, displaced in the most oil-bearing stratum. A number of researchers (Fomin, 2011; Kontorovich, Kostyreva, 2015; etc.) recognize the presence of zones of highly transformed organic matter of the Bazhenov deposits themselves, for example, at the Chupal and Malobalyksk deposits, confirming this by pyrolytic and charcoal characteristics, and also by an elevated temperature gradient. Additional heating of sediments and an increase in catagenesis in comparison with closely spaced areas, where the deposits of the Bazhenov formation are on gradations of the catagenesis MK_1-MK_2, were also facilitated by the faults fixed in these territories.

On the other hand, studies published in recent years sufficiently substantiate the mixed nature of bitumen in the Bazhenov deposits and the possibility of formation of the oil bearing capacity at the expense of other sources of generation. So, in the work (Soboleva, 2017), when interpreting the results of the detailed hydrocarbon composition of a large sample of oils (more than 80 oil samples from the West Siberian oil and gas basin), it was assumed that in addition to the "own OM of the Bazhenov oil and gas source formation, hydrocarbon fluids from Vasyugan, Tyumen formations and possibly Paleozoic rocks took part in the generation of oil content. The flow of light liquid hydrocarbons and gases occurred along fault zones of different genesis and duration of existence".

Of course, the identification of oil deposits in the shale formations of bazhenites, domanicites, melinites is quite a difficult task. Since the time of I.M. Gubkin, and to this day, there are heated debates about the oil-generating capabilities of the Upper Devonian Domanic formation of the Volga-Urals. Its oil source properties are

not in doubt, but the scale of the possible separation of micronized oil from the stratum is subject to discussion. However, in the depositions of the Domanic formation, residual micro-oil (now called shale oil) is found in the decompressed fractured interlayer reservoirs, and from the bituminous siliceous-carbonate rock formations inflows of hydrocarbons are produced of semi-industrial and industrial nature (Dakhnova, Mozhegova, 2015; Stoupakova et al., 2015; Mukhametshin, Punanova, 2016). I.N. Plotnikova et al. (2017), on the basis of in-depth studies of the geochemical characteristics of the bitumen from Semilukskian horizon and the oil of the Eifelian-Frasnian terrigenous complex, it was concluded that, along with the syngenetic scattered matter, mobile bitumen identical to the oil of the underlying terrigenous deposits of Pashian and the Timanian horizons. In this regard, the authors consider bitumen in the Domanic stratum as migratory, and the deposits of the Domanic facies themselves should be regarded as "accumulative or accumulative-generation system, oil deposits of which were formed due to oil systems generated in other sources."

Similar conclusions were obtained by a detailed study of the composition of the CEB of clayey deposits from the menilite formation of the Oligocene age (Upper Paleogene) of the Ciscarpathian marginal trough of the North-Ciscarpathian oil and gas basin. Investigation of the relationship between oil and Om of rocks allowed us to distinguish two varieties of bitumen – syngenetic and epigenetic, significantly differing in the MPC content. The syngenetic type was revealed in samples from the areas of Tanyavsky, Pasechnyansky and Shodnitsky. It is characterized by a low value of β (up to 7-8%) and high concentrations of vanadylporphyrins (V_p) (up to 1.6% on the CEB), which indicates a low stage of the transformation of OM. In epigenetic bitumen obtained from sediments from the areas of Rozhnyatovsky, Dolinsky, as well as in the oil from the Dolinsky, Tanyavsky, Rozhnyatovsky, Shodnitsky, Bitkovsky, Lopushnyansky deposits, there are no V_p from the depths from 2513 to 4712 m.

This circumstance, as well as the features of hydrocarbon composition and the distribution of oxygen-containing groups, indicate a higher catagenic transformation. Based on the revealed genetic differences in the composition of the oils and OM of rocks, and also the different degrees of their catagenetic transformation, menilite clay black shales probably were not the only generating sources for hydrocarbon systems from the Cenozoic section of Ciscarpathian. The formation of oil deposits may have been due to mixing, or due to the migration of liquid hydrocarbons from the more deeply submerged zones of the development of the Meso-Paleozoic sedimentary complex (Maevsky et al, 1992).

Summarizing the above rather extensive material on the features of the distribution of OM in the sediments of the Bazhenov Formation of the Western Siberian oil and gas basin and other regions with the spread of such a black shale formation, we can state the presence of zones with the introduction of highly transformed epigenetic bitumen catastrophically altered by deep processes, which, in our view, increases the prospects of the oil and gas potential of the region due to the additional source of hydrocarbons, besides the OM of the Bazhenov deposits. These sources can be associated with oil-producing Jurassic (Vasyugan and Tyumen formations) and deep-buried pre-Jurassic sedimentary deposits – Triassic and Paleozoic.

Assessment of oil and gas potential prospects of Lower-Middle Jurassic and pre-Jurassic deposits

By 2016, 902 hydrocarbon fields have been discovered within the Western Siberian oil and gas basin, including 350 with deposits in the Jurassic complex. The largest number of deposits (624 deposits at 210 fields) was found in the Tyumen formation; in the Bazhenov formation there were 80 deposits. The largest initial open oil reserves are concentrated in the Lower-Middle Jurassic oil and gas bearing complex of the central and northern regions of the basin (17.6 billion tons, geological reserves), The smallest are in the Bazhenov formation (0.6 billion tons, extracted reserves) (Skorobogatov, 2017). In our previous studies, the issues of assessing the prospects of oil and gas potential of the Jurassic and pre-Jurassic deposits were thoroughly worked out (Vinogradova, Punanova, 2006; Chakhmakhchev et al., 2003; Punanova, Shuster, 2012; Dmitrievsky et al., 2012; Shuster, Punanova, 2016). Let us briefly discuss the main points.

According to the representations (Shemin et al., 2001) the most informative indicators of prospect evaluation in relation to the Jurassic deposits of the Nadym-Taz interfluve are tectonic and lithologic-facies, since they control the development of the largest hydrocarbon accumulations here. Yu.N. Karogodin (2004) attaches great importance to the role of geodynamic processes in the formation of unique fields in the northern and arctic regions of Western Siberia. It was here, in contrast to other regions of Western Siberia, during the Neogene-Quaternary period, intensive structural-formational movements with the formation of uplifts with amplitudes of more than 200 m were manifested. Skorobogatov (2003), who believes that, depending on the tectonic structure of the sedimentary basin, the lithological and facial characteristics of the sedimentary cover and the geothermal regime, the conditions of ontogenesis of hydrocarbons are significantly different and lead to the formation of differently large and phase states of deposits.

Based on the above considerations, we paid special attention to the lithologic-facies situation of sedimentation, the staginess of the catagenetic transformation of OM sediments, and the structural features of the region in connection with the scale of the fields. The material is illustrated by schematic diagrams (Fig. 4, 5).

An analysis of the relationship between the scale of fields and structural elements has revealed the confluence of unique and large fields to large positive structural elements – mega and meso swells. When allocating the tectonic zones, the materials of V.A. Kontorovich et al, G.G. Shemin et al. were used (Fig. 5). In the Jurassic deposits, the largest fields are confined to positive structures of the first order (megaswells) and second order (meso swells), as well as to positive structures that complicate the megamonoclinal sides. The Bovanenkovo field (large in terms of reserves in J_{1-2}) is located on the Bovanenko-Nurminsky megaswell; Novoportovsk field (unique in reserves in J_{1-2}) – at the South Yamal meso-swell; Novogodny field (large in terms of reserves in J_3) – at Vyngapurovsky megaswell, Urengoysky field (average in reserves in J_{1-2} and J_3) – at the Central Urengoy meso-swell. The Kharampursky field (large in reserves in J_3) is located in the East-Pur megamonocline. Small fields tend to arches and hollows (megatroughs and deflections). For example, in the North arch, deposits are found exclusively with small reserves. However, this relationship does not exclude the possibility of discovering on the same structures fields with other categories of reserves.

Analyzed by us (Punanova, Vinogradova, 2006; 2008), the thicknesses, the distribution of formations, the size of hydrocarbon reserves and their phase state

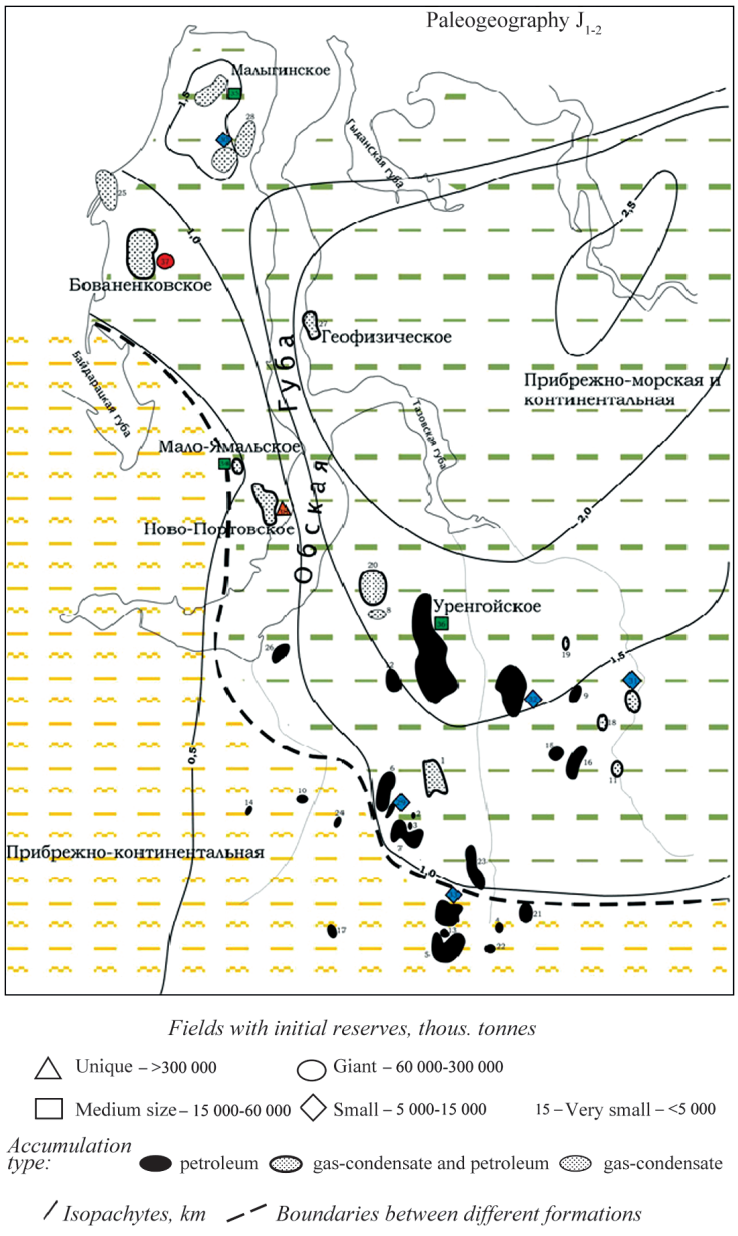

Fig. 4 Schematic map of the distribution of hydrocarbon accumulations of different phase states in the Lower-Middle Jurassic oil and gas bearing complex in connection with facies features of sediments

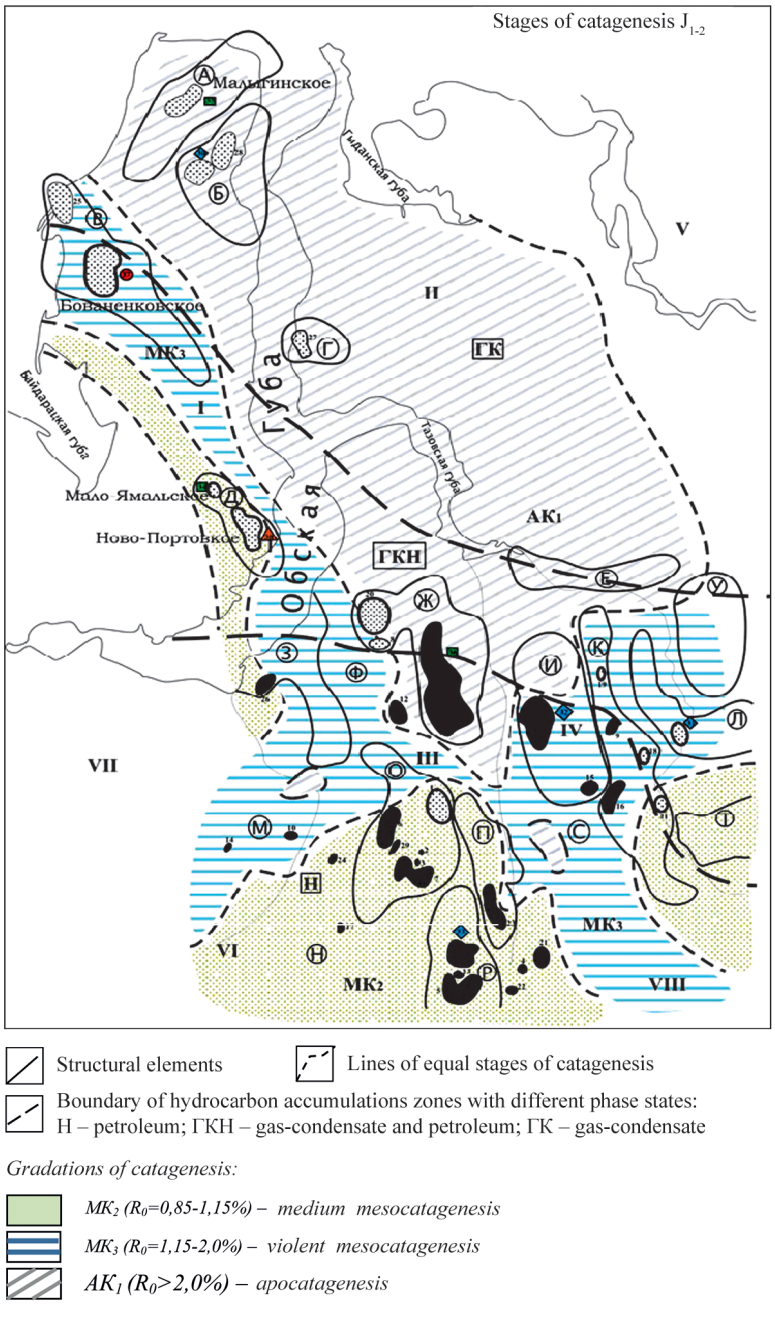

Fig. 5 Schematic map of hydrocarbon accumulations of different phase states in the Lower-Middle Jurassic oil and gas bearing complex in connection with the catagenesis of the Jurassic basal horizons. Conventional designations: fields by initial reserves and type of deposit – see Fig. 4. Oil and gas bearing areas: I – Yamal; II – Gydansky; III – Nadym-Pursky; IV – Pur-Tazovsky; V – Yenisei-Khatanga (Ust-Yenisei); VI – Sredneobsky; VII – Frolovsky; VIII – Vasyugansky. Structural elements: А – North Yamal megaval; Б – Middle-Yamal megaval; В – Bovanenkovo-Nurminsky inclined megaval; Г – Geophysical mezoval; Д – South Yamal mezoval; Е – Tazovsky megaval; Ж – Central-Urengoi mezoval; З – Medvezhye-Nuginsky inclined megaval; И – Srednepursky oblique megaprogib; К – Russian-Chasel megaval; Л – Thermokarst high; М – Nadym hemisyneclise; Н – South-Nadym megamonoclysis; О – North arch; П – Etypurovsky megaval; Р – Vyngapurovsky megaval; С – East-Pursky megamonoclinal; Т – Upper Tolkinsky arch; У – Mangazeya zone of uplifts; Ф – Nerutinsky depression.

are shown in Fig. 4. The Lower-Middle Jurassic oil and gas bearing complex in the northern regions of the West Siberian oil and gas basin is represented (Nemchenko, 2000; Rudkevich et al., 1988) by two formation series – two sandy-silty-clay formations:

- coastal-marine and continental, rhythmically-horizontal-layered;
- coastal-continental lenticular-layered.

The differences in formations are manifested in the more marine nature of the former and the continentality of the latter. Both formations are gray-colored and dark-colored, sub-carboniferous. They contain OM of humus and sapropel-humus type. The amount of C_{org} in clay and argillic varieties ranges from 2 to 3%. If the thicknesses of the first formation vary from 0.5 km in the south-west to 2.5 km in the northeast, then the thickness of the deposits of the second formation, distributed in the south-western and southern parts of the region, varies

from 0.5 to 1 km. O.I. Bostrikov et al. (2012), on the Leontievskian horizon of the Tyumen formation of the Jurassic, most widely developed in the region under investigation (covering more than 80% of the territory of the Western Siberian oil and gas basin), shows the next range of changes in C_{org}: in the deposits of the deep shelf in the central part of the Yamal-Gydan region the C_{org} content reaches its maximum values (up to 3%), decreasing to the south and south-west to 1%. The type of OM is expressed by the proportion of aquatic (sapropel) components (the rest of the OM is represented by the humus terrigenous constituent of mostly higher plants). This share varies from 75% to 25%. Within the Yamal-Gydan region, the deep-sea shelf sea prevailed. Clay and clayey-aleuritic sediments with a content of aquatic components in the range of 50-75% were accumulated here. The southwestern frame of the Yamal-Gydan region is characterized at this time by sediments of the shallow shelf with a smaller content of aquatic components up to 25-50%.

An analysis of the material concerning the stage-by-stage transformation of the region's OM reveals a significant diversity of viewpoints of the researchers (Nemchenko, 2000; Fomin et al., 2001) and various patterns on the maps of the catagenetic transformation zones of OM. When constructing schematic maps of catagenesis of the Lower-Middle Jurassic and Upper Jurassic oil and gas bearing complexes, we used a map of A.N. Fomin et al. (2001) as the basis of the constructions, as the most representative, based on large factual material.

The degree of catagenetic transformation of the OM of the basal horizons of the Jurassic varies considerably over the territory and is represented by the entire catagenesis scale – from grades PC_3 to AC_{1-3}. The least transformed OM (PC_3) is observed on the western peripheral outer side of the basin. The zone of weak mesocatagenesis of OM (R_0 = 0.5 – 0.85%) is adjoined by a thin strip from the east to this region. The largest areas of the northern part of the West Siberian oil and gas basin are represented by three gradations of catagenesis (Fomin et al, 2001): the stages of MC_2, MC_3 and AC_1, i.e. moderate, severe mesocatagenesis and apocatagenesis. The schematic map (Fig. 5) shows the boundaries of the distribution zones of the three stages of the transformation of OM and associated HC fields with different reserves. Here, too, the boundaries of the zones with hydrocarbon accumulations of different phase composition are given (Vinogradova, Punanova, 2006).

Considered three stages of the catagenetic transformation of OM in the Jurassic basal horizons relate to the types of hydrocarbon accumulations corresponding to the phase state: zone of moderate catagenesis is oil deposits area; gas-condensate-oil deposits prevail in the zone of strong mesocatagenesis, the zone of apocatagenesis is a region of gas condensate deposits with a low condensate factor. The allocated zones are most likely continued in the southern waters of the Kara Sea.

Comparison of the staged catagenetic transformation of Jurassic OM with the value of the initial hydrocarbon reserves did not reveal a direct relationship between them. As was noted by many geochemists and confirmed by the study, the degree of catagenesis of OM determines the type of hydrocarbon fluid: with increasing gradations of catagenesis, the type of deposit varies from oil to gas-condensate-oil and gas-condensate.

Thus, the analysis of the spatial distribution of fields in terms of geological reserves in the Lower-Middle Jurassic oil and gas bearing complex showed a fairly clear connection with the structural features of the region. Dependence of reserve values on the paleofacial environment of sedimentation and sediment thickness, as well as on the catagenetic transformation of the initial OM, was outlined (Vinogradova, Punanova, 2006; Punanova, Vinogradova, 2006; 2008).

The common point for characterizing the oil and gas bearing complexes under investigation is the presence of sufficiently thick oil and gas source strata in each complex, which due to the catagenetic conditions (the "oil and gas window") became oil and gas producing, capable of generating large amounts of bitumen and gases. The presence of traps and low-permeability screens-tires contributed to the accumulation of hydrocarbons formed and their safety. The observed nature of propagation over the area and the section of hydrocarbon accumulations of different phase states corresponds to the evolutionary development of the strata and their original OM, i.e. stages of their catagenetic transformation: from deep pure gas deposits through transitional and oil to accumulations of protocatalogenetic gases and naphthenic condensates and oils of early generation. The established and predicted boundaries of hydrocarbon distribution zones of accumulations of different phase states in the studied oil and gas bearing complexes in the north of Western Siberia correspond to the gradations of the catagenetic transformation of the initial OM and its facies-genetic composition (Vinogradova, Punanova, 2006). The deposits of the Lower- Middle Jurassic age, containing mainly OM of humic nature (carbonaceous and sub-glacial continental formations), are classified as gas-producing, which led to the concentration of large gas and gas-condensate deposits in these sediments. The type of OM in sediments of the Upper Jurassic age is characterized as mixed, humus-sapropelic, which is a source of predominantly oil accumulations.

Thus, by the size of geological reserves, statistical regularities in the distribution of resources, their spatial distribution and the phase state of the clusters, each investigated oil and gas bearing complex of Mesozoic

deposits in the northern regions of Western Siberia is independent, and the scale of accumulations is controlled by factors inherent in each complex individually. It is the tectonic, lithologic-facies and catagenetic features of the processes of oil and gas generation that control both the phase state of the deposits and the differentiation of accumulations in terms of geological resources (Punanova, Vinogradova, 2008).

The estimation of the oil-generation potential, carried out by pyrolytic methods based on drilling Tyumensky SG-6 and Yen-Yakhinsky SG-7, and also the study of samples from Paleozoic deposits of the northern frame of the Western Siberian oil and gas basin significantly changed the negative views of many researchers on the possibility of oil generation of Paleozoic OM sediments (Belokon et al., 1994; Gorbachev et al., 1996; Dmitrievsky et al., 2012; Ekhlakov et al., 2000; Kontorovich et al., 2001; Lopatin et al., 1997, 1999; Prasolov et al., 2000; Khakhaev et al., 2008; Chakhmakhchev et al., 2004; etc.).

According to the analysis of core from SG-6 within the Tyumen, Kotukhtinsky, Yagelny, Novy Urengoy and Varengayakhinsky formations, productive, medium-productive and highly productive oil and gas source rocks with increased contents of sapropel-humus type OM and bitumen are widely developed. In the Paleozoic deposits underlying the effusive-sedimentary stratum of the Triassic, the oil and gas source rocks are developed, which, in terms of productivity, are classified as productive and highly productive oil and gas reservoirs.

Studies of the core and sludge from the well SG-7 indicate that increased values of the generation potential of rocks are recorded in the deposits of the Pokursky, Tangalov, Bazhenov and Tyumen formations. The main zone of oil formation is fixed in the depth interval 2850-4700 m, in which the concentration of free and sorbed hydrocarbons (up to 1.6 mg HC/g of rock) sharply increases, the values of the productivity index and Tmax increase. The gas generation properties of the rocks are preserved up to the bottom of the sedimentary strata (6921 m). Almost throughout the entire well section, including the effusive rock complex, there is intensive migration of hydrocarbon fluids. In the Paleozoic sections of the northern frame of the Western Siberian oil and gas basin (outcrops of the Polar Urals on the Shchuch'insky outburst, the Western Taimyr and the Nizhne-Pursky swell), based on pyrolysis data on the characterization of the oil- and the distribution of HC biomarkers, strata are identified that have favorable oil-production parameters. The HC accumulation zones can be expected within structures similar to the Nizhne-Pursky swell, where these rocks are located in the main zone of oil generation, as well as in other regions where these deposits lie at considerable depths and are covered by good impermeable beds (Kostyreva et al., 2008; Boldushevskaya et al., 2008; Kiryukhina et al., 2012).

Based on the significant differences in the intensity of paleoheating of sedimentary strata in the entire territory of the West Siberian oil and gas basin with depth depending on the age of the basement consolidation (Kontorovich et al., 2008; Fomin, 2011), we predict the depths of HC generation processes in accordance with Rº and paleotemperatures. The highest generation indices of oil and gas producing sequences and greater depths of detection of oil accumulations (up to 4,200 m) can be expected in areas of Pre-Baikal basement, and Jurassic strata will be the main oil-producing strata in the areas of rigid paleo-heating. The depths of the discovery of oil accumulations here are limited to 3200 m (Table 1) (Dmitrievsky et al., 2012).

Based on the analysis of geochemical indicators, most researchers believe that the oil of the Jurassic and pre-Jurassic complex (the contact zone of the basement and the cover) form a group with a single fluid dynamic system and a common source of oil and gas formation, close in physicochemical characteristics and hydrocarbon composition. Both Lower Jurassic and Upper Jurassic deposits are recognized as petroleum deposits (Moskvin et al., 2001; etc.). However, the comparison of the contents of the biophilic elements V,

Cycle of basement consolidation (Kontorovich et al, 2008; Fomin, 2011)	Main areas of accumulation (Kontorovich et al, 2008; Fomin, 2011)	Temperature gradient	Probable lower boundaries of HC generation, m	
			of oil	of light oil and GC
Pre-Baikal	Prienisesky, part of the Mansiysky syneclise, Surgutsky and Nizhnevartovsky arches	Low	4200	5200
Gercinsky, Caledonsky	Central and South-East parts of West Siberia	Medium	3650	4400
Triassic reefs, granitoid massif and fluid-conducting faults in basement	Shaimsky, Krasnoleninsky and others arches	Intense	3200	4050

Table 1. Estimated depths of oil and gas generation processes

Ni, Fe, Mo, Cu in oil and bitumen of the Shaim region with the data on rare-earth elements (REE) (Fedorov et al., 2010) on the Khanty-Mansiysk, Danilovsky, Lovinsky, Martymya-Teterivsky, etc., attests to the essential difference between the Paleozoic naphthids and the weathering crust from the Jurassic ones. Also, sharp differences in the oils of the Jurassic, Triassic and Paleozoic complexes according to ME indicators are evident in the Nyurol region (Punanova, 2002). All these facts are probably connected with the presence of local foci of oil formation in the Paleozoic and pre-Jurassic deposits. These data confirmed the conclusions made by us on the basis of thermolysis of Bazhenov deposits. Thus, when comparing the hydrocarbons and ME compositions of naphthys of the Jurassic and Paleozoic complexes, it is concluded that there are two possible sources of oil generation. This syngenetic OM of the sedimentary Paleozoic and OM, generated by Jurassic sedimentary and Triassic volcanic-sedimentary deposits.

Conclusion

In connection with the sharp heterogeneity of the structure in exploration areas and fields in dense massive rocks, expressed in a "chaotic" distribution of reservoir rocks with different filtration-capacity properties and oil and gas inflow zones, it is necessary to take a new approach to choosing the location and depth of the designed wells on promising areas. At the stage of preliminary drilling of exploratory wells, it is necessary to conduct seismic operations using scattered waves, which allow detecting in the zones and areas of increased energy of scattered waves, i.e. reservoir rocks. Moreover, zones with the maximum energy values correspond to the section intervals with the best reservoir properties of the reservoir rocks and the maximum oil rates in the wells. This technology can be used in the low-permeability strata of the Bazhenov formation.

By the features of the OM distribution in the sediments of the Bazhenov formation of the Western Siberian oil and gas basin and in the black shale formations of other regions, the zones of introduction of highly transformed epigenetic bitumen, catagenically altered by deep processes, have been identified. In our opinion, it improves the prospects of the oil and gas potential of the region under study at the expense of the additional source of hydrocarbons, besides the OM of the Bazhenov formation itself. These sources can be associated with oil-producing Jurassic (Vasyugan and Tyumen formations) and deep-buried pre-Jurassic sedimentary deposits – Triassic and Paleozoic.

Summarizing the rather extensive material, it can be stated that a number of the facts revealed that it is possible to assess the prospects of the Jurassic and deeply buried pre-Jurassic deposits of the Western Siberian oil and gas basin from a new perspective. Such new arguments include traced zones of highly transformed OM in the bitumen of the Bazhenov formation, indicating the presence of generation foci in the underlying sedimentary strata, geochemical data on in situ oil formation processes in the Paleozoic complex, favorable geochemical conditions of pre-Jurassic deposits, which is expressed in relatively high Corg content and bitumen, in moderate and sufficient catagenetic heating of subsoil, high realized generation potential. In combination with other geological prerequisites – reservoirs and impermeable beds, the studied sediments can be considered as a promising object for the discovery of oil and gas fields in it. Moreover, the most promising areas are the epigenetic migratory bitumen zone that extends through the Yugansky depression, the Koltogorsky basin, the Salymsky uplift and further north-west to the Yamal Peninsula and possibly to the Kara Sea. The new arguments give an additional impetus to the wide deployment of scientifically grounded work on the Jurassic and deep pre-Jurassic horizons of the West Siberian oil and gas basin – the lower floor of the oil and gas bearing both within its northern part (Ob, Taz and Gydan Gulfs) and in marine areas that will confirm the predictions the founder of oil geology acad. A.A. Trofimuk, that Paleozoic oil in Western Siberia really is the "gold substrate" of its Mesozoic wealth.

Acknowledgements

The article is written in the framework of the state contract (the topic «Fundamental problems of geology, geochemistry and hydrogeology of oil and gas bearing sedimentary basins. Feasibility of significant factors for the effective forecast of large hydrocarbon accumulations in unstructured conditions», No. AAAA-A16-116022510269-5).

References

Belokon' T.V., Gorbachev V.I., Pevzner L.A. et al. (1994). A new stage in the study of structure and oil and gas potential of the deep horizons of the north of Western Siberia (based on the Tyumen superdeep well drilling data). *Geologiya, metody poiskov, razvedki i otsenki mestorozhdeniy toplivno-energeticheskogo syr'ya*: Obzor [Geology, methods of prospecting, exploration and evaluation of fuel and energy raw materials fields: Review], Moscow: ZAO Geoinformmark, 32 p. (In Russ.)

Boldushevskaya L.N., Ladygin S.V., Nazimkov G.D. et al. (2008). Organic matter of the Paleozoic deposits of the Western Taimyr and the Western part of the Yenisei-Khatanga regional trough, paleotectonic reconstructions by geological and geochemical data. *Fundament, struktury obramleniya Zapadno-Sibirskogo mezozoysko-kaynozoyskogo osadochnogo basseyna, ikh geodinamicheskaya evolyutsiya i problemy neftegazonosnosti* [Basement, frame structures of the West Siberian Mesozoic-Cenozoic sedimentary basin, their geodynamic evolution and oil and gas bearing problems], Novosibirsk, pp. 23-25. (In Russ.)

Bostrikov O.I., Larichev A.I., Fomichev A.S. (2011). Geochemical aspects of Lower and Middle Jurassic sediments of the West-Siberian Plate in view of hydrocarbon potential evaluation. *Neftegazovaya geologiya. Teoriya i praktika = Oil and gas geology. Theory and practice*, 6(3). http://www.ngtp.ru/rub/1/31_2011.pdf. (In Russ.)

Bochkarev V.S., Brekhuntsov A.M., Deshchenya N.P. et al. (2000). Geological and tectonic models of the north of Western Siberia and the problem of hydrocarbon deposits search in deep horizons. *Sb. «Kriterii otsenki neftegazonosnosti nizhe promyshlenno osvoennykh glubin i opredelenie*

prioritetnykh napravlenii geologorazvedochnykh rabot» [Coll. papers: "The criteria for assessing oil and gas content below the industrially exploited depths and determination of priority areas for geological exploration"], Perm, pp. 201-202. (In Russ.)

Chakhmakhchev V.A., Punanova S.A. (1992). To the problem of diagnostics of oil reservoirs on the example of Bazhenov deposits of Western Siberia. *Geokhimiya = Geochemistry*, 1, Pp. 99-109. (In Russ.)

Chakhmakhchev V.A., Punanova S.A., Vinogradova T.L. (2003). Geological and geochemical forecast of oil and gas content of deep-buried sediments in the north of the West Siberian oil and gas bearing basin. *Geologiya, geofizika i razrabotka neftyanykh i gazovykh mestorozhdenii = Geology, geophysics and development of oil and gas fields*, 6, pp. 4-10. (In Russ.)

Dakhnova M.V., Mozhegova S.V. (2015). Geochemical criteria for forecasting the oil content of the domanic (Bazhenov) deposits – the source of shale oil. *Chernye slantsy: geologiya, litologiya, geokhimiya, znachenie dlya neftegazovogo kompleksa, perspektivy ispol'zovaniya kak al'ternativnogo uglevodorodnogo syr'ya: Mater. vseross. nauch.-prakt. konf.* [Black Shales: Geology, Lithology, Geochemistry, Importance for the Oil and Gas Complex, Prospects for Use as an Alternative Hydrocarbon Material: Proc. All-Russian. Sci.-Pract. Conf.], Yakutsk: Akhsaan, pp. 124-128.(In Russ.)

Dmitrievskii A.N., Shuster V.L., Punanova S.A. (2012). Doyurskii kompleks Zapadnoi Sibiri – novyi etazh neftegazonosnosti. Problemy poiskov, razvedki i osvoeniya mestorozhdenii uglevodorodov [The pre-Jurassic complex of Western Siberia as the new stage of oil and gas content. Problems of prospecting, exploration and development of hydrocarbon deposits], Lambert Academic Publishing, Saarbruchen, Germany, 135 p. (In Russ.)

Ekhlakov Yu.A., Dikovskiy A.A. et al. (2000). Tyumen superdeep well as a reference section for study of oil and gas content criteria below the industrially exploited depths in the north of the West Siberian oil and gas basin. *Kriterii otsenki neftegazonosnosti nizhe promyshlenno osvoennykh glubin i opredelenie prioritetnykh napravleniy geologo-razvedochnykh rabot* [Criteria for assessing oil and gas content below the industrially exploited depths and determining priority areas for geological exploration works], Perm, pp. 116-118. (In Russ.)

Fedorov Yu.N., Maslov A.V., Ronkin Yu.L., Lepikhina O.P. (2010). Mikroelementnaya kharakteristika syrykh neftey Shaimskogo i Sredneobskogo neftegazonosnykh rayonov Zapadnoy Sibiri: novye dannye. Degazatsiya [Microelement characteristics of crude oils of Shaim and Sredneobsky oil and gas bearing regions of Western Siberia: new data. Degassing]. Moscow: GEOS, 586 p. (In Russ.)

Fomin A.N., Kontorovich A.E., Krasavchikov V.O. (2001). Catagenesis of organic matter and prospects of oil and gas content of the Jurassic, Triassic and Paleozoic deposits of the northern regions of the West Siberian megabasin. *Geologiya i geofizika = Geology and geophysics*, 42(11-12), pp. 1875-1888. (In Russ.)

Fomin A.N. (2011). Catagenesis of organic matter and prospects of oil and gas content of the sedimentary deposits of the Triassic of the West Siberian megabasin. *Gornye vedomosti*, 9, pp. 11-15. (In Russ.)

Karogodin Yu.N. (2004). The role of geodynamic processes in the formation of a unique Urengoy-Yamburg gas-bearing zone in the north of Western Siberia. *Tezisy Vtoroi mezhd. konf. «Geodinamika neftegazonosnykh basseinov»* [II Int. Conf.: Geodynamics of oil and gas basins, Abstracts], V. 2, Moscow, Gubkin Russian State University of oil and gas, pp. 41-44. (In Russ.)

Khakhaev B.N., Gorbachev V.I., Bochkarev V.S. et al. (2008). The main results of superdeep drilling in the West Siberian oil and gas province. *Sb. dokladov «Fundament, struktury obramleniya Zapadno-Sibirskogo mezozoisko-kainozoiskogo osadochnogo basseina ikh geodinamicheskaya evolyutsiya i problemy neftegazonosnosti»* [Coll. papers: Basement, frame structures of the West Siberian Mesozoic-Cenozoic sedimentary basin, their geodynamic evolution and oil and gas bearing problems], Novosibirsk, pp. 224-227. (In Russ.)

Kiryukhina T.A., Ul'yanov G.V., Dzyublo A.D. et al. (2011). Geochemical aspects of oil-gas content of Jurassic and pre-Jurassic deposits of the north of Western Siberia and the adjacent shelf. *Gazovaya promyshlennost' = Gas industry*, 7, pp. 66-70. (In Russ.)

Kostyreva E.A., Fomin A.N., Belyaev S.Yu. et al. (2008). Organic geochemistry of the Paleozoic deposits of the Shchuch'inskii protrusion of the Polar Urals. *Sb. dokladov: Fundament, struktury obramleniya Zapadno-Sibirskogo mezozoysko-kaynozoyskogo osadochnogo basseyna, ikh geodinamicheskaya evolyutsiya i problemy neftegazonosnosti* [Coll. papers: Basement, frame structures of the West Siberian Mesozoic-Cenozoic sedimentary basin, their geodynamic evolution and oil and gas bearing problems], Novosibirsk, pp. 127-131. (In Russ.)

Kontorovich A.E., Burshtein L.M., Kazanenkov V.A., Kontorovich V.A., Kostyreva E.A., Ponomareva E.V., Ryzhkova S.V., Yan P.A. (2014). The Bazhenov suite is the main reserve of unconventional oil in Russia. *Georesursy, geoenergetika, geopolitika = Georesources, geoenergetics, geopolitics*, 2(10). http://oilgasjournal.ru/vol_10/kontorovich.html (In Russ.)

Kontorovich A.E., Kostyreva E.A. (2015). Organic geochemistry of bitumen Bazhenov suite of central regions of Western Siberia. *Chernye slantsy: geologiya, litologiya, geokhimiya, znachenie dlya neftegazovogo kompleksa, perspektivy ispol'zovaniya kak al'ternativnogo uglevodorodnogo syr'ya: Mater. vseross. nauch.-prakt. konf.* [Black Shales: Geology, Lithology, Geochemistry, Importance for the Oil and Gas Complex, Prospects for Use as an Alternative Hydrocarbon Material: Proc. All-Russ. Sci.-Pract. Conf.], Yakutsk: Akhsaan, pp. 150-154. (In Russ.)

Kontorovich A.E., Fomin A.N., Krasavchikov V.O., Istomin A.V. (2008). Catagenesis of the organic matter of the Mesozoic and Paleozoic deposits of Western Siberia. *Litologicheskie i geokhimicheskie osnovy prognoza neftegazonosnosti: Sb. materialov VNIGRI* [Lithological and geochemical foundations of oil and gas potential: Coll. papers of VNIGRI], St.Petersburg, pp. 68-77. (In Russ.)

Lopatin N.V., Emets T.P. (1999). Oil-producing properties and catagenesis of clay rocks of Mesozoic-Permian stratotypes revealed by the Tyumen superdeep well SG-6. *Geologiya, geofizika i razrabotka neftyanykh mestorozhdenii = Geology, geophysics and development of oil fields*, 6, pp. 9-19. (In Russ.)

Maevskii B.I., Chakhmakhchev V.A., Razumova E.R., Punanova S.A. et al. (1992). On the origin of hydrocarbon deposits in the Paleogene sediments of Precarpathia. *Otechestvennaya geologiya = Domestic geology*, 10, pp. 9-16. (In Russ.)

Moskvin V.I., Kostyreva E.A., Moiseeva N.V. et al. (2001). Geochemistry of oils of the Shaim region. *Tezisy dokl. nauch.-prakt. konf. «Geokhimiya v praktike poiskovo-razvedochnykh rabot na neft' i gaz»* [Abstracts Sci.-Pract. Conf. "Geochemistry in the practice of oil and gas prospecting], Moscow, VNIGNI, pp. 101-102. (In Russ.)

Mukhametshin R.Z., Punanova S.A. (2016). Paleozoic oils specific features of the Ural-Volga central regions and Domanic stratum as a source of their formation. *Geologiya, geofizika i razrabotka neftyanykh i gazovykh mestorozhdeniy = Geology, geophysics and development of oil and gas fields*, 6, pp. 45-51. (In Russ.)

Nemchenko N.N. (2000). Izbrannye trudy, posvyashchennye problemam nefti i gaza [Selected works devoted to the problems of oil and gas]. Moscow, OAO «VNIIOENG», 456 p. (In Russ.)

Neruchev S.G., Rogozina E.A., Zelichenko I.A. et al. (1986). Neftegazoobrazovanie v otlozheniyakh domanikovogo tipa [Oil and gas formation in the deposits of domanic type]. Leningrad: Nedra, 448 p. (In Russ.)

Nikolaev A.V. (1991). Development of non-traditional methods in geophysics. *Sb.: Fizicheskie osnovy seismicheskogo metoda* [Coll. papers: Physical foundations of the seismic method], Moscow: Nauka, pp. 5-17. (In Russ.)

Plotnikova I.N., Ostroukhov S.B., Laptev A.A., Gazizov I.G., Emel'yanov V.V., Pronin N.V., Salikhov A.D., Nosova F.F. (2017). Migration Aspect in the Oil-Bearing Capacity of the Domanic Formation in Tatarstan. *Georesursy = Georesources*, 19(4), Part 2, pp. 348-355. DOI: https://doi.org/10.18599/grs.19.4.7

Punanova S.A. (2002). Geochemical features of Paleozoic oils of the West Siberian oil and gas bearing basin. *Neftekhimiya = Petrochemistry*, 42(6), pp. 428-436. (In Russ.)

Punanova S.A. (2017). Applied metallogeny of naphthids. *Aktual'nye problemy nefti i gaza = Actual problems of oil and gas*, 2(17), 13 p. http://oilgasjournal.ru. (In Russ.)

Punanova S.A., Vinogradova T.L. (2006). Forecast of the phase state of hydrocarbon clusters in the Mesozoic deposits of the north of Western Siberia. *Geokhimiya = Geochemistry*, 9, pp. 983-995. (In Russ.)

Punanova S.A., Vinogradova T.L. (2008). Gas-oil-bearing complexes of northern regions of Western Siberia and features of their geological resources. *Geologiya nefti i gaza = The geology of oil and gas*, 3, pp. 20-30. (In Russ.)

Punanova S.A., Chakhmakhchev V.A. (1992). Experimental studies of the transformation of the microelement composition of naphthides during the processes of their migration, catagenesis and hypergenesis. *Sb. «Modelirovanie neftegazoobrazovaniya»* [Coll. papers: Modeling of oil and gas formation], Moscow: Nauka, pp. 119-124. (In Russ.)

Punanova S.A., Shuster V.L. (2012). Geological-geochemical conditions for oil and gas content availability of Pre-Jurassic deposits located on West-Siberian platform. *Geologiya, geofizika i razrabotka neftyanykh i gazovykh mestorozhdenii = Geology, geophysics and development of oil and gas fields*, 6, pp. 20-26. (In Russ.)

Rudkevich M.Ya., Ozeranskaya L.S. Chistyakova N.F. et al. (1988). Neftegazonosnye kompleksy Zapadno-Sibirskogo basseina [Oil and gas bearing complexes of the West Siberian basin], Moscow: Nedra, 181 p. (In Russ.)

Skorobogatov V.A. (2017). Jurassic productive complex of Western Siberia: past, present, future. *Vestnik gazovoi nauki = Bulletin of gas science*, 3(31), pp. 36-58. (In Russ.)

Skorobogatov V.A. (2003). Genetic reasons for the unique gas and oil content of the Cretaceous and Jurassic deposits of the West Siberian province. *Geologiya, geofizika i razrabotka neftyanykh i gazovykh mestorozhdenii = Geology, geophysics and development of oil and gas fields*, 8, pp. 8-14. (In Russ.)

Soboleva E.V. (2017). Formation of the oil composition of the Yu0 Bazhenov formation, Salym oil field. *Georesursy = Georesources*, Special issue, Part 2, pp. 144-154, DOI: http://doi.org/10.18599/grs.19.15 (In Russ.)

Stoupakova A.V., Sokolov A.V., Soboleva E.V., Kiryukhina T.A., Kurasov I.A., Bordyug E.V. (2015). Geological survey and petroleum potential of Paleozoic deposits in the Western Siberia. *Georesursy = Georesources*, 2(61), pp. 63-76. DOI: http://dx.doi.org/10.18599/grs.61.2.6 (In Russ.)

Shemin G.G., Nekhaev A.Yu., Fomin A.N. et al. (2001). Criteria and assessment of the prospects of oil and gas content of deep-buried sequences in the lower Jurassic of the north of the West Siberian NGP. *V kn. «Kriterii otsenki neftegazonosnosti nizhe promyshlenno osvoennykh glubin i opredelenie prioritetnykh napravlenii geologo-razvedochnykh rabot»* [Book 1: "The criteria for assessing oil and gas content below the industrially exploited depths and determination of priority areas for geological exploration"], Perm, pp. 107-132. (In Russ.)

Shuster V.L. (2003). Problemy neftegazonosnosti kristallicheskikh porod fundamenta [Problems of oil and gas content of crystalline basement rocks], Moscow: «Geoinformtsentr», 48 p. (In Russ.)

Shuster V.L., Punanova S.A. (2014). Development of Unconventional Hydrocarbon Sources in Western Siberia and Evaluation of Oil and Gas Prospects. *Georesursy = Georesources*, 4(59), pp. 53-58. (In Russ.)

Shuster V.L., Punanova S.A. (2016). Justification of Oil and Gas Potential of the Jurassic-Paleozoic Deposits and the Basement Formations of Western Siberia. *Georesursy = Georesources*, 18(4), Part 2, pp. 337-345, DOI: 10.18599/grs.18.4.13

Vinogradova T.L., Punanova S.A. (2006). Hydrocarbon accumulations of Jurassic deposits in the north of Western Siberia and features of their geological resources. *Doklady RAN = Proc. of the Russian Academy of Sciences*, 410(2), pp. 220-224. (In Russ.)

About the Authors

Svetlana A. Punanova – DSc (Geology and Mineralogy), Leading Researcher

Oil and Gas Research Institute of the Russian Academy of Sciences

3 Gubkin str., Moscow, 119333, Russian Federation

E-mail: punanova@mail.ru

Vladimir L. Shuster – DSc (Geology and Mineralogy), Professor, Chief Researcher

Oil and Gas Research Institute of the Russian Academy of Sciences

3 Gubkin str., Moscow, 119333, Russian Federation

Manuscript received 16 February 2018;
Accepted 18 April 2018; Published 30 June 2018

ORIGINAL RESEARCH ARTICLE

DOI: https://doi.org/10.18599/grs.2018.2.81-87

Lithological and biostratigraphic characteristics of the Upper Silurian and Lower Devonian deposits of the southwestern part of the field named after Roman Trebs

T.M. Mavrinskaya[1], E.N. Savelyeva[2], K.D. Shumatbaev[2]*

[1]Institute of Geology of Ufa Scientific Center of the Russian Academy of Sciences, Ufa, Russian Federation

[2]BashNIPIneft LLC, Ufa, Russian Federation

Abstract. A conodont sequence from the Przhidolian stage of the Upper Silurian and almost the entire Lokhkovian stage of the Lower Devonian has been established in the sections of the Upper Silurian-Lower Devonian on the southwestern part of the field named after Roman Trebs (Timano-Pechora oil and gas province). According to the conodonts, two biostratigraphic subdivisions are distinguished in the rank of layers with fauna in the Upper Silurian and three of them in the Lokhkovian stage of the Lower Devonian. The layers can be compared with the standard conodont zonal scale. The Silurian-Devonian boundary has a complex rationale for biostratigraphic data (conodonts), cyclostratigraphy, and logging data (electrical and radioactive methods). The Lower Devonian deposits are overlain by terrigenous packs of the Timanian horizon of the Frasnian stage. The break in the sedimentation covers the interval from the Praghian stage of the Lower Devonian to the Dzhierskian horizon of the Frasnian stage of the Upper Devonian inclusively. The regularity of the placement of reservoir rocks in the section of wells is analyzed and their relation to the cyclicity of sedimentation is noted.

Key words: Silurian, Devonian, conodonts, logging, lithology, cyclicity

Recommended citation: Mavrinskaya T.M., Savelyeva E.N., Shumatbaev K.D. (2018). Lithological and biostratigraphic characteristics of the Upper Silurian and Lower Devonian deposits of the southwestern part of the field named after Roman Trebs. *Georesursy = Georesources,* 20(2), pp. 81-87. DOI: https://doi.org/10.18599/grs.2018.2.81-87

Introduction

The field named after Roman Trebs is located within the Timan-Pechora oil and gas province, tectonically associated with the northeastern slope of the Bolshezemelsky Arch. Geological studies of the Lower Paleozoic in the northern part of the Timan-Pechora province have been carried out since the last century by many researchers: D.V. Nalivkin, V.V. Menner, N.V. Taninskaya, A.I. Antoshkina, V.N. Puchkov, S.V. Melnikov, T.M. Beznosova, Z.P. Yuryeva, Iyu. Valiukevichus, Yu.V. Deulin, G.A. Chernov, A.I. Pershina, N.B. Rasskazova, V.S. Tsiganko and others. As a result of these studies, stratigraphic dismemberment of Paleozoic deposits was carried out, paleogeographic reconstructions were made, geological and facial maps were created, sedimentation models were constructed, which allowed reconstructing the stages of paleobasin evolution and reconstructing sedimentation conditions for individual periods of time.

This article is devoted to the dismemberment of the Silurian and Devonian deposits discovered by a series of wells, the determination of their stratigraphic volume and identification of the position and nature of the boundary based on the results of biostratigraphic (by conodont), cyclostratigraphic, geophysical studies of wells. Two wells A and B were taken as the basis, which characterize the most completely the section under consideration.

As a stratigraphic basis, the Stratigraphic Scheme for the Middle and Upper Paleozoic of the Russian Platform (1990) was used in the dismemberment.

Lithological characteristics of the Upper Silurian and Lower Devonian section in the wells A and B

The deposits of the Upper Silurian and the Lower Devonian of the Bolshezemelsky Arch are related to the formations of the shallow-marine paleoshelf of the epicontinental sea. They have a cyclic structure reflecting the transgressive-regressive sedimentation.

As a rule, the lower elements of the cyclites are composed of dark-colored clayey and clay-carbonate rocks, for which, according to the logging data, high indications of gamma ray logging with relatively low

*Corresponding author: Elena N. Savelyeva
E-mail: savelevaen@bashneft.ru

values of neutron logging and specific electric resistance (Fig. 1). When the sea level rises, they are usually the first to form in the submerged parts of the coastal zones under the reducing environment.

The average elements of the cyclites in many cases are represented by limestones the micrite and nodular-layered, distinguished by low indications of gamma-ray logging and high indications of neutron logging and high specific electric resistance. They are formed during stagnation in an open sea basin with normal salinity in the zone of lower sublittoral, in a more calm hydrodynamic situation.

Biogermic, organogenous-detrital dolomitic limestones and porous dolomites are the upper members of the cyclites, which correspond to low gamma-ray logging indications and mean values of neutron logging, high values of specific electric resistance in oil-saturated intervals and low in water saturated ones. They are formed in shallow conditions in the zone of upper sublittoral.

The replacement of biogermal limestones or porous dolomites with argillaceous rocks reflects the beginning of a new transgressive stage. Important reference points are packs of basal conglomerates, whose sign according to the logging data are the increased values of natural radioactivity in the gamma-ray logging. They are formed during the erosion of the underlying strata at the onset of a new transgression of the sea.

The Lower Devonian deposits occur in a clinoform on the eastern slope of the Bolshezemelsky Arch, the thickness of the sediments decreases from east to west and southwest to complete wedging (Yur'eva, Valiukevichus, 2014).

Well A is west of the Central Block of the field named after R. Trebs, in the zone of wedging and reduction of D_1 stratum thickness, and well B is located in the south-eastern part of the Central Block, almost at the eastern boundary of the Khoreyversky depression. In the context of the latter, a comparative increase in the volume of the Lower Devonian deposits is observed.

The Upper Silurian. Przhidolian stage. Grebenskian horizon. In the well A, two cyclites are identified in the sediments of the Grebenskian horizon (Fig. 2). The first cyclite includes the packs 1-3. It is represented by a complete set of elements of the cyclite: clayey rocks in the base (pack 1), layered limestones with interlayers of bioclastic and organogenic differences in the middle part (pack 2) and dolomites porous and clayey in the upper part (pack 3). In a pack of limestones of the middle part conodonts were found: *Coryssognathus* aff. *dubius* (Rhodes), *Oulodus (= Delotaxis)* cf. *elegans* (Walliser), *Ozarkodina* aff. *cornidentata* (Branson et Mehl), *Ozarkodina* cf. *eosteinhornensis* (Walliser), characteristic of the Przidolian stage of the Upper Silurian. In the porous dolomites oil saturation is noted. The total thickness of the cyclite in well A is 25.9 m.

The second cyclite contains packs 4-6. It begins with nodular-layered limestones (pack 4), overlapping with a clear contact underlying porous dolomites. ,The following conodonts were found in the limestones: *Oulodus* cf. *elegans detortus* (Walliser), *Oulodus* cf. *elegans elegans* (Walliser), *Ozarkodina* cf. *confluens* (Branson et Mehl), common in the Przhidolian stage, the conodontic zone detorta. Organogenic-detrital and biohermous bryozoan limestones with intercalations of clayey and oolitic limestones are more developed (pack 5). In organogenic-clastic limestones, the Upper-Przhidolian conodonts were encountered: *Oulodus* cf. *elegans detortus* (Walliser), *O.* cf. *elegans elegans* (Walliser), *Ozarkodina* aff. *nasuta* (Viira), *Oz.* cf. *denticulata* (Viira), *Oz.* cf. *siluricus (*Branson et Mehl), *Oz.* cf. *swetlanae* (Mashkova). The cyclite ends with dolomites dense massive, alternating with dolomite clayey thin-layered (pack 6), the formation of which took place in the lagoon environment.

In the section of well B, Silurian deposits are represented by two sedimentation cyclites. At the base of the first cyclite (packs 1-6) mudstones lie, which are replaced by clayey limestones with argillite interlayers (pack 1). The latter in turn overlap with limestones unevenly-clayey micro-grained, nodular-layered (packs 2,3). In the limestones of packs 1 and 3, conodonts of the Upper Silurian *Coryssognathus* aff. *dubius* (Rhodes), *Ozarkodina* cf. *confluens* (Branson et Mehl), *Oz.* cf. *denticulata* (Viira) are found. Cyclite is completed with clayey dolomite that is not clearly-layered, porous, porous-cavernous, with areas of relic organogenic structure (packs 4-6). The porous-cavernous dolomites are characterized by oil saturation.

The second cyclite is represented by packs 7-9. The lower part of it is composed of interbedded mudstones and clayey dolomites (pack 7). The middle part (pack 8) is composed of dolomites micro-grained and cloddy, unevenly clayey, in places with a relic organogenic structure. In the upper part of the cyclite there are dolomites porous, porous-cavernous, oil saturation is noted (pack 9).

Lower Devonian. Lokhkovian stage. Ovinparmian horizon. In the well A, three cyclites are distinguished in the deposits of the Ovinparmian horizon (Fig. 2).

Packs 7-10 are included in the first cyclite. It begins with basal conglomerates (pack 7). In the debris there are conodonts of the Grebenskian horizon of the Upper Silurian: *Oulodus* cf. *siluricus* (Branson et Mehl), *Ozarkodina* sp., *Panderodus* sp., *Wurmiella* sp. In addition to the large carbonate debris, clastic and argillaceous material is present in the rocks that came from erosion of rocks from the adjacent land. On the conglomerates there are mudstones (pack 8), which are replaced by limestones clotted, cloddy, clayey (pack 9).

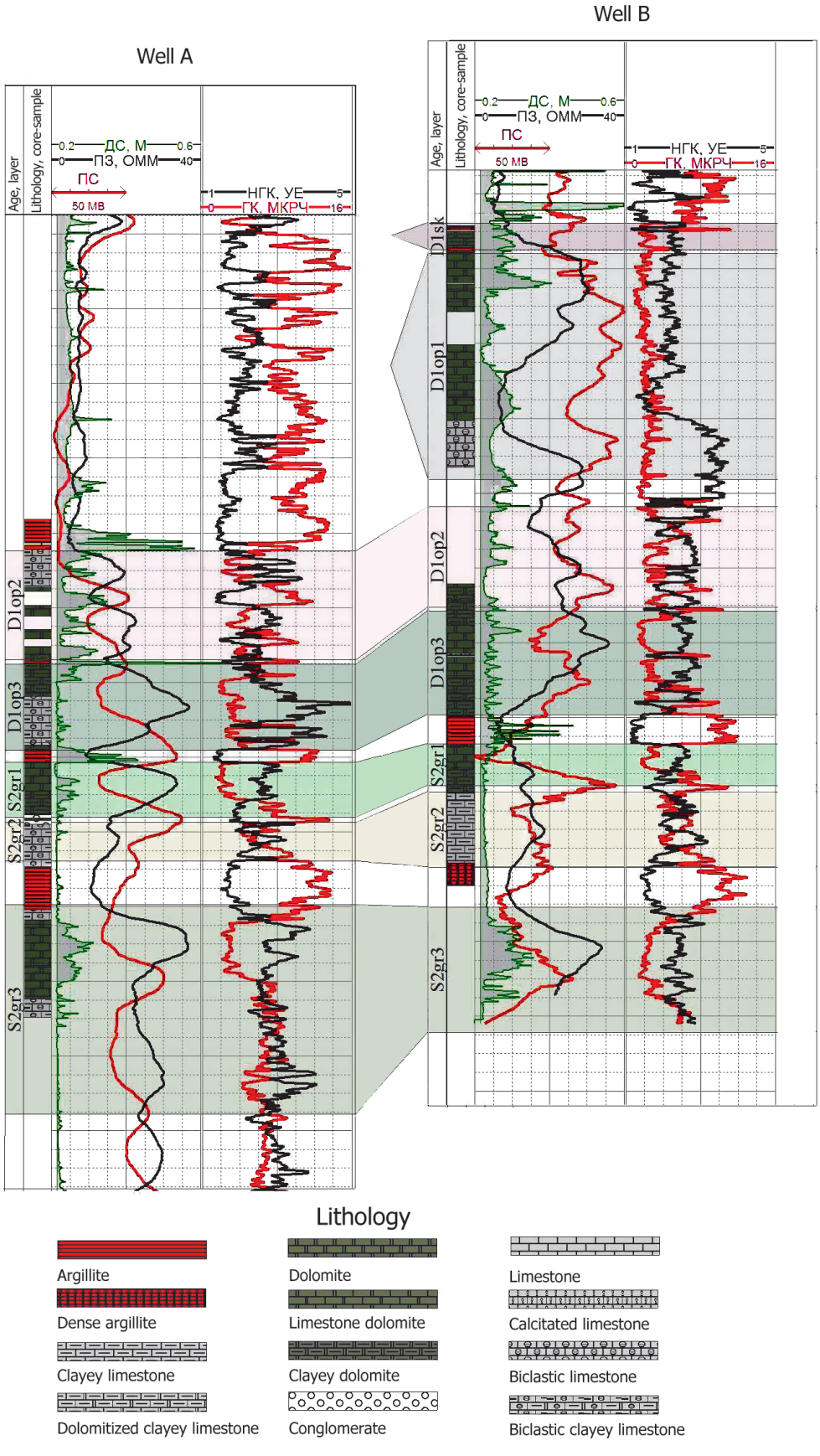

Fig. 1. Correlation scheme for wells A and B

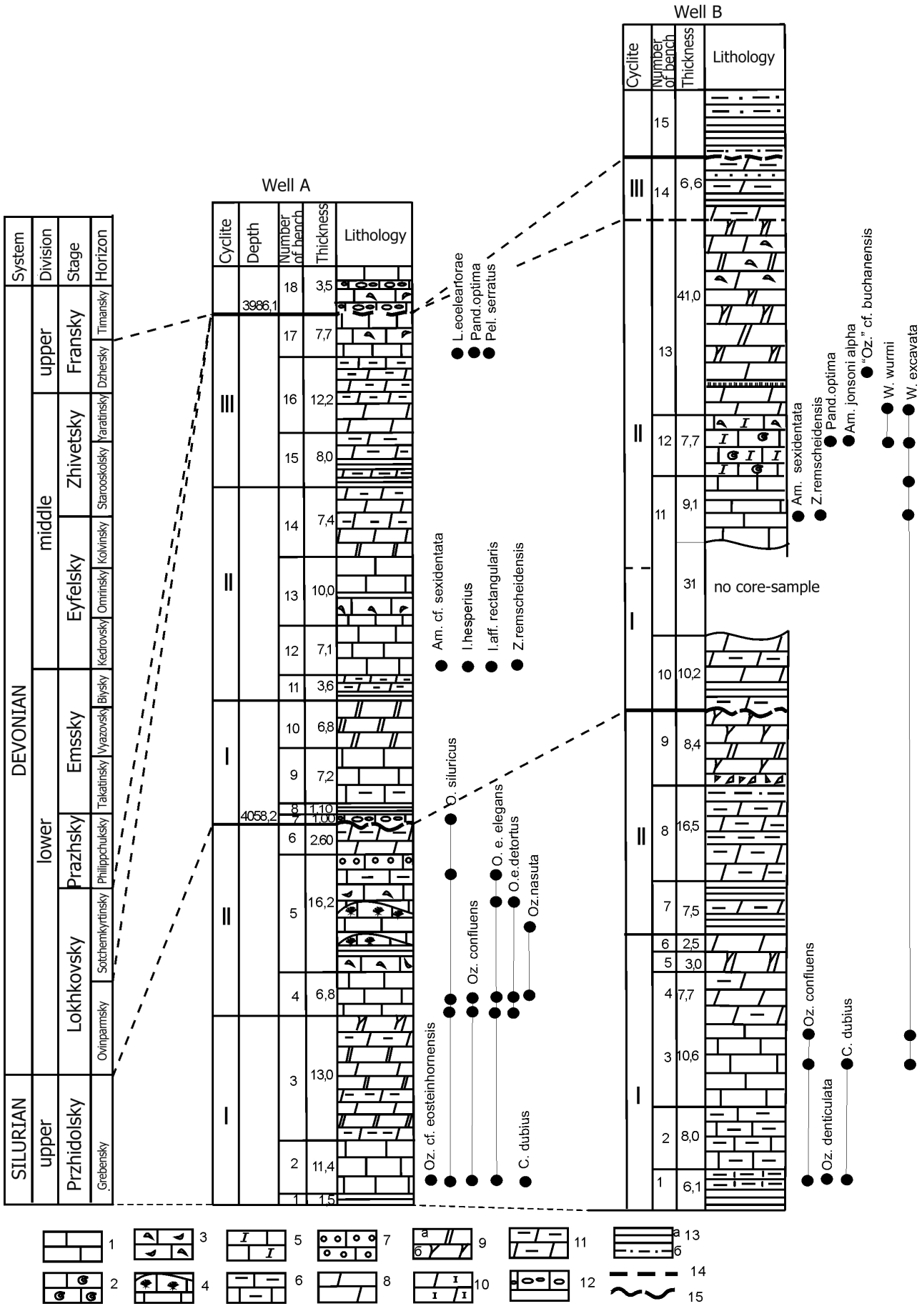

Fig. 2. Correlation of geological sections along wells A and B. Conodont distribution in sections. 1-6 – limestones: 1 – layered, 2 – organogenic, 3 – bioclastic, 4 – biohermic, 5 – dolomite, 6 – clayey; 7 – oolitic; 8-11 – dolomites: 8 – dense, 9a – porous, 9b – cavernous, 10 – calcareous, 11 – clayey; 12 – conglomerates, 13 – a) mudstones, b) siltstones, 14-15 – assumed boundaries: 14 – conformable, 15 – non-conformable.

In limestones, there are structures of landslides, which allow us to assume their formation in shallow-water conditions on the slopes of organogenic structures. Cylite is completed by porous dolomites with significant oil saturation. The thickness of the cyclite is 16.1 m.

The second cyclite contains packs 11-14. Clay-carbonate rocks are laid at its basis (11). They overlap limestones nodular-layered (pacl 12) with conodonts *Icriodus* cf. *hesperius* (Klapper et Murphy), *Icriodus* aff. (Branson et Mehl), *Panderodus unicostatus* (Branson et Mehl), *Zieglerodina remscheidensis remscheidensis* (Ziegler), characteristic of the Lower Lokhkovian of the Lower Devonian. Above the section, limestones are microgranular with interlayers of bioclastic (pack 13). The upper part of the cyclite is represented by alternating dolomites, porous, dense and clay (pack 14), with single interbeds of dolomites with relic biogermic algal texture. The thickness of the second cyclite is 34.0 m.

The third cyclite is incomplete, it includes packs 15-17. The lower part of it is composed of interbedded mudstones and clayey dolomites (pack 15). The upper layers (pack 16) are represented by dolomites as nodular-layered and clayey, ending with clayey limestones interbedded with limestone nodular-layered. In the latter, conodonts of *Amydrotaxis* sp., *Lanea* cf. *eoeleanorae* Murphy et Valenzuela-Ríos, *Pandorinellina optima* (Moskalenko), *Pelekysgnathus* cf. *serratus Jentzsch* are found, common in the Middle Lokhkovian of the Lower Devonian.

The limestones of the Middle Lokhkovian are covered by a pack of intermingling limestone conglomerates and limestones with organogenic detritus, 1.35 m thick. They contain a pack of red-colored terrigenous-carbonate rocks of the Timanian horizon.

In the well B, three cyclites are determined in the Lower Devonian sediments, (Fig. 2). The section of the first cyclite is characterized by a core in an incomplete volume. There is a core of only the lower element of the cyclite. It is represented by dolomites, microgranular dense slightly calcareous, unevenly clayey, with thin interlayers of dark gray clay material. The fragments of the recrystallized shell fauna (pack 10) are found in some places. The second cyclite includes packs 11-13. Pack 11 is composed of limestones microgranular, dense with fragments of shell fauna. As a result of leaching, which occurred along organic residues, a thin porosity is observed. Conodonts *Amodrotaxis* cf. *sexidentata* Murphy et Matti, *Oulodus* sp., *Pelekysgnathus* sp., *Zieglerodina* cf. *remscheidensis* (Ziegler) have been found in limestones, characteristic for the upper part of the Lower Lokhkovian. The upper pack 12 is represented by organogenic limestones. In them conodonts of the Middle Lokhkovian *Amydrotaxis* cf. *jonsoni* (Klapper) *morphotype alpha* Klapper et Murphy, *Pandorinellina* cf. *optima* (Moskalenko) are found. In the next pack 13 – dolomites are unevenly oil-saturated, fine-grained, porous-cavernous with lens-like inclusions of sulfates; silicification is observed. In the fine-grained dolomites, rare conodonts are represented by *Wurmiella wurmi* (Bischoff et Sannemann), and *'Ozarkodina'* cf. *buchanensis* (Philip), *Oulodus* sp. The species '*Ozarkodina' buchanensis* is widespread in the Upper Lokhovian deposits of the Lower Devonian of the Southern Tien-Shan (Bardashev, Ziegler, 1992). The third cyclite completes the Lower Devonian section. It is represented only by the first element of the cyclite, which is formed by dolomite clayey with thin interlayers of mudstone (pack 14).

Taking into account the lithological characteristics of the pack 14 (well B), and also taking into account the findings of the Upper Lokhkovian conodonts *'Ozarkodina' buchanensis* in the pack 13, we can assume the presence of sediments of the lower stratum of the Sochkyrtinskian horizon in the section of well B. This assumption is confirmed in the interpretation results of geophysical data (Fig. 1). The red-colored terrigenous rocks of the Timanian-Sargaevian horizon of the Frasnian stage of the Upper Devonian lie above.

Biostratigraphic dismemberment of well sections by conodonts

Distribution of conodonts in the Silurian-Lower Devonian section of wells A and B is extremely uneven. It largely depends on the facial composition of the rocks. The conditions for the formation of the Silurian and Lower Devonian deposits in the epicontinental Timan-Pechora paleobasin varied from the lagoon to the lower sublittoral of the high sea (Taninskaya, 2010). Changes in sedimentation environments were controlled by sea level fluctuations. The main finds of conodonts are made in layered limestones formed in the conditions of the lower sublittoral. Conodonts are not found in clayey rocks and porous dolomites. The taxonomic diversity of conodonts is small. But they are represented by stratigraphically important species, allowing the dismemberment of the section and its correlation with the standard conodont scale.

Biostratigraphic dismemberment was performed according to the section of the most representative well A and supplemented with materials obtained from well B.

In well A there are biostratigraphic subdivisions in the rank of layers with fauna containing species-indices of the standard conodont scale.

In the Upper Silurian sediments, the following biostratigraphic sequence is established:

Layers with *Ozarkodina* cf. *eosteinhornensis* (Walliser) respond to pack 2. Along with the nominal species in the conodont complex, *Coryssognathus* aff. *dubius* (Rhodes), *Oulodus (= Delotaxis)* cf. *elegans* (Walliser), *Ozarkodina* aff. *cornidentata*

(Branson et Mehl) are found. Species *Ozarkodina* cf. *eosteinhornensis* (Walliser) is a zonal standard conodont zone of the eosteinhornensis of the Przhidolian stage of the Upper Silurian (Melchin et al., 2012).

Layers with *Oulodus* cf. *elegans detortus* (Walliser) are highlighted in packs 4-5. *Oulodus* cf. *elegans* (Walliser), *Ozarkodina* cf. *confluens* (Branson et Mehl), *O.* aff. *nasuta* (Viira), *Oz.* cf. *denticulata* (Viira), *Oz.* cf. *swetlanae* (Mashkova) are also found here. The lower boundary of the layers is determined by the appearance of *O. e. detortus*, a zonal species of the detortus zone – the upper conodont zone of the Przidololian stage of the Upper Silurian (Melchin et al., 2012).

In zone B, zonal species of *Ozarkodina eosteinhornensis*, *Oulodus elegans detortus* have not been identified. But the presence of typical Silurian species *Ozarkodina* cf. *confluens* and *Coryssognathus* aff. *dubius* in a section and features of its structure allow us to make a comparison with Przhidolian deposits of well A.

The Lower Devonian sequence includes:

Layers with *Icriodus hesperius* (Klapper et Murphy), *Icriodus* aff. *rectangularis* (Carls et Gandl) are allocated in pack 12. In the conodonts complex, *Zieglerodina remschedensis* (Ziegler) and elements of *Amydrotaxis* cf. *sexidentata* Murphy et Matti are also present. Finds here of the early species of *Icriodus* define the lower reaches of the Lokhkovian stage of the Lower Devonian. *Icriodus hesperius* is a zonal species of the conodont zone of the same name, which is the lowest zone of the Lower Lokhkovian of the Lower Devonian (Becker et al., 2012). Types of *Icriodus* aff. *rectangularis* (Carls et Gandl) and *Amydrotaxis* cf. *sexidentata* Murphy and Matti appear somewhat later at the end of the I. hesperius zone. The joint finding of these taxa shows that the given interval of the section is not the basis of the Devonian. The layers are compared with the upper part of the hesperius zone of the Lower Lokhkovian of the Lower Devonian. A complex of conodonts with *Amydrotaxis* cf. *sexidentata* Murphy et Matti, *Zieglerodina remschedensis* (Ziegler) was found in the well B in the pack 11 (Fig. 2), which can be compared with the upper part of the zone hesperius – the woschmidti zone of the Lower Lokhkovian.

Layers with *Lanea* cf. *eoeleanorae, Pandorinellina optima* are identified in the pack 17. The identified cosmopolitan conodonts, their presence in the complex, determines the assignment of these layers to the Middle Lokhkovian of the Lower Devonian (the conodont zones of the omoalpha-eleanorae of the standard scale). Based on the conodont data, the volume of the Lower Devonian in the well A corresponds to the Lower-Middle Lokhkovian. In the well B, Middle Lokhkovian beds are characterized by the species *Amydrotaxis* cf. *jonsoni* (Klapper), *alpha morphotype* Klapper et Murphy, *Pandorinellina* cf. *optima* (Moskalenko). Species have a wide geographical distribution and are characteristic of the Middle Lokhkovian of the Lower Devonian. In the section of the well, an evolutionary sequence of species of Amydrotaxis is observed (Murphy, Matti, 1982).

In the well B, younger layers with *'Ozarkodina'* cf. *buchanensis* (Philip). This species was encountered at the top of the Middle and Upper Lokhov formations of the Shishkat section in the Southern Tien Shan (Bardashev, Ziegler, 1992). The Lower Devonian deposits cover the red-colored terrigenous deposits of the Upper Devonian.

Characteristics of the Silurian-Lower Devonian boundary

In accordance with the developed models of sedimentogenesis for the Late Silurian - Early Devonian time, the Silurian-Lower Devonian boundary within the Bolshezemelsky Arch is of a transgressive nature. A sharp drop in sea level at the end of Przhidolian time led to a partial erosion of the deposits of the Przhidolian stage, expressed in the development of erosion surfaces in the dolomites, a reduction in their capacity. The beginning of the transgressive stage is reflected in the formation of dark-colored clay rocks at the base of the Lower Devonian deposits; sometimes basal conglomerates are noted (Yur'eva, Valiukevichus, 2014; Taninskaya, 2010).

Since the sections of the wells do not have a layered faunistic characteristic, the boundary is established with some degree of conventionality. Lithologically, it is expressed by a sharp change in the porous, clayey and cavernous dolomites lying in the roof of the Grebenskian horizon, dark-colored clayey rocks at the base of the lower Devonian, sometimes with basal conglomerates, as in well A. Biostratigraphically, the boundary is characterized by the disappearance of characteristic Silurian fauna species and the appearance of the Lower Devonian conodontic fauna in overlying layers.

Conclusion

As a result of the conducted studies, it was established that the Upper Silurian-Lower Devonian and Upper Devonian structural complexes participating in the section of wells A and B are separated by a surface of deep erosion non-conformity covering the interval from the Praghian stage of the Lower Devonian to the Djierian horizon of the Frasnian stage of the Upper Devonian inclusively.

In sections of the Grebenskian horizon of the Przhidolian Stage of the Upper Silurian and the Ovinparmian horizon of the Lokhovian Stage of the Lower Devonian, a conodont sequence is established in the wells, comparable to the standard conodont scale. Two biological subdivisions with layers of fauna in the Grebenskian horizon and two in the Ovinnparmian horizon were identified.

The Silurian-Devonian boundary, discovered by the investigated wells, has a transgressive character, expressed by a sharp change in porous and cavernous dolomites by argillites and clay-carbonate rocks. In the well A at the level of the Silurian-Lower Devonian boundary, there is a layer of basal conglomerates.

The deposits of the Upper Silurian, the Lower Devonian, are cyclical. The presence of reservoir rocks - porous and porous-cavernous dolomites formed during regression, screened by layers of impenetrable clay rocks formed in transgressive stages, creates favorable conditions for the accumulation of oil.

Acknowledgements

The authors are grateful to the O.V. Artyushkova, Head of the Paleozoic Stratigraphy Laboratory of the Institute of Geology, Ufa Federal Research center of RAS, for critical comments and helpful advice when writing an article. The authors express their gratitude to the reviewer for useful critical comments.

When writing the article, the results of studies conducted on the theme of state contract No. 022-2014-0003 were additionally used.

References

Bardashev I.A. and Ziegler W. (1992). Conodont biostratigraphy of Lower Devonian Deposits of the Shihskat section (Southern Tian-Shan, Middle Asia). *Courier Forschungsinstitut Senckenberg,* 154, pp. 1-29.

Becker R.T., Gradstein F.M. and Hammer O. (2012). Devonian Period. In: Geologic Time Scale 2012. Gradstein, F.M., Ogg, J.G., Schmitz, M.D. and Ogg, G.M. (eds.). *Amsterdam: Elsevier*, Vol. 1, Chapter 20, pp. 525-558.

Melchin M.I., Sadler P.M. and Cramar B.D. (2012). Silurian Period. In: Geologic Time Scale 2012. Gradstein, F.M., Ogg, J.G., Schmitz, M.D. and Ogg, G.M. (eds.). *Amsterdam: Elsevier*, Vol. 1, Chapter 20, pp. 489-523.

Murphy M.A. and Matti J.G. (1982). Lower Devonian conodonts (hesperius-kindlei Zones), Central Nevada. University of California publications in Geological Sciences, V. 123, 83 p.

Reshenie Mezhvedomstvennogo regional'nogo stratigraficheskogo soveshchaniya po srednemu i verkhnemu paleozoyu Russkoi platformy [Decision of the Interdepartmental Regional Stratigraphic Meeting on the Middle and Upper Paleozoic of the Russian Platform]. (1990). Leningrad: VSEGEI, 60 p. (In Russ.)

Taninskaya N.V. (2010). Sedimentologicheskie kriterii kollektorov v sredneordoviksko-nizhnedevonskikh otlozheniyakh Timano-Pechorskoi provintsii [Sedimentological criteria of reservoirs in the Middle Ordovician-Lower Devonian sediments of the Timan-Pechora province]. *Neftegazovaya geologiya. Teoriya i praktika = Oil and gas geology. Theory and practice*, 5(4), pp. 1-28. (In Russ.)

Yur'eva Z.P., Valiukevichus Iyu. (2014). Nizhnedevonskaya karbonatnaya klinoforma Khoreiverskoi vpadiny Timano-Severoural'skogo regiona [The Lower Devonian carbonate clinoform of the Khoreyver depression in the Timan-Severouralsk region]. *Litosfera = The Lithosphere*, 2, pp. 26-38. (In Russ.)

About the Authors

Tatyana M. Mavrinskaya – Researcher of the Paleozoic Stratigraphy Laboratory, Institute of Geology of Ufa Scientific Center of the Russian Academy of Sciences

16/2 K. Marx str., Ufa, 450077, Russian Federation

Elena N. Savelyeva – PhD (Geology and Mineralogy), Head of the Lithology Laboratory, BashNIPIneft LLC

86/1 Lenina str., Ufa, 450006, Russian Federation

E-mail: savelevaen@bashneft.ru

Kirill D. Shumatbaev – Deputy Head of the Well Log Interpretation Department, BashNIPIneft LLC

86/1 Lenina str., Ufa, 450006, Russian Federation

Manuscript received 9 April 2018;
Accepted 10 June 2018; Published 30 June 2018

ORIGINAL RESEARCH ARTICLE

DOI: https://doi.org/10.18599/grs.2018.2.88-101

Geological structure features of Menzelinsky, Timerovsky and Olginsky fields of the Republic of Tatarstan as a result of their genetic nature

N.V. Nefyodov[1], V.B. Karpov[2], Yu.M. Arefiev[3], A.V. Kalmykov[4], G.A. Nikiforov[5]*

[1]*TatRITEKneft, territorial branch of RITEK JSC, Nurlat, Russian Federation*

[2]*RITEK JSC, Moscow, Russian Federation*

[3]*Institute for Problems of Ecology and Subsoil Use of Tatarstan Academy of Sciences, Kazan, Russian Federation*

[4]*NPP Cherny klyuch LLC, Kazan, Russian Federation*

[5]*Institute of Mechanics and Engineering, FRC Kazan Science Center of the Russian Academy of Sciences, Kazan, Russian Federation*

Abstract. The Menzelinsky, Timerovsky and Olginsky fields are located in the northeast of the Republic of Tatarstan and are associated with uplifts, sharply pronounced along the Tulskian surface of the Lower Carboniferous. With a small area of uplifts (1.5-2.2 km across), they are distinguished by a considerable (220-380 m) height and steep wings (up to 40°) of the carbonate rock array overlapped by the Radaevskian-Tulskian terrigenous strata. The carbonate array is represented by deposits of the Tournaisian-Famennian age on the arches of uplifts and by Famennian deposits on their wings. It is accepted to classify such carbonate structures as frameless reefs formed on local seabed areas with a combination of specific conditions for their continuous growth. In the opinion of the authors of the present article, characterized and similar uplifts were formed due to erosion-karst processes that took place on the Tournaisian continental land after the regression of the Tournaisian Sea in the east of the Russian Platform. Erosion and karst processed the limestone paleosurface of the continent during the entire Kosvinian time. As a result of the Late Radaevskian-Bobrikovian cycle of marine transgression, the entire Tournaisian-Famennian surface was covered by the terrigenous rock strata of Radaevskian-Tulskian on the wings of the uplifts and by Bobrikovian-Tulskian strata – on the arches.

Keywords: uplift, carbonate rocks, terrigenous strata, frameless reefs, erosion, karst, regression, transgression

Recommended citation: Nefyodov N.V., Karpov V.B., Arefiev Yu.M., Kalmykov A.V., Nikiforov G.A. (2018). Geological structure features of Menzelinsky, Timerovsky and Olginsky fields of the Republic of Tatarstan as a result of their genetic nature. *Georesursy = Georesources,* 20(2), pp. 88-101. DOI: https://doi.org/10.18599/grs.2018.2.88-101

The Menzelinsky, Timerovsky and Olginsky fields are located in the northeast of the Republic of Tatarstan. Tectonically, the Menzelinsky and Timerovsky fields are confined to the Aktanysh-Chishminsky trough of the Kama-Kinel Troughs System (KKTS), the Olginsky field is confined to the southeastern slope of the North Tatar arch (Voitovich et al., 1998).

The fields were discovered in the last decade on the uplifts revealed by the seismic survey of CDP 2D and partly 3D on the reflecting Y horizon (the roof of the Tulskian horizon of the Lower Carboniferous). The uplifts have been drilled by exploratory and production wells. Oil production in the fields is carried out from the Tournaisian-Upper Devonian carbonate-bearing reservoir rocks. Oil deposits were also discovered in the Bobrikovian-Tulskian sandstone beds on the arched parts of the uplifts.

* *Corresponding author: Nikolay V. Nefyodov*
E-mail: nnefedov@tatritek.ru

The uplifts, including the stratigraphic and lithologic-facies section of the sedimentary strata on them, and the oil deposits in the Tournaisian-Upper Devonian interval, have characteristic and general structural features that distinguish them from most of the uplifts known in Tatarstan with oil deposits in the Lower Carboniferous rock complex. These features are related to the genetic nature of the characterized uplifts, as well as their position in certain tectonic zones.

With a small area in the plan (1.5-2.2 km across) the uplifts are distinguished by a high altitude along the top of the carbonate rock array: 380 m – West-Yurtovsky (Menzelinsky field), 280 m – Timerovsky and 220 m – South-Izhevsky (Olginsky field).

The dip angles of the uplifts flanks along the Tulskian surface vary from 4˚30’ to 12˚30’, whereas on the roof of the underlying carbonate layer – from 17˚40’ to 40˚30’, that is, the uplifts are multiply steeper.

The cut of the sedimentary strata on all three uplifts is practically the same, and the degree of expression along the top of the Tulskian sediments is somewhat

different. At the South-Izhevsky uplift (the Olginskoye field), the Tulskian surface is located according to well data for abs. mark from -832.0 to -911.0 m (exceeding 79 m), on the Menzelinsky – from -937.0 to -1043.0 m (exceeding 109 m), on Timerovsky – from -968.0 to -1092.0 m (exceeding 124 m). The Tulskian-Bobrikovian terrigenous strata on the Menzelinsky and Timerovsky fields have the same structure and the same thickness – 32 to 99 m at Timerovsky and 34 to 99 m on the Menzelinsky, which indirectly attests to the same conditions for its accumulation (Table 1). At the Olginsky field, the Tulskian-Bobrikovian deposits have a thickness of 24-77 m. The natural increase in the thickness of this rock complex toward the Nizhnekamsk trough is associated with the leveling of the "ancient" geomorphological depression enhanced by the erosion-karst processes in the post-Tournaisian time, the terrigenous strata formed as a result of the Radaevskian-Bobrikovian marine transgression. The thickness of the Radaevskian clay deposits in the Menzelinsky and Timerovsky fields is the same – 17-146 m and 14-148 m, respectively. On the Olginsky field it is less – 12-78 m. Radaevskian clayey stratum lies on characteristic formations according to logging data, representing frequent interbedding of carbonate rocks and clays. The thickness of the interlayers varies within 0.6-2.0 m. When comparing the sections of neighboring wells, individual interlayers do not correlate with each other, although the overall shape of these formations remains more or less constant, and the upper and lower boundaries are fairly distinct (Fig. 1-3).

The upper boundary, corresponding to a change in the clay-carbonate strata to clayey Radaevskian stratum, is practically unambiguous on logs. The lower boundary, corresponding to the change in the clay-carbonate stratum of interlayering on the Carbonate rocks of the Tournaisian-Famennian age in the arched wells and the Famennian ones – in the rest (and most of them), is not clear in all wells (Fig. 1-3). This stratum of interbedding, in our opinion, is a kind of weathering crust of the Tournaisian continent, which was eroded and karsted into the Kosvinskian (Elkhovskian) time, is a kind of foreslope. The thickness of the foreslope is not constant: it is smaller in the arched wells (6-13 m) and increases up to 135 m in the Timerovskian uplift area in the well, which is hypsometrically lower than the rest on the roof of the Tulskian sediments.

On the profile through the Menzelinsky and Timerovsky fields (Fig. 4), the maximum thickness of the foreslope is confined to the deflection between the uplifts. In individual wells, there is no "foreslope": at the Menzelinskoye field – in well No. 898-2, Timerovsky field – in wells Nos. 843, 2869; Olginsky field – in wells Nos. 2411, 2433.

The formation of the foreslope lies on different stratigraphic subdivisions of the carbonate sequence. In the arched wells – No. 895, 895D of Menzelinsky, No. 2802 of Timerovsky, No. 2411, 2418, 2419 of the Olginsky field – the trail covers the Tournaisian limestones, in the other wells – Zavolzhskian, and the lowest in the structures – the Dankovo-Lebedyanskian ones. The thickness of the Tournaisian deposits preserved from erosion varies from 10 m at the Olginsky field to 27 m at the Timerovsky field. In the well No. 2411 of Olginsky field, the Tournaisian interval has a thickness of 50 m and is represented by all horizons of the stage, whereas in the remaining wells that have opened the Tournaisian sediments, the latter are represented by the Malevskian-Upinskian strata (Fig. 5).

The roof of Zavolzhskian overhorizon, which is the supporting surface in the analysis of the Tournaisian-Famennian carbonate deposits, is recorded by the characteristic type of curves of the resistivity, spontaneous polarization, radioactivity logs. It is noteworthy that the thickness from the roof of Tulskian horizon to the roof of the Zavolzhskian overhorizon is 75 m at the Menzelinsky field, 78 m at the Timerovsky field and 80 m at the Olginsky field, i.e. is a value of the same order with thicknesses at other deposits of the Republic of Tatarstan (Zyuzeevsky, Tavelsky, etc.). These facts largely support the thesis of the inheritance of the Tulskian surface from the Zavolzhskian (and from the Tournaisian paleosurface) on the entire eastern part of the Republic of Tatarstan and the erosion-karst nature of the modern Tournaisian (or Tournaisian-Famennian in the troughs of the KKTS) of the relief (Kharitonov et al., 2015).

Uplift (field)	Thickness, m				
	C1tl+C1bb	C1rd	C1t	From top C1tl to D3zv	Weathering crust (foreslope)
1	2	3	4	5	6
West-Yurtovsky (Menzelensky)	34-99	17-146	12-14	75	7-67
Timerovsky	32-99	14-148	27	78	6-135
South-Izhevsky (Oginsky)	24-77	12-78	10-26	80	13-42

Table 1. Thickness of stratigraphic complexes of the Lower Carboniferous

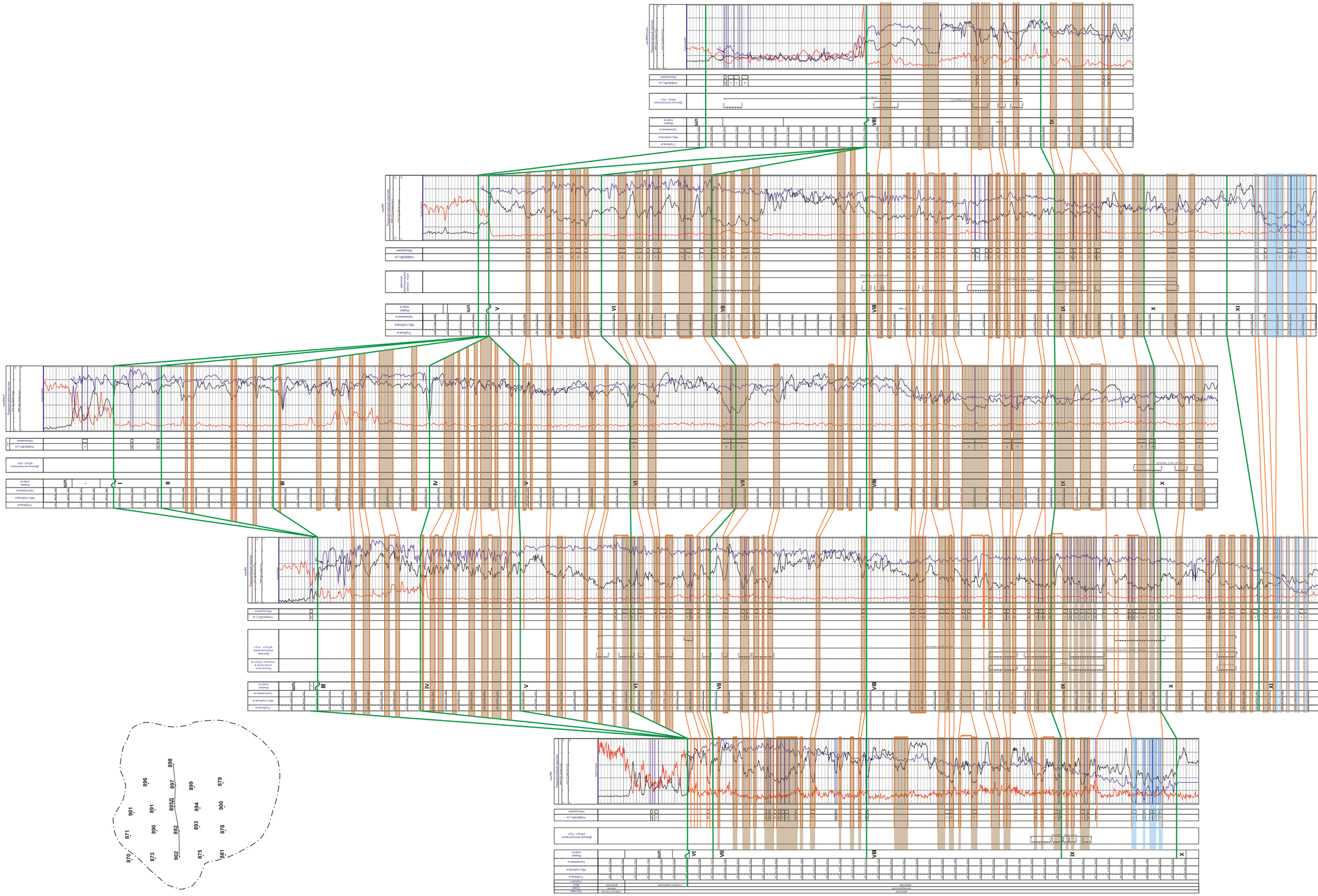

Fig. 1. Correlation scheme of the Lower Carboniferous-Upper Devonian sediments for the wells of the Menzelinsky field of the Republic of Tatarstan

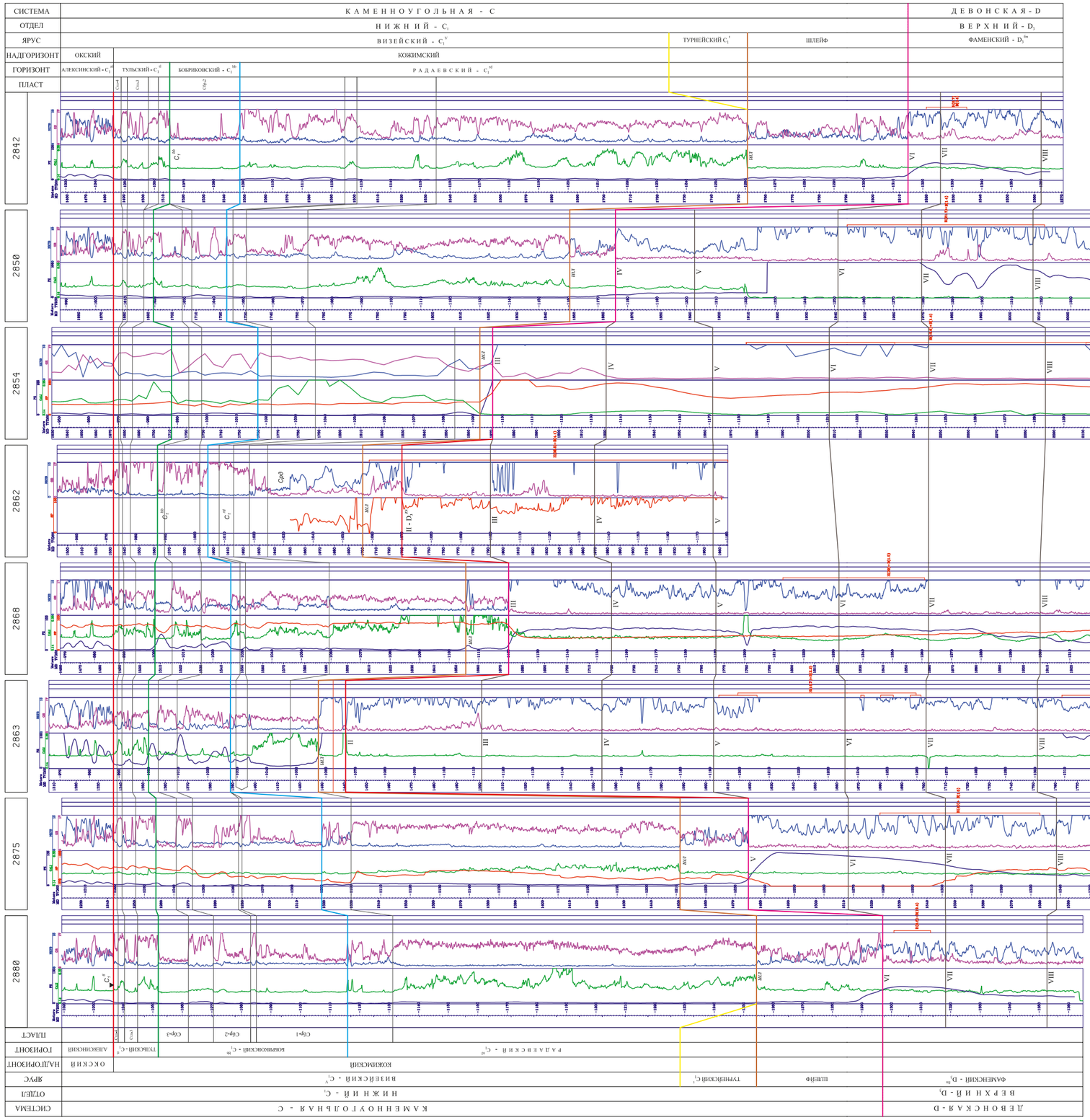

Fig. 2. Correlation scheme of the Lower Carboniferous-Upper Devonian sediments for the wells of the Timerovsky field of the Republic of Tatarstan

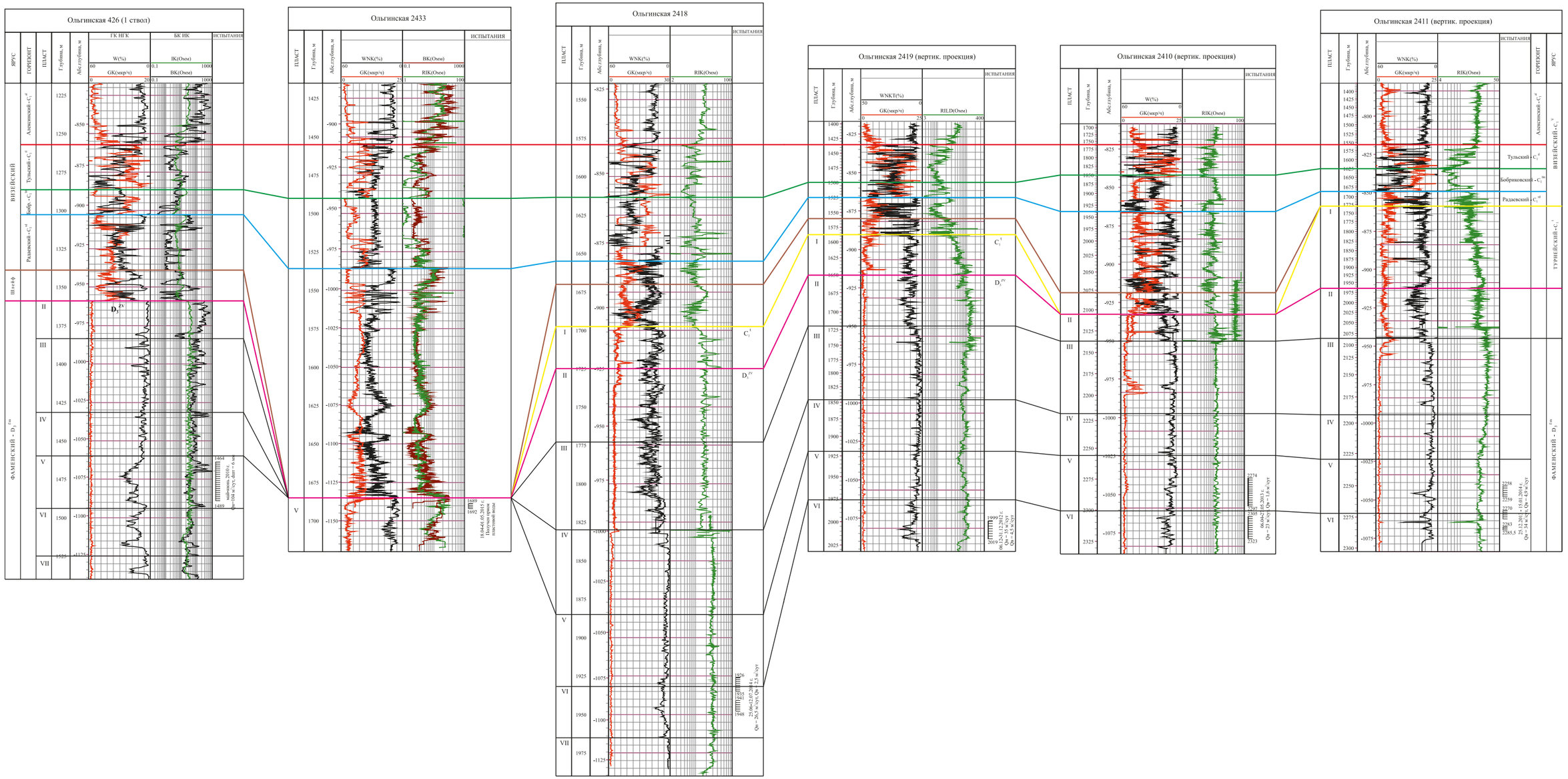

Fig. 3. Correlation scheme of the Lower Carboniferous-Upper Devonian sediments for the wells of the Olginsky field of the Republic of Tatarstan

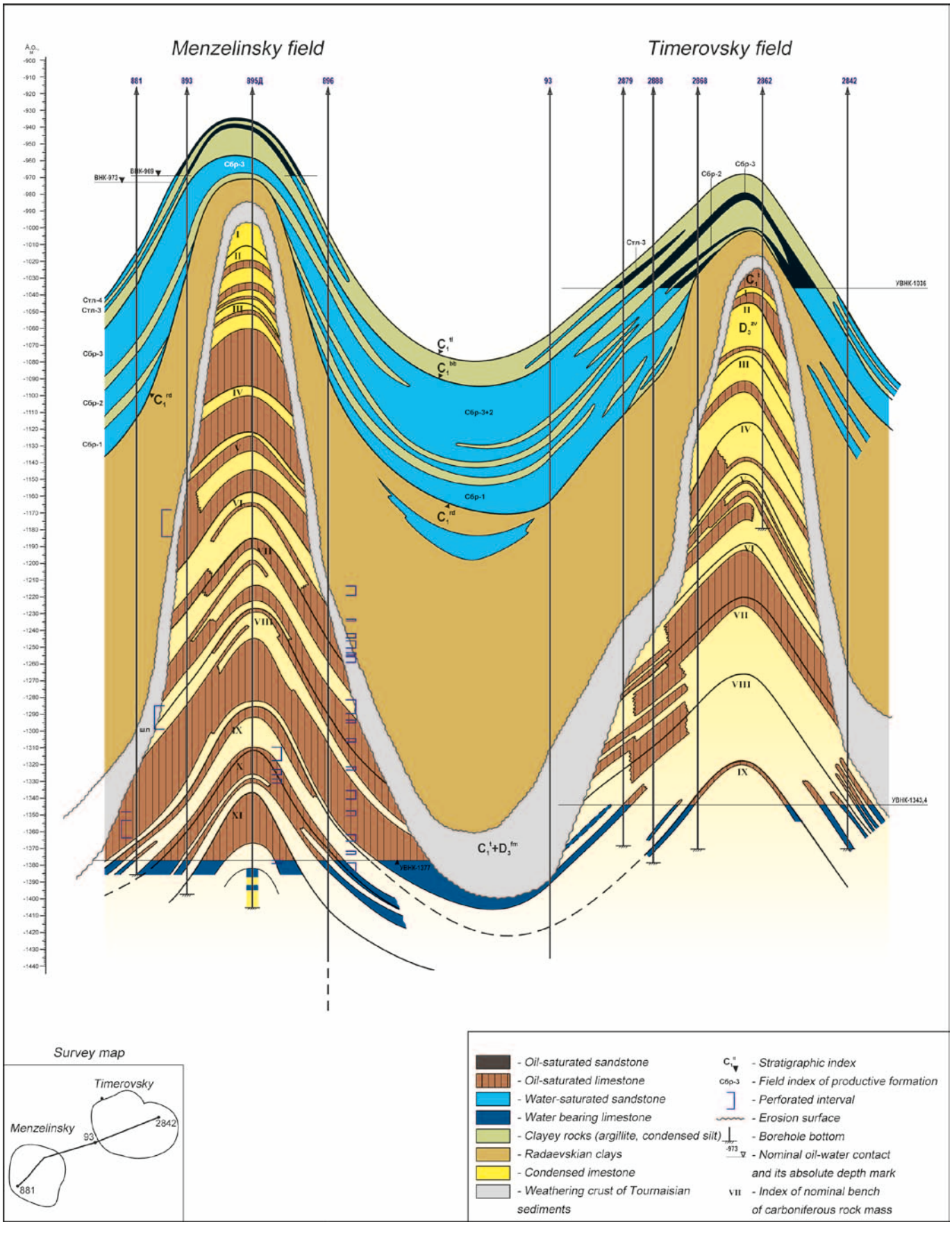

Fig. 4. Schematic geological scheme of the Lower Carboniferous-Upper Devonian sediments for the wells of the Menzelinsky and Timerovsky fields

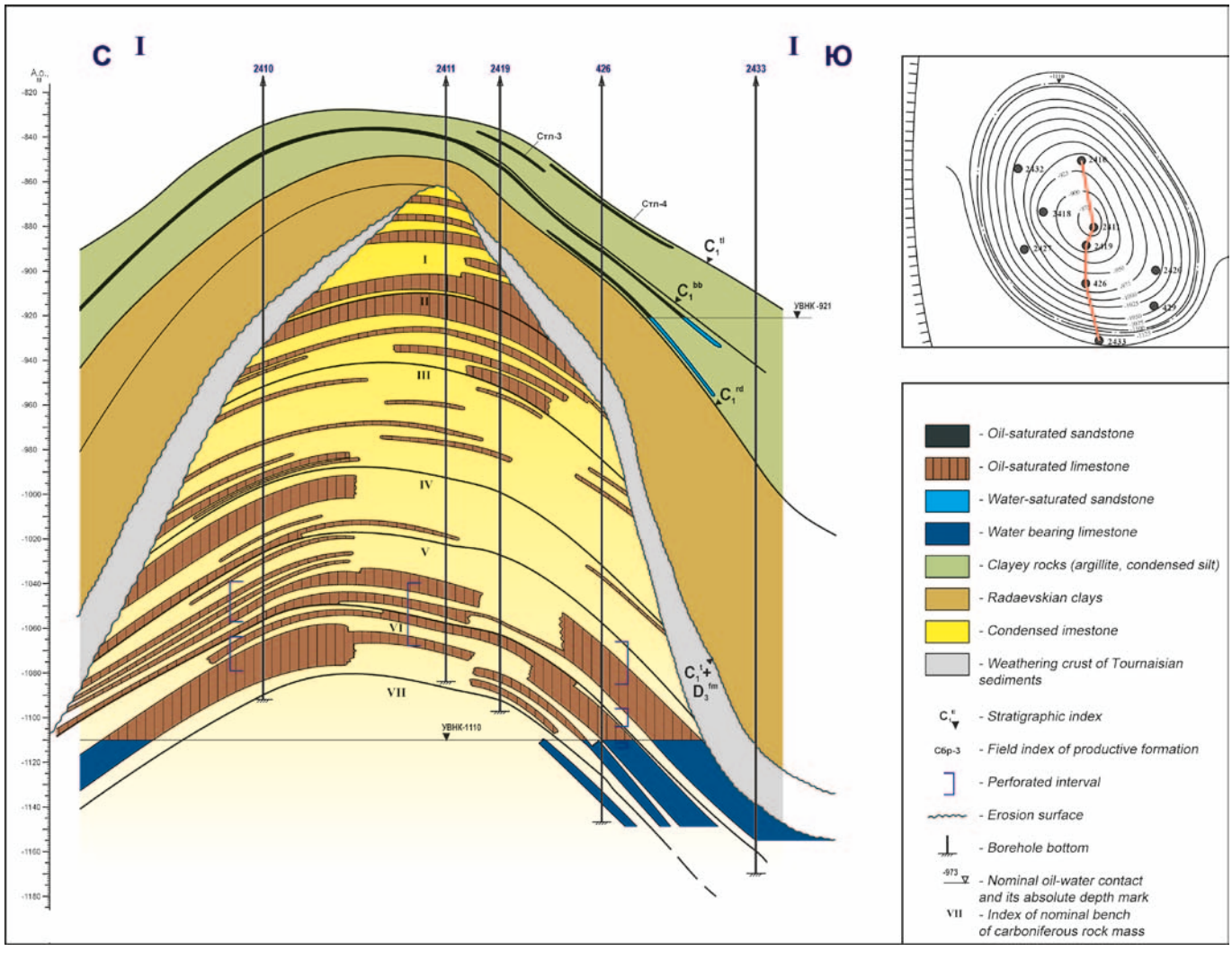

Fig. 5. Schematic geological scheme of the Lower Carboniferous-Upper Devonian sediments for the wells of the Olginsky field

Their modern conical shape and relatively steep slopes are due to the processes of erosion and karst, which continued throughout the Kosvinian time, and not to local layering of organic remains on a limited area. The cores of the reef-building structures are confined, apparently, to the thickness of the over-Rechitskian age. The roof of the Middle Fammenian is not lithologically expressed, therefore, it is impossible to carry it out with sufficient confidence in the curves of the apparent resistivity, radioactivity and other logs. Since there was no break in the sedimentation at the boundary of the Late-Middle-Famenian times, the Dankovian-Lebedyanskian deposits conformably envelope to the Slovetskian-Yeletskian, and the surface of the Zavolzhskian sequence repeats the Dankovian-Lebedian sequence.

Structural forms, similar to the three above described, are traditionally considered to be biohermic structures – reef-building structures successively formed by different-aged cores – Retchitskian-Dankovian-Lebedyanskian, Cherepetskian and Kizelovskian, which have their own structural features (Volkov, 2008; Gubaidullin et al. 1973, Shakirov, 2003; Larochkina, 2013). Carbonate strata of a later age envelop the earlier ones, increasing in thickness on the arch of the structure and decreasing on its wings to minimum values. For theoretical substantiation of the formation of such structures, they were classified, according to V.G. Kuznetsov, as non-framed reefs (Volkov, 2008). The remains of marine organisms – foraminifera, crinoids, bryozoans, solitary corals, various algae – concentrated on a small section of the bottom, overlapping each other and thereby ensuring vertical growth of the reef. Favorable conditions for local prosperity of organic life were created due to the fact that the Menzelinsky, Timerovsky, and Olginsky reefs, for example, were located in the junction zone of the regional Prikamsky and Bakhchsarai faults, mobile tectonically and provided the inflow of heat necessary for the prosperity of organic life from the earth's interior into the sea basin.

Thus, for the appearance of a frameless reef and its continuous growth until the end of the Kizelovskian time, an indispensable combination of several conditions was required, the main ones the lowering of the lower boundary of the photic layer to the level of the bottom

surface due to fluctuations in the sea basin level and the high density of disjunctive dislocations per unit of that area, where the remains of marine organisms accumulated (Volkov, 2008). It should be noted that the distance between the Menzelinsky and Timerovsky reefs is only 2.6 km, although the first of them is confined to the axial zone of the Nizhnekamsk trough, which is part of the CKSP system, and the second – to its internal side zone. These zones according to (Larochkina, 2013; Muslimov et al., 1999) differed by differentiated subvertical movements due to the rise and immersion of the corresponding territories. However, the causes and results of multidirectional motions of the earth's crust at the "junction" of the axial and side parts of the deflection and at such a short distance are not given.

Apparently, the whole strata of rocks, including the crystalline basement, were involved in differentiated and various-amplitude subvertical movements. And since the amplitude of such movements reached several tens of meters, in the sedimentary stratum (the Lower Carboniferous-Devonian), disjunctive dislocations with a displacement of the blocks on either side of these dislocations would inevitably arise. However, traces of similar displacements of the same-aged strata of the Tournaisian-Devonian section in the traversed wells were not recorded either within the troughs of KKTS or outside it.

Even if we suppose the growth of the top of the reef in such a limited space – first cone-shaped, and then more and more steep, then the question arises: how did the hydrodynamic regime of the sea basin and, in a broad sense, the weather and climate conditions of that time affect such underwater structures? The sea currents, the depth of the wave impact zone, including the powerful storms, inevitably had to affect the top of the frameless reef, washing off part of the accumulated non-precipitated rainfall and redepositing them beyond the base of the reef.

The structure of the modern relief of the Tournaisian surface, in our opinion, is determined by two main genetic factors that have manifested themselves in different periods of geological history. The first in time is sedimentary, rock-forming; the second – erosion-karst, rock-destroying and at the same time rock-transforming.

The sedimentation factor created a mass of Tournaisian limestones deposited on the surface of the Zavolzhskian formations under the conditions of the continuity of the Tournaisian sea basin from the Upper Devonian. There were no geological "shocks" and "transformations" at the turn of geological epochs – late Devonian and early Carboniferous – in the vast sea basin that occupied the whole northeast and eastern parts of the Russian platform. In this large space, there was a stable marine regime with a changed hydrochemical situation, which manifested itself in the replacement of compacted dolomitized and gypsum-bearing mainly crystalline and pelitomorphic limestones of the Volga region on structurally and texturally diverse organogenic-detrital and crystalline limestones interbedded with densely compacted dolomitic limestones of Tournaisian age.

A diverse organic life flourished in the Tournaisian sea basin – plankton and bottom (foraminifera, ostracods, pelecypods) organisms, various fish species, attached forms (solitary corals, crinoids, spiriery, etc.) and various plant forms – blue-green, scarlet, tubular algae (phytoplankton) (Antropov, 1972). Sedimented carbonate silt had both chemogenic and organogenic-clastic nature. Their distribution according to the area of the sea bottom was determined by many factors: the unevenness of the bottom relief, the change in the direction and strength of the sea currents, the depth of the waves, the frequency and intensity of the storms and sea currents that led to the tsunami. These factors violated the ideal sequence of sedimentation and often obscured it. Therefore, it is extremely difficult to identify any specific cycles of sedimentation in a lithologically monotonous Tournaisian-Famennian sequence. Significant role was played also by the processes of transformation of originally deposited silt-like sediments – processes of lithogenesis (diagenesis, epigenesis and hypergenesis). They determined partly the variety of structural and textural features of the carbonate section and its stratification (Khisamov et al., 2010).

The second factor – erosion-karst, which included two processes that occurred simultaneously, but with varying intensity. This factor manifested itself after the regression of the Tournaisian sea basin, caused by a large-scale transformation of the Earth's surface on the Russian platform (Igolkina et al., 1977). The consequence of regression was the formation of a vast continental land area, folded from the surface by carbonate muds, to a varying extent, lithotified. Processes of erosion and karst had determined the forms of the relief of the modern Tournaisian surface.

The period of the interruption in sedimentation that began at the end of the turn of the century continued throughout the Elkhovian period and part of the early times. In this segment of geological history, the continental surface began to undergo simultaneously both erosion and karsting. All the basic conditions for karsting were formed (Gvozdetskii, 1954): the presence of a soluble rock – limestone; their permeability, which was determined by the texture-structural features of carbonate silt and resulting fracturing due to dehydration during removal from sea level; active movement of surface waters due to frequent and intense storm currents in hot and humid climates; the aggressiveness of atmospheric water due to the high content of carbon dioxide in the Earth's atmosphere. On the exposed bottom of the Tournaisian Sea, the West-Yurtovsky,

Timerovsky and South-Izhevsky uplifts were allocated in the form of hills, arched parts of which were larger in area than their modern swells.

The intensity of the karst processes that created the modern sculptural appearance of the West-Yurtovsky and Timerovsky uplifts was determined by the position of the latter in the Nizhnekamsk trough of the ancient deposition, which divided the Northern and Southern Tatar arches in the Archaean period of their consolidation. This deflection existed for a very long geological time and was only lightened at the end of the Visean century as a result of the Radaevskian-Tulskian marine transgression. In the geological literature, however, the opinion prevails that the Nizhnekamsk trough, like the whole of the KKTS, is an intraformational deflection located above the monoclinal slope along the top of the terrigenous Devonian and formed as a result of prolonged differentiated and multidirectional movements of its parts – sides and axial region (Larochkina, 2013; Muslimov et al., 1999).

According to our ideas about the time and conditions for the formation of the Nizhnekamsk trough, its severity in the relief of the Tournaisian seabed, which became part of the continental land in the Kosvinian period, contributed to the widespread development of erosion and karst processes on its surface. Frequent and strong rain streams processed slopes of uplifts; temporary river streams, changing their direction and channel and flowing into the deflection, unevenly blurred its sides, dissolving the slightly lithified carbonate rocks and transferring their insoluble residue to the most lowered areas of the relief. They also moved and mixed fragments that accumulated in the slopes of the slopes and formed partly due to the collapse of the cornices of denser and organogenic-detrital limestones on the slopes of the uplifts. The deflections dividing the uplifts went deeper; residual – from dissolution and collapse – the formation of redeposited, changing the places of their accumulations. Naturally, the transferred fragments, the size of which, apparently, could reach several meters, are well recorded on logs of wells. The fragments contained faunal remains, and their structure could be very different. As a result of the Radaevskian transgression, the fragments were mixed with clay material deposited in the basin. If you agree with the opinion of E.B. Grunis (Grunis, 2010) about the instantaneous geological character of the Late Radayevskian transgression, it should be assumed that its force also contributed to the change in the relief forms and the redistribution of carbonate debris along the area and along the vertical.

The erosion-karst processes that occurred on the post-Tournaisian continent created a modern relief of the Tournaisian-Famennian surface, and, secondly, played a decisive role in the formation of the void space of the part of carbonate section that was affected by them. The current thickness of the carbonate deposits of the Tournaisian and Famennian ages is described as a sequence of interbedding of various types of complexly constructed reservoir rocks and dense differences of the same rocks with mutual crossings along the lateral and along the horizontal. Thicknesses and the number of effective and dense interlayers within one local uplift vary from well to well without apparent pattern, although in general the distribution of rock packs containing dense and porous-permeable interlayers is quite confident.

The carbonate layer deposited in the marine basin was characterized by a variety of textural-structural types of rocks and was characterized by primary porosity and permeability, macro- and micro-lamination (Kozina et al., 1973). After the regression of the marine basin, the carbonate, unlithified silt exposed onto the day surface was dehydrated, turned into a "crust" of rocks, which cracked with the formation of numerous and predominantly subvertical cracks. It is believed, however, that for reefgenic structures like the Menzelinsky, Timerovsky and neighboring reefs, the fracture is associated with tectonic processes occurring in the body of the crystalline basement and in the sedimentary layer overlapping the basement (Volkov, 2008; Shakirov, 2003).

The exposed bottom of the regressed Tournaisian Sea was distinguished by a dismembered relief – the presence of different in area and height and relatively shallow uplifts, separated by deflections and depressed portions.

On its surface there were open karst processes, in the thickness of rocks – a closed karst. These processes included both the dissolution of the primary rock and the mechanical action by rain storms. Storm streams removed an insoluble residue from the surface, and high temperatures promoted the warming of rocks from the surface and increased solubility of limestones. The open karst thus denuded the upper part of Kizelian sediments in different depths, depending on the nature of the relief and "purity" of the limestone, as a result of which there are no complete sections of the Tournaisian stage in Tatarstan.

The more contrasted the Tournaisian relief, the more processing it was subjected to from the surface. Greater solubility was possessed by fine-grained and pure limestones of lesser extent – limestone organogenic-detrital and clay (Kozina et al., 1973). As a consequence, protrusions, cornices, steps, niches formed on the slopes of the uplifts. Over time, protrusions and cornices collapsed under the influence of continued dissolution and gravity, and their fragments were transported to the lowered parts of the relief, forming a kind of weathering crust and breccia interlayers, which were taken for the erosion of those deposits on which the breccia interlayers lie.

Those parts of the Tournaisian uplifts had undergone particularly strong processing, that adjoined the slopes,

as rain streams flowed over them, and the surface of the slopes warmed up well. A large role in the underground karst was played by the sedimentary layering of carbonate rocks and the thickness of their various structural differences. This should be taken into account when evaluating the effective thicknesses of wells drilled at one local elevation, since the effective thicknesses in the two adjacent wells can not differ by an order of magnitude if they are due to their appearance to the same process. In the development of Tournaisian (and Tournaisian-Famennian) sediments, the highest oil rates are often observed in wells located on the slope parts of the uplifts, in which the reservoir properties indicators of the productive formation are usually higher (Muslimov et al., 1999).

In the modern tropical countries, positive karst forms of relief are widespread: high and steep remnants in the form of pillars, towers, cones and dome-shaped forms.

Local elevations of the Menzelinsky, Timerovsky and neighboring reef-like structures have a characteristic dome-shaped form. This form seems to be typical for all Tournaisian-Famennian uplifts in the axial zone of the Nizhnekamsk trough and is less common outside its borders. Most of the Tournaisian uplifts have smoother shapes.

In our opinion, the shape and size of modern uplifts in the Nizhnekamsk trough are determined primarily by erosion and karst processes. The significant height of the void-porous reservoir on the uplifts is entirely due to its formation by an underground karst.

Main conclusions

1. The surface of the Tulskian horizon, taken for the reflecting horizon U under seismic constructions, corresponds to the Tournaisian paleosurface, inherited in turn from the Famennian-Zavolzhskian, since there was no break in the sedimentation on the border of the Famennian and Tournaisian centuries.

2. The thickness of rocks enclosed between the roof of the Tulskian horizon of the Visean Stage of the Lower Carboniferous and the roof of the Zavolzhskian overhorizon of the Famenian Stage of the Upper Devonian remains relatively constant (70-80). This means that the thicknesses of the Tournaisian horizon preserved from erosion and karst also vary within a narrow range.

3. The modern surface of the Tournaisian deposits is formed by erosion-karst processes that dominated the Tournaisian continent, formed after the regression of the Tournaisian sea basin in the entire east of the Russian platform.

4. The wide development of karst was facilitated by the combination of the conditions necessary for its manifestation: geological – the presence of a thick layer of permeable and fractured limestones, the duration of the continental break; geomorphological – a dissected surface, inherited from the Famennian, with its positive and negative forms of relief; climatic – humid and warm climate, a large amount of sediments in the form of showers with the formation of temporary water flows and a high content of carbon dioxide in the atmosphere.

5. Surface karst in combination with wind and river erosion created a variety of modern structural forms of the Tournaisian-Famennian surface; The deep (underground) karst formed a hollow-fractured volume of oil and water-containing reservoirs in the Tournaisian and Tournaisian-Famennian strata.

6. The Tournaisian-Famennian relief in most of the territory of the Republic of Tatarstan is blocked by Radaevskian clays containing a spore-pollen complex of Elkhovian appearance.

7. The transgression of the marine basin took place in two stages: in the Late Radaevskian and Radaevskian-Bobrikov time. The established marine regime in the territory of the Republic of Tatarstan is at the beginning of the Tulskian time.

References

Antropov I.A. (1972). Organogennye postroiki devona i rannego karbona tsentral'noi chasti Russkoi platformy i usloviya ikh razvitiya [Organogenic structures of the Devonian and the Early Carboniferous of the central part of the Russian Platform and the conditions for their development]. *Litologiya i paleogeografiya paleozoiskikh otlozhenii Russkoi platform* [Lithology and paleogeography of Paleozoic deposits of the Russian platform]. Moscow: Nauka Publ., pp. 282-291. (In Russ.)

Gvozdetskii N.A. (1954). Karst. Moscow, Geografgiziz, 351 p. (In Russ.)

Grunis E.B. (2010). Novye predstavleniya teorii geologicheskikh protsessov i perspektiv neftegazonosnosti Russkoi platformy [New ideas of the theory of geological processes and prospects of oil and gas potential of the Russian platform]. *Innovatsii i tekhnologii v razrabotke, dobyche i pererabotke nefti i gaza* [Innovations and technologies in development, production and processing of oil and gas], Kazan: Fen, pp. 90-101. (In Russ.)

Gubaidullin. A.A., Al'tmark M.S. O vliyanii pozdnefranskikh organogennykh postroek na paleografiyu famenskogo i turneiskogo basseinov v predelakh yugo-vostoka Tatarii [On the influence of lateorganic organogenic buildings on the paleography of the Famennian and Tournaisian basins within the southeast of Tatarstan]. *Doklady AN SSSR = Proc. of the USSR Academy of Sciences*, 211(4), Moscow, pp.936-938. (In Russ.)

Igolkina N.S., Krivskaya T.Yu. (1977). Dovizeiskii pereryv na Russkoi platform [Dovizeysky break on the Russian platform]. *Sovetskaya geologiya = Soviet geology*, (7), pp.71-78. (In Russ.)

Kharitonov R.R., Aref'ev Yu.M. (2015). Some Features of the Structure of Lower Carboniferous Strata of Zyuzeyevsky Field. *Georesursy = Georesources*, 4(63), Vol.2, pp. 17-24. DOI: http://dx.doi.org/10.18599/grs.63.4.20 (In Russ.)

Khisamov R.S., Gubaidullin A.A., Bazarevskaya V.G., Yudintsev E.A. (2010). Geologiya karbonatnykh slozhno postroennykh kollektorov devona i karbona Tatarstana [Geology of carbonate complex reservoirs of the Devonian and the Carboniferous of Tatarstan. Kazan: Fen, 283 p. (In Russ.)

Kozina E.A., Khairetdinov N.Sh. (1973). Vliyanie veshchestvennogo sostava i struktury karbonatnykh porod na ikh kollektorskuyu kharakteristiku [Influence of the material composition and structure of carbonate rocks on their reservoir characteristics]. *Proc. TatNIPIneft,* Kazan, XXII, pp. 69-74. (In Russ.)

Larochkina I.A. (2013). Kontseptsiya sistemnogo geologicheskogo analiza pri poiskakh i razvedke mestorozhdenii nefti na territorii Tatarstana [The concept of systematic geological analysis in prospecting and exploration of oil fields in the territory of Tatarstan]. Kazan: Fen, 229 p. (In Russ.)

Muslimov R.Kh., Vasyasin G.I., Shakirov A.N., Chendarov V.V. (1999). Geologiya turneiskogo yarusa Tatarstana [Geology of the Tournaisian Stage of Tatarstan]. Kazan: Monitoring, 186 p. (In Russ.)

Shakirov A.N. (2003). Geologicheskie osnovy primeneniya metodov uvelicheniya nefteotdachi v produktivnykh otlozheniyakh paleozoya Tatarstana [Geological foundations of EOR application in productive deposits of Paleozoic of Tatarstan]. St. Petersburg: Nedra, 372 p. (In Russ.)

Voitovich E.D., Gatiyatullin N.S. (1998). Tektonika Tatarstana [Tecktonics of the Tatarstan]. Kazan: Kazan Univer. Publ., 139 p. (In Russ.)

Volkov D.S. (2008). Osobennosti i metody izucheniya geologicheskogo stroeniya verkhnedevonsko-kamennougol'nykh otlozhenii severo-vostoka Respubliki Tatarstan i poisk organogennykh postroek v osevoi zone Kamsko-Kinel'skoi sistemy progibov. *Avtoref. dis. kand. geol.-min. nauk* [Features and methods of studying the geological structure of the Upper Devonian-Carboniferous deposits of the northeast of the Republic of Tatarstan and the search for organogenic structures in the axial zone of the Kamsko-Kinel 's system of deflections. Abstract Cand. Geol.-Min. Sci. Diss.]. Moscow, 26 p. (In Russ.)

About the Authors

Nikolay V. Nefyodov – Director
TatRITEKneft, territorial branch of RITEK JSC
1b Leningradsky str., Nurlat, 423040, Russian Federation
E-mail: nnefedov@tatritek.ru

Valery B. Karpov – Deputy Director General for Field Development – Chief Geologist, RITEK JSC
3 Bolshaya Ordynka, Moscow, 115035, Russian Federation

Yuri M. Arefiev – Senior Reserсher, Laboratory of Geological and Environmental Modeling
Institute for Problems of Ecology and Subsoil Use of Tatarstan Academy of Sciences
28 Daurskaya St., Kazan, 420087, Russian Federation

Alexander V. Kalmykov – Head of the Laboratory of Hydrodynamic Research
NPP Cherny klyuch LLC
1 Akhtyamov str., Kazan, 420021, Russian Federation

Grigory A. Nikiforov – Researcher
Institute of Mechanics and Engineering, FRC Kazan Science Center of the Russian Academy of Sciences
2/31, Lobachevsky St., Kazan, 420111, Russian Federation

Manuscript received 3 April 2018;
Accepted 1 June 2018;
Published 30 June 2018

ORIGINAL RESEARCH ARTICLE

DOI: https://doi.org/10.18599/grs.2018.2.102-107

Definition of the reservoir permeability field according to pressure measurements on wells with the use of spline function

A.V. Elesin[*], *A.Sh. Kadyrova, A.I. Nikiforov*

Institute of Mechanics and Engineering, FRC Kazan Scientific Center of the Russian Academy of Sciences, Kazan, Russian Federation

Abstract. The problem of reservoir permeability identification based on known well pressures under conditions of single-phase fluid filtration is considered in the article. The permeability field is identified in the spline function class from the solution of the inverse coefficient problem for the filtration equation. The problem of identification is reduced to the problem of minimizing the residual function, having the form of a sum of squares of the difference between the pressure values known from measurements at the wells and obtained with the help of a numerical model. Minimization of the residual function is carried out by the Levenberg-Marquardt method. The solutions of model problems of permeability identification for a two-dimensional reservoir, penetrated by a system of production and injection wells, are presented. The calculated permeability fields are close to the true fields. The example of a problem with errors in pressure measurements shows the stability of the solution.

Keywords: permeability identification, spline function, residual function

Recommended citation: Elesin A.V., Kadyrova A.Sh., Nikiforov A.I. (2018). Definition of the reservoir permeability field according to pressure measurements on wells with the use of spline function. *Georesursy = Georesources,* 20(2), pp. 102-107. DOI: https://doi.org/10.18599/grs.2018.2.102-107

Introduction

In solving tasks of single-phase fluid filtration, field of the reservoir permeability must be known. In practice, permeability is usually determined only at individual points of the reservoir by hydrodynamic methods or by the results of core studies. In this paper, the permeability field is identified in the class of spline functions from the solution of the inverse coefficient tasks for the filtration equation. Methods for solving inverse coefficient tasks are divided into explicit and implicit tasks (Sun, 1994). In explicit methods, the values of the parameters are determined from the solution of the nonlinear system of equations (Golubev et al., 1978; Zinoviev, 1984). In this case, the pressure field must be known. If pressure values are known only at the wells, the parameter values are determined only in the wellbore regions.

In implicit methods, iterative procedures are used to determine the values of parameters of the entire reservoir, in which only pressure values are used in wells (Neuman, Carrera, 1986; Khairullin et al., 2006; Elesin et al., 2009; Khairullin et al., 2017). Unlike the proposed approach, the reservoir parameters are represented in the form of piecewise-constant functions.

The use of spline functions is one of the parametrization methods (Sun, 1994), and in this case for the obtained permeability field, no further processing and correction is required in most cases and it can be easily and unambiguously converted to any grid. To solve inverse tasks, in addition to the data needed to solve a direct hydrodynamic task, additional information is used. In the present work, such information is taken to be the bottomhole pressure, which is known along with well production rates. The flow rate is used to solve a direct task for determining the pressure field. Known wellhead pressures are included in the residual function, in the process of minimization of which the field of reservoir permeability is determined. To minimize the residual function, the classical Levenberg-Marquardt method is used. The stability of the solution to the errors in pressure measurements is investigated.

Formulation of the task

Single-phase stationary filtration in a two-dimensional layer is described by the equation (Aziz, Settari, 1982; Basniev et al., 1986):

$$\nabla(\sigma\nabla p) = q, \quad (1)$$

where $\sigma = kh/\mu$ – coefficient of hydroconductivity, k – permeability, h – thickness of the reservoir, μ – viscosity of the liquid, p – pressure, $q = \sum_{i=1}^{M} Q_i \delta(x_i, y_i)$, Q_i, (x_i, y_i) –

[*] *Corresponding author: AndreyV. Elesin*
E-mail: elesin@imm.knc.ru

flow rate and coordinates of the i-th well, M – number of wells, $\delta(x_i, y_i)$ – delta function. For equation (1), the boundary conditions are given:

$$p\big|_{\Gamma_1} = p_\Gamma, \quad \frac{\partial p}{\partial \vec{n}}\bigg|_{\Gamma_2} = w, \tag{2}$$

where $\Gamma_1+\Gamma_2=\Gamma$ – boundary of the reservoir Ω, $\vec{n}$ – the normal vector to the reservoir boundary, w – normal component of the filtration rate.

Equation (1) with boundary conditions (2) is solved numerically. To approximate the spatial variables, the method of control volumes on a rectangular grid is used. The resulting system of linear algebraic equations is solved by the method of conjugate gradients with preconditioning as an incomplete Kholesky decomposition (Golub, Van Loan, 1999; Hill, 1990; Larabi, De Smedt, 1994).

The determination of the pressure field from solution (1)-(2) is a direct task. The inverse task is to determine permeability values in all control volumes at known pressure points at individual points. To obtain a unique solution of the inverse task, it is necessary that the number of identifiable parameters does not exceed the number of known pressure values. Since in solving practical tasks the number of control volumes covering the design area (layer) is much larger than the number of known pressures, two approaches are commonly used to reduce the number of identifiable parameters. In the first approach, the calculated region is divided into zones, each of which is characterized by a constant value of permeability. The second approach uses different interpolation options.

First, the permeability values at the interpolation nodes are determined, and the remaining values are obtained by interpolation throughout the calculation area. In this paper, unlike the second approach, in the course of solving the inverse task, the field of permeability in the form of a spline function is directly restored (Ashkenazy, 2003; Harder, Desmarais, 1972), the number of determining parameters of which corresponds to the number of wells with known bottomhole pressure.

Interpolation by a spline function

Let us assume that the values of a certain quantity a_i are known at the points $P_i(x_i,y_i)$, $i=1, n$, of a two-dimensional region. The task of interpolation is to construct a spline function $\varphi(x,y)$ (spline surface) defined on the whole region so that its values at the points P_i coincide with the values a_i. Points are called interpolation nodes. Interpolation by a spline surface has a simple mechanical meaning. The spline surface is a model of an elastic thin plate bent under the action of external forces applied at points P_i. Finding such a spline surface is to solve the variational task of finding the minimum free energy of a thin plate. The spline-surface equation has the form:

$$\varphi(x,y) = \sum_{i=1}^{n} c_i r_i^2 \ln r_i^2 + c_{n+1} + c_{n+2}x + c_{n+3}y, \tag{3}$$

where $r_i^2 = (x-x_i)^2 + (y-y_i)^2$. To determine coefficient c_i, $i=1,n+3$, of spline function $\varphi(x,y)$, it is necessary to solve the system of equations:

$$\varphi(x_i,y_i)=a,\ i=q,\ n,$$

$$\sum_{i=1}^{n} c_i = 0,\ \sum_{i=1}^{n} x_i c_i = 0,\ \sum_{i=1}^{n} y_i c_i = 0$$

For n > 3 there is solution to this system, and the solution is unique, if among the points (x_i,y_i), $i=1,N$, there are at least three points not lying on one line (Ashkenazy, 2003).

Method for solving the inverse task

A frequently used method for solving inverse coefficient tasks is to reduce them to the tasks of minimizing the residual function (Sun, 1994). In this paper, the residual function is constructed from known pressure values and has the form,

$$J(\boldsymbol{K}) = \frac{1}{2}\sum_{j=1}^{M}\left(p_j - p_j^*\right)^2, \tag{4}$$

where $\boldsymbol{K}$ – the control vector, arguments of which $\tilde{k}_i = \ln k_i$, k_i – permeability values at the spline interpolation nodes, p_j, p_j^* – pressure tasks, obtained as a result of solving equation (1), and known from the well measurements, M – the number of known pressure values.

The minimization process is carried out in two stages. At the first stage, the permeability of the entire reservoir is considered constant and is determined in the process of minimizing the residual function by the gradient method (Panteleev, Letova, 2005). At each iteration of the gradient method, the permeability is recalculated using formula:

$$\boldsymbol{K}^n = \boldsymbol{K}^{n-1} - \rho \boldsymbol{g},$$

where $\boldsymbol{g}$ – gradient of the residual function, pitch ρ is determined by the golden section method. The resulting permeability value is then used as the initial value. At the second stage, the permeability values at the interpolation nodes are determined in the process of minimizing the residual function by the Levenberg-Marquardt method (Aziz, Settari, 1982; Dennis, Schnabel, 1988; Panteleev, Letova, 2005). The new parameter values at each iteration of the Levenberg-Marquardt method are calculated by the formula:

$$\boldsymbol{K}^n = \boldsymbol{K}^{n-1} - \left(\boldsymbol{H} + \mu_n \boldsymbol{E}\right)^{-1} \boldsymbol{g},$$

where $\boldsymbol{E}$ – the unit matrix, $\mathbf{H} = \mathbf{A}^T\mathbf{A}$ – the approximate

matrix of the second derivatives, $\boldsymbol{A} = \left\{ \frac{\partial p_j}{\partial \tilde{k}_l} \right\}$ – the sensitivity matrix, μ_n – the Marquardt parameter, n – the iteration number. The initial value of the Marquardt parameter is chosen one order of magnitude larger than the maximum singular number of the matrix **H**. If the residual function is decreased at the current iteration $J(\boldsymbol{K}^n) < J(\boldsymbol{K}^{n-1})$ the Marquardt parameter is halved, if the descending condition is violated, the Marquardt parameter is doubled until this condition is satisfied. Then, a new iteration is performed. Elements of the sensitivity matrix are computed numerically.

The process of minimizing the residual function was stopped by fulfilling one of two criteria: the achievement of a given accuracy with respect to pressure measurements $\max_{j=1,M} \left| p_j - p_j^* \right| < \delta$ or the slow convergence of the minimization process $J^n - J^{n+1} < 0{,}01 J^n$ during 3 iterations.

Model tasks

In the model tasks, the exact solution is always known. This allows us to test the solution methods and evaluate the sufficiency of the initial data to obtain an exact solution. The model tasks of reservoir permeability identification are constructed as follows. First, the formation points (interpolation nodes) are selected in which permeability values are specified. From these values, the spline function (3) is constructed and the permeability field of the entire reservoir is calculated, which is taken as the true permeability field. Then, from the solution of Eq. (1) using the Peaceman formula (Peaceman, 1978), the pressure values at the wells are determined. After that, it is assumed that the permeability values are unknown and it is required to determine them in the process of minimizing the residual function (4) from known well pressures.

The model task 1

A rectangular reservoir with dimensions of 2000 m × 2000 m with a capacity of 10 m, opened by 5 injection wells and 20 producing wells is considered. The radius of the wells is 0.1 m. A pressure of 20 MPa is set at the boundary of the reservoir. The viscosity of the liquid is 10 mPas. The coordinates of the wells, their production rates and the given permeability values ktr are given in Table 1. The coordinates of the interpolation nodes of the spline function coincide with the well coordinates (Fig. 1). To approximate the filtration equation (1) with respect to spatial variables, the layer is covered by a square grid with a step of 40 m (2500 reference volumes).

No.	x, m	y, m	$Q^{(*)}$, m^3/day	Permeability, mkm^2				
				k_{tr}	k_1	k_2	k_3	k_4
1	300	300	40	0,1	0,100	0,099	0,100	0,100
2	740	140	35	5	4,819	18,809	5,160	4,851
3	1060	140	35	2	2,007	2,805	2,069	2,013
4	1340	340	-100	0,6	0,600	0,581	0,598	0,600
5	1620	180	45	4	3,978	7,966	4,176	3,997
6	620	740	-150	0,75	0,750	0,725	0,747	0,750
7	1020	540	60	0,8	0,801	0,814	0,803	0,801
8	1420	660	50	2,4	2,405	2,665	2,433	2,407
9	1860	740	30	2,8	2,791	4,718	2,908	2,802
10	300	900	60	3	3,004	3,962	3,080	3,012
11	500	1140	70	0,9	0,900	0,943	0,904	0,901
12	940	1060	80	3,4	3,405	4,049	3,463	3,411
13	1220	820	40	1,2	1,201	1,295	1,211	1,202
14	1460	1140	-100	3	2,997	2,719	2,965	2,994
15	1900	1020	40	0,88	0,880	0,986	0,890	0,881
16	340	1460	50	5	5,028	6,993	5,190	5,043
17	740	1540	-100	2,1	2,097	1,920	2,076	2,095
18	1140	1300	60	2,4	2,403	2,636	2,427	2,406
19	1420	1420	80	0,4	0,400	0,407	0,401	0,400
20	1780	1540	-150	2	2,000	1,868	1,985	1,998
21	220	1820	30	5	4,709	23,095	5,056	4,742
22	700	1860	40	1,7	1,705	2,043	1,736	1,708
23	1140	1660	45	0,2	0,200	0,202	0,200	0,200
24	1300	1860	50	0,5	0,500	0,525	0,502	0,500
25	1820	1820	40	0,1	0,100	0,101	0,100	0,100

(*) Q<0 injection wells, Q>0 producing wells.

Table 1. The values of flow rate and permeability (true and calculated) in the wells (model task 1)

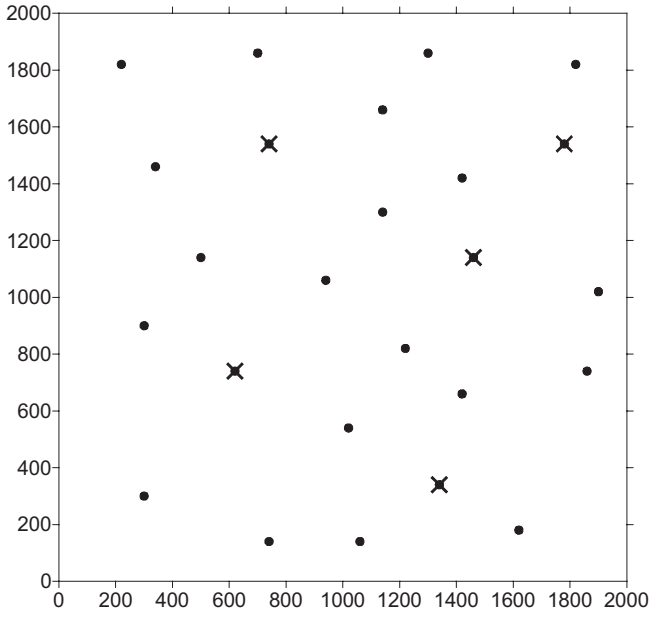

Fig. 1. Producing (●) and injection (×) and injection wells

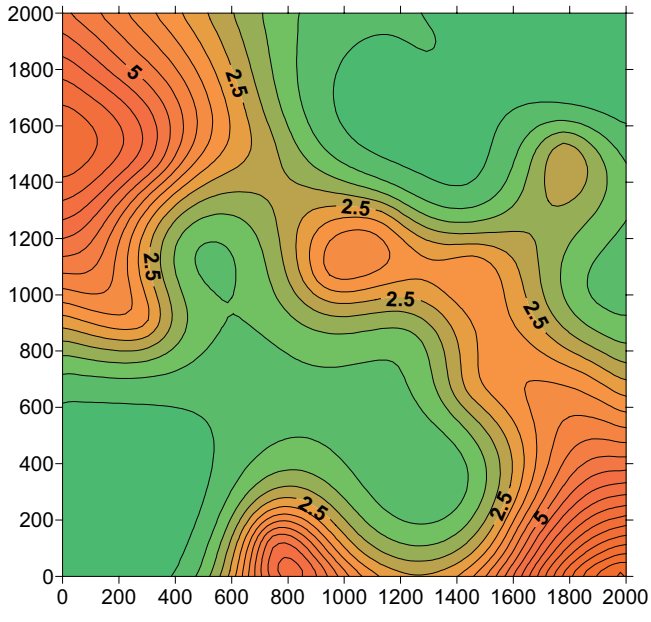

Fig. 2. Calculated permeability field (Model task 1 without errors in pressure measurements)

To study the stability of the solution, random errors εi were introduced into the pressure measurements. The results of solving the model task without error and with errors in pressure measurements are given in Table 1. The solution k_1 was obtained without error in pressure measurements (ε_i = 0 MPa), solutions k_2, k_3, k_4 were obtained in tasks with errors in pressure measurement $|\varepsilon_i|$<0,1 MPa, $|\varepsilon_i|$<0,01 MPa, $|\varepsilon_i|$<0,001 MPa respectively. When solving tasks, both with an error and without an error in measuring pressure, a predetermined accuracy of δ = 0,01 МПа is achieved. The calculated permeability values without error in pressure measurements are close to the true ones (Fig. 2).

From the results of the solution of tasks with errors in pressure measurements, it can be seen that with decreasing error, the values of the parameters approach the true values. Note that the maximum relative deviations in model task 1 are observed at the interpolation nodes with the maximum permeability values. This is explained by the fact that at the same values of flow rate, the value of bottomhole pressure at the well is more sensitive to a change in permeability at its small values, which is clearly seen from the Peaceman formula. Therefore, in order to achieve a given pressure accuracy, the small permeability values should be closer to the true values in comparison with the larger permeability values.

The model task 2

In the first model task, the true and calculated permeability fields were determined from the same nodes of interpolation of the spline function. The second model task differs from the first in that the true field of permeability was constructed from the interpolation nodes located at the nodes of the square grid with steps of 1000 m (9 knots). The coordinates of the interpolation nodes in solving the inverse task coincided with the well coordinates. The true permeability values obtained in the result of the solution of the second model task on wells without an error in pressure measurements are given in Table 2.

The corresponding permeability fields are shown in Fig. 3, 4. When solving the task, a predetermined accuracy of δ = 0,01 MPa from measurements of pressure at the wells was achieved. The calculated permeability field is close to the true field.

No.	k_{tr}	k	No.	k_{tr}	k	No.	k_{tr}	k
1	0,342	0,340	10	0,408	0,408	19	0,415	0,414
2	0,397	0,397	11	0,441	0,441	20	0,381	0,381
3	0,417	0,416	12	0,499	0,498	21	0,313	0,314
4	0,404	0,404	13	0,456	0,454	22	0,368	0,367
5	0,351	0,351	14	0,402	0,402	23	0,421	0,420
6	0,460	0,460	15	0,296	0,296	24	0,413	0,413
7	0,462	0,461	16	0,377	0,377	25	0,422	0,422
8	0,401	0,401	17	0,418	0,419			
9	0,300	0,302	18	0,458	0,457			

Table 2. Permeability values (true and calculated) at wells, mkm² (model task 2)

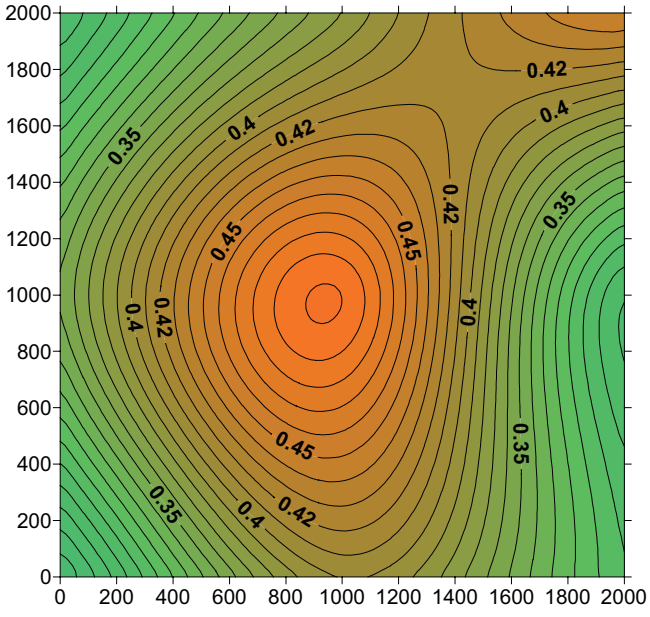

Fig. 3. True permeability field (model task 2)

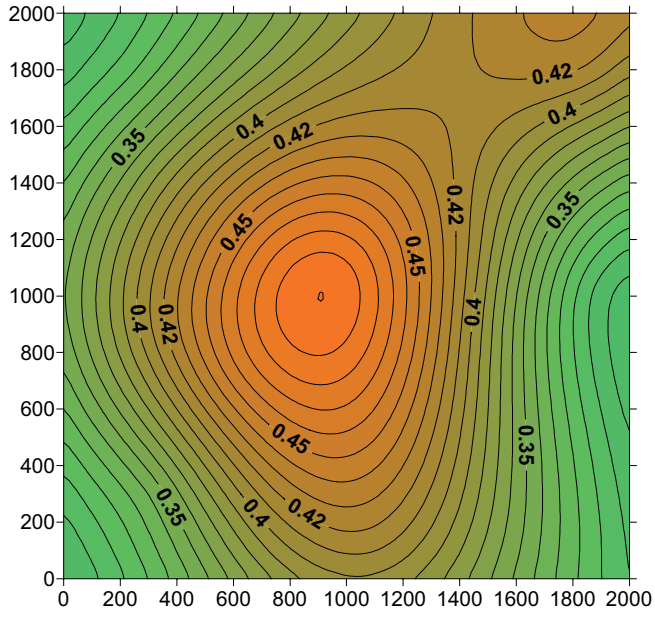

Fig. 4. Calculated permeability field (model task 2)

Conclusion

The model tasks of identifying the permeability of a two-dimensional formation, opened by a system of producing and injection wells, were determined based on pressure measurements at wells under conditions of stationary single-phase fluid filtration. The permeability field was approximated by a spline function, constructed from the values at the wells. Unknown permeability values at the wells were determined in the process of minimizing the residual function using the Levenberg-Marquardt method. When solving model tasks without errors in pressure measurements, the calculated permeability fields practically coincide with the given fields. For the task with errors in pressure measurements, the stability of the solution obtained is shown.

References

Ashkenazy V.O. (2003). Splayn-poverhnosti: Osnovy teorii i vychislitel'nye algoritmy [Spline surfaces: Fundamentals of theory and computational algorithms]. Tver: Tverskoy gos. un-t, 82 p. (In Russ.)

Aziz Kh., Settari A. (1982). Petroleum Reservoir Simulation. Moscow: Nedra, 407 p. (In Russ.)

Basniev K.S., Vlasov A.M., Kochina I.N., Maksimov V.M. (1986). Podzemnaya gidravlika [Underground hydraulics]. Moscow: Nedra, 303 p. (In Russ.)

Carrera J., Newman Sh.P. (1986). Estimation of Aquifer Parameters Under Transient and Steady State Conditions: 3. Application to Synthetic and Field Data. *Water Resour. Res*., 22(2), pp. 228-242.

Dennis J.E., Schanabel R.B. (1988). Numerical Methods for Uncostrained Optimization and Nonlinear Equations. Moscow: Mir., 440 p. (In Russ.)

Elesin A.V., Kadyrova A.SH., Mazurov P.A. (2009). Dvuhshagovye metody Levenberga-Markvardta v zadache identifikacii koehfficienta fil'tracii [Two-step Levenberg-Markvardt methods in the problem of identifying the filtration coefficient]. *Georesursy = Georesources*, 32(4), pp. 40-42. (In Russ.)

Golub G.H., Van Loan C.F. (1999). Matrix Computations. Moscow: Mir, 548 p. (In Russ.)

Golubev G.V., Danilaev P.G., Tumashev G.G. (1978). Opredelenie gidroprovodnosti neodnorodnyh neftyanyh plastov nelokal'nymi metodami [Determination of hydroconductivity of inhomogeneous oil reservoirs by nonlocal methods]. Kazan: Kazan Univer. Publ., 168 p. (In Russ.)

Harder R.L., Desmarais R.N. (1972). Interpolation using surface splines. *Journal of Aircraft*, 9(2), pp. 189-191.

Hill M.C. (1990). Solving groundwater flow problems by conjugate-gradient methods and the strongly implicit procedure. *Water Resour. Res*. 26(9), pp.1961-1969.

Khairullin M.Kh., Khisamov R.S., Shamsiev M.N., Farkhullin R.G. (2006). Interpretation of the results of well hydrodynamic research by regularization methods. Moscow-Izhevsk: SRC "Regular and chaotic dynamics"; Institute of Computer Science, 172 p. (In Russ.)

Khairullin M.Kh., Badertdinova E.R., Nazimov N.A. (2017). Multisensor Research Technologies of Oil Horizontal Wells on Fields of the Republic of Tatarstan. *Georesursy = Georesources*, 19(3), Part 1, pp. 234-238. DOI: https://doi.org/10.18599/grs.19.3.14.

Larabi A., De Smedt F. (1994). Solving three-dimensional hexahedral finite element groundwater models by preconditioned conjugate gradient methods. *Water Resour. Res*, 30(2), pp. 509-521.

Panteleev A.V., Letova T.A. (2005). Metody optimizacii v primerah i zadachah [Optimixation methods in examples and tasks]: 2nd publ. Moscow: Vysshaya shkola, 544 p. (In Russ.)

Peaceman D.W. (1978). Interpretation of well block pressures in numerical reservoir simulation. *Soc. Petrol. Eng. Journal*, 18(3), pp. 183-194.

Sun N.-Z. (1994). Inverse Problems in Groundwater Modeling. Kluwer Acad., Norwell, Mass., 337 p.

Zinoviev N.P. (1984). Identifikaciya gidroprovodnosti v sluchae uprugogo rezhima fil'tracii v neftyanom plaste [Identification of the hydraulic conductivity in the case of an elastic filtration regime in oil reservoir]. *Issled. po prikl. matem*. [Studies of applied mathematics], 11, Part 2, pp. 78-84. (In Russ.)

About the Authors

Andrey V. Elesin – PhD (Physics and Mathematics), Senior researcher of the Laboratory of mathematical modeling of hydrogeological processes

Institute of Mechanics and Engineering, FRC Kazan Scientific Center of the Russian Academy of Sciences

2/31, Lobachevsky St., Kazan, 420111, Russian Federation

E-mail: elesin@imm.knc.ru

Alfiya Sh. Kadyrova – PhD (Physics and Mathematics), Senior researcher of the Laboratory of mathematical modeling of hydrogeological processes

Institute of Mechanics and Engineering, FRC Kazan Scientific Center of the Russian Academy of Sciences

2/31, Lobachevsky St., Kazan, 420111, Russian Federation

Anatoly I. Nikiforov – DSc (Physics and Mathematics), Chief researcher of the Laboratory of mathematical modeling of filtration processes

Institute of Mechanics and Engineering, FRC Kazan Scientific Center of the Russian Academy of Sciences

2/31, Lobachevsky St., Kazan, 420111, Russian Federation

Manuscript received 12 February 2018;
Accepted 24 May 2018;
Published 30 June 2018

ORIGINAL RESEARCH ARTICLE

DOI: https://doi.org/10.18599/grs.2018.2.108-114

Hydraulic fracturing efficiency evaluation in the vicinity of a single well for a reservoir with two fractures

Yu.I. Yakhina
Termosim LLC, Kazan, Russian Federation
E-mail: vib-210@mail.ru

Abstract. The solution of fluid flow problem in an unbounded homogeneous reservoir penetrated by a single well with two intersecting fractures with taking into account their hydrodynamic resistance is constructed and investigated. A general integral representation of the perturbed pressure field is obtained using the instantaneous point-source. As a particular case, the quasi-stationary operating mode of the well is considered. The accuracy and limitations of the obtained asymptotic solutions are estimated. A comparative analysis obtained results is done. Well productivity and the pseudoskin factor for the fractures system are determined, explicit analytical expressions for these characteristics are constructed. In the course of computational experiments, the interaction of intersecting fractures at different opening angles are investigated. An estimate of the efficiency of repeated hydraulic fracturing of the productive formation is obtained. It is shown that the maximum flow is achieved for a perpendicular arrangement of the fractures, and the distribution of the outflow (inflow) along the flat vertical fracture essentially depends on its relative filtration resistance.

Keywords: hydraulic fracturing, crack azimuth of repeated fracturing, efficiency of repeated fracturing, quasi-stationary operation of well, pseudoskin factor of repeated fracturing, filter resistance in cracks, instantaneous point-source, fracture hydrodynamics

Recommended citation: Yakhina Yu.I. (2018). Hydraulic fracturing efficiency evaluation in the vicinity of a single well for a reservoir with two fractures. *Georesursy = Georesources,* 20(2), pp. 108-114. DOI: https://doi.org/10.18599/grs.2018.2.108-114

Introduction

In order to involve undrained and weakly drained mineral resources in development, hydraulic fracturing is used. This technology contributes to the creation of a high-conductive fracture, which allows increasing the productivity of producing wells or injectivity of injection wells. According to expert assessments of hydrodynamic studies, the hydraulic fracturing of the reservoir is the most effective geological and technical measure that guarantees an increase in the efficiency of poorly permeable reservoirs development. One of the first studies of stationary single-phase inflow to a well with a single fracture of hydraulic fracturing is presented in the paper (Prats, 1961). Theoretical calculations show that the fracturing allows several times to increase the well production by activating the weakly draining zones, the volume of extraction or injection depending on the conductivity and fracture length (Cinco-Ley et al., 1978; Meehan et al., 1989).

A review of a number of other publications and an analysis of the efficiency of fracturing in a well with a single vertical fracture in a circular feed loop was carried out (Morozov, 2016) on the basis of various estimates of productivity and the generalized pseudoskin factor concept (Economides et al., 2002).

With a significant reduction in the production rates with respect to the initial regimes, a second fracturing is performed. At the same time, to ensure full coverage of the reservoir and introduction of new reserves, a method of reorientation of the azimuth is used, which makes it possible to realize the development of the fracture in a direction different from the first hydraulic fracturing.

Repeated hydraulic fracturing is one of the most common methods of intensifying the extraction of mineral reserves and increasing reservoir productivity, which makes the task of analyzing and predicting its effectiveness topical. In a particular case, the problem of a stationary inflow to a well with several vertical fractures with uniformly distributed inflow along the fractures in the region bounded by the circular feed circuit was considered in the work (Raghavan, Joshi, 1993). A similar problem of a steady uniformly distributed inflow to two fractures with different geometric characteristics at a given intersection angle was solved numerically in (Lihtarev, Pestrikov, 2010).

In the framework of this study, theoretical issues related to the analysis of the unsteady hydrodynamic regime of one and two intersecting fractures of different

azimuth are considered taking into account their hydraulic resistance in an unbounded homogeneous reservoir. The efficiency of re-fracturing at different opening angles was estimated. Explicit analytical expressions are obtained for the productivity of the well and the pseudoskin factor.

General integral representation of the disturbance in the reservoir pressure field

During the operation of the well, fluid movement in the near-wellbore zone occurs due to the potential energy of the reservoir elastic state, as a result of lowering pressure at the bottom of the well. At the same time, the volume of liquid increases, and the porosity, and possibly the permeability, decreases due to the expansion of the formation skeleton. In the case of fluid injection in the formation, the flow of injected fluid is maintained by increased pressure at the bottom, and the filtration process develops in the opposite direction.

The main characteristic of filtration processes is the field of reservoir pressure, which, in the case of unsteady elastic filtration in a porous medium with distributed sources, is described by the piezoconductivity equation (Charnyy, 1963):

$$\frac{\partial P}{\partial t} = \varkappa \Delta P + \frac{q^*}{m_0 \beta}; \quad |x|, |y|, |z| < \infty, t > 0,$$

where $\varkappa = k/(\mu\beta m_0)$ is the conductivity coefficient, which determines the propagation velocity of pressure perturbations $P(x,y,z,t)$ in a porous medium with permeability k, porosity m_0, elastic capacity coefficient β, liquid viscosity μ; $q^*(x,y,z,t)$ is the density of distributed sources, which is the amount of fluid entering the volume unit of the medium per unit time t; Δ is the differential Laplace operator in a system of Cartesian coordinates (x,y,z).

Let there be no perturbation of pressure in the reservoir at the initial moment of time, then the solution of the piezoconductivity equation for zero initial conditions can be written in a general integral form using the method of instant point sources (Carslaw, Jaeger, 1964; Tikhonov, Samarskii, 1999):

$$P(x,y,z,t) = \int_0^t \iiint_{-\infty}^{+\infty} \frac{q^*(\xi,\eta,\zeta,\tau)}{m_0\beta} G^*(\xi,\eta,\zeta,x,y,z,t-\tau - \tau) d\xi\, d\eta\, d\zeta\, d\tau, \quad (1)$$

where $G^*(\xi,\eta,\zeta,x,y,z,t-\tau)$ is the influence function of the instantaneous point source, which is the pressure perturbation at the point (x,y,z) at time t, caused by a single instantaneous point source at the point (ξ,η,ζ) at time $t = \tau$:

$$G^*(\xi,\eta,\zeta,x,y,z,t-\tau) = \left(\frac{1}{2\sqrt{\pi\varkappa(t-\tau)}}\right)^3 e^{-\frac{(x-\xi)^2+(y-\eta)^2+(z-\zeta)^2}{4\varkappa(t-\tau)}}.$$

The total inflow or outflow of fluid Q in a well with fractures per unit time is, by definition, equal to:

$$Q(t) = \iiint_{-\infty}^{\infty} q^*(\xi,\eta,\zeta,t)\, d\xi\, d\eta\, d\zeta.$$

We use the obtained representation (1) to study the filtration process when liquid is injected in a homogeneous isotropic reservoir with a thickness h in the vicinity of an injection well with two flat vertical fractures created as a result of hydraulic fracturing and intersecting at an angle α (Fig. 1). In order to simplify further reasoning, we assume that fractures of length $2x_f$ and width δ_f are symmetrically disposed about the axis of the well, have the same geometry and identical hydrodynamic properties. The flow rate $Q(t)$ pumped into the well is distributed evenly along the thickness of the reservoir (fracture height) with the surface density $q(x,t)$. Here, q is the amount of liquid injected per unit of formation thickness from a unit of fracture length per unit time. The density of the distributed source along the fracture, taking into account the smallness of the opening of the discontinuity, δ_f, is determined by the relation: $q^*(x,y,z,t) \approx q(x,t)/\delta_f$ (at $q^* = 0$ outside the fracture $|y| > \delta_f/2$).

In view of the linearity of the problem under consideration and the identity of the fractures , the perturbation of the pressure field created by them can be regarded as the sum of the perturbations caused by single fractures , one of which is located along the x axis as shown in Fig. 1, and the other, a repeated fracture , is directed along the axis with coordinates:

$$\begin{pmatrix} x' \\ y' \end{pmatrix} = \begin{pmatrix} \cos\alpha & -\sin\alpha \\ \sin\alpha & \cos\alpha \end{pmatrix} \begin{pmatrix} x \\ y \end{pmatrix}.$$

Assuming homogeneity of the reservoir and uniformity of vertical injection, the general integral representation of the pressure field (1) after integration over η is transformed to the form:

$$P(x,y,t) = \frac{\mu}{4\pi k} \int_0^t \int_{-x_f}^{x_f} \frac{q(\xi,\tau)}{(t-\tau)} \left[e^{-\frac{(x-\xi)^2+y^2}{4\varkappa(t-\tau)}} + e^{-\frac{(x'-\xi)^2+y'^2}{4\varkappa(t-\tau)}} \right] d\xi d\tau. \quad (2)$$

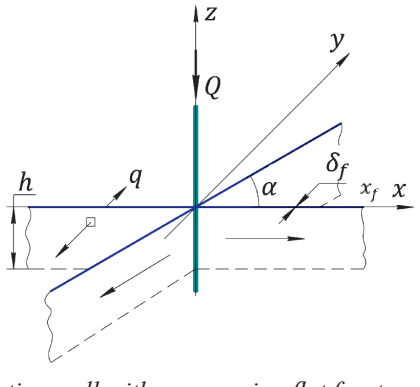

Fig. 1. Injection well with suppressing flat fractures

The total flow rate Q takes the form:

$$Q(t) = 2h \int_{-x_f}^{x_f} q(x,t)\, dx.$$

Single fracture hydrodynamics

Hydraulic fracturing of the productive formation allows creating a fracture with a high permeability $k_f >> k$, which leads to a decrease in the hydraulic resistance of the bottomhole zone and, as a consequence, to an increase in the filtration surface. For the same reason, the transient processes of pressure redistribution in the Pf fracture occur very rapidly, and the fluid flow at each instant of time can be described by a stationary filtration equation (Meehan et al., 1989):

$$\frac{k_f \delta_f}{\mu} \frac{\partial^2 P_f}{\partial x^2} = q;\ 0 < x < x_f, t > 0. \quad (3)$$

By assumption, the homogeneous fracture consists of two differently directed «wings» symmetrical with respect to the well, which allows us to consider the liquid filtration region in only one direction of the fracturing (for example, in the interval $0 < x < x_f$), as shown in Fig. 2.

At the bottom of the well, there is a perturbation of the fluid pressure P_w, relative to the reservoir, and the inflow from the end is considered negligible. Thus, equation (3) is supplemented by boundary conditions:

$$P_f(x,t)|_{x=0} = P_w,\ \left.\frac{\partial P_f}{\partial x}\right|_{x=x_f} = 0.$$

The solution of the problem formulated above, which describes the process of filtration in a fracture, can be represented in the form:

$$P_f(x,t) = P_w - \frac{\mu}{k_f \delta_f}\left[\int_0^x \xi q(\xi,t) d\xi + x\int_x^{x_f} q(\xi,t) d\xi\right],$$

$$0 < x < x_f. \quad (4)$$

Relation (4) relates the pressure distribution along the fracture to the liquid flow density $q(x,t)$, and should be considered together with equation (2) at $y = 0$:

$$P_f(x,t) = \frac{\mu}{4\pi k}\int_0^t \int_{-x_f}^{x_f} \frac{q(\xi,\tau)}{(t-\tau)}\left[e^{-\frac{(x-\xi)^2}{4\varkappa(t-\tau)}} + e^{-\frac{(x'-\xi)^2+y'^2}{4\varkappa(t-\tau)}}\right] d\xi\, d\tau, \quad (5)$$

where $0 < x < x_f$, $t > 0$, $x' = x\cos\alpha$ and $y' = x\sin\alpha$.

To determine the distributed inflow along the fracture, combining equations (4) and (5), we obtain the integral equation:

$$P_w = \frac{\mu}{4\pi k}\int_0^t \int_{-x_f}^{x_f} \frac{q(\xi,\tau)}{(t-\tau)}\left[e^{-\frac{(x-\xi)^2}{4\varkappa(t-\tau)}} + e^{-\frac{(x'-\xi)^2+y'^2}{4\varkappa(t-\tau)}}\right] d\xi\, d\tau +$$

$$+ \frac{\mu}{k_f \delta_f}\left[\int_0^x \xi q(\xi,t) d\xi + x\int_x^{x_f} q(\xi,t) d\xi\right], \quad (6)$$

where $0 < x < x_f$ and $t > 0$.

Quasistationary well regime with intersecting fractures

As preliminary estimates show, under unchanged operating conditions of the well (constant bottomhole pressure P_w or constant flow rate Q), the quasistationary filtration regime in the reservoir, characterized by the time-invariant profile of the relative distribution of the inflow along the fracture

$$\overline{q}(x) = q(x,t)/< q >,$$

where $< q >= Q(t)/(4hx_f)$ is set at $\varkappa t/x_f^2 \geq 100$.

In this case, the integral equation (6) takes the form:

$$P_w = -\frac{\mu Q(t)}{4hx_f}\left\{\frac{1}{4\pi k}\int_0^{x_f} \overline{q}(\xi)\left[Ei\left(-\frac{(x+\xi)^2}{4\varkappa t}\right) + \right.\right.$$

$$+ Ei\left(-\frac{(x'+\xi)^2+y'^2}{4\varkappa t}\right) + Ei\left(-\frac{(x-\xi)^2}{4\varkappa t}\right) +$$

$$\left.\left. + Ei\left(-\frac{(x'-\xi)^2+y'^2}{4\varkappa t}\right)\right] d\xi + \right.$$

$$\left. + \frac{1}{k_f \delta_f}\left[\int_0^x \xi\, \overline{q}(\xi)\, d\xi + x\int_x^{x_f} \overline{q}(\xi)\, d\xi\right]\right\}. \quad (7)$$

Here $Ei(-x) = -\int_x^{\infty} \frac{e^{-u}}{u} du$ – is integral exponential function, for small values of the argument (Abramovitz, Stegun, 1979):

$$Ei(-x) \approx \ln(1.781x).$$

Accordingly, in the quasi-stationary approximation, instead of (7) for large values of time t, we have:

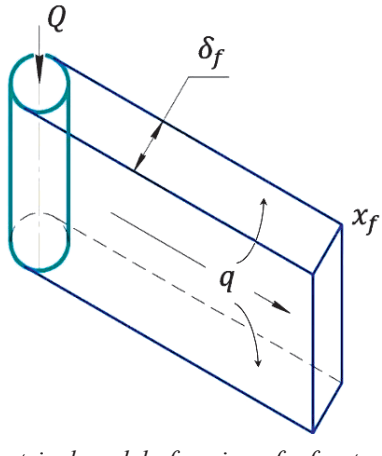

Fig. 2. Geometrical model of a wing of a fracture

$$P_w = -\frac{\mu Q(t)}{4hx_f}\left\{\frac{1}{4\pi k}\int_0^{x_f}\overline{q}(\xi)\left[ln\left(\frac{(x+\xi)^2}{2.2458\,\varkappa t}\right)+\right.\right.$$

$$+ ln\left(\frac{(x-\xi)^2}{2.2458\,\varkappa t}\right) + ln\left(\frac{(x'+\xi)^2+y'^2}{2.2458\,\varkappa t}\right)+$$

$$\left.\left.+ ln\left(\frac{(x'+\xi)^2+y'^2}{2.2458\,\varkappa t}\right) + ln\left(\frac{(x'-\xi)^2+y'^2}{2.2458\,\varkappa t}\right)\right]d\xi +\right.$$

$$\left.+\frac{1}{k_f\delta_f}\left[\int_0^x \xi\,\overline{q}(\xi)\,d\xi + x\int_x^{x_f}\overline{q}(\xi)\,d\xi\right]\right\}, \qquad (8)$$

where $x' = x\cos\alpha$ и $y' = x\sin\alpha$.

The numerical solution of the distributed flow rate of liquid along a fracture in the presence of a filtration resistance

Here and below, the following typical values for the injection conditions of the liquid (water) are accepted in the calculations: the pressure at the bottom is $P_w = 4.053\cdot10^6$ Pa (40 atm), the fracture half-length is $x_f = 100$ m, the fracture width is $\delta_f = 0.2$ m, the piezoconductivity coefficient is $\varkappa = 2.78$ m^2/s (10^4 m^2/hour), the permeability of the reservoir is $k = 10^{-13}$ m^2 (100 mD), the viscosity of the fluid is $\mu = 0.001$ Pa·s (1 cps), the operating time of the well is t = 360000 sec (100 hours).

The results of the computational experiments presented in Fig. 3a have shown that the distribution of the inflow along the fracture essentially depends on its relative filtration resistance, $kx_f/(k_f\delta_f)$. At the end of the fracture , a sharp increase in the outflow is observed, which is associated with a change in the character of the liquid flowfrom the linear to the quasiradial one.

In turn, for a known injection density $q(x,t)$, which takes into account the filtration resistance in the fractures, the quasi-stationary pressure distribution in the reservoir can be calculated on the basis of the asymptotic representation of the general equation (2):

$$P(x,y,t) = -\int_0^{x_f}\frac{\mu q(\xi,t)}{4\pi k}\left[Ei\left(-\frac{(x+\xi)^2+y^2}{4\varkappa t}\right)+\right.$$

$$+ Ei\left(-\frac{(x-\xi)^2+y^2}{4\varkappa t}\right) + Ei\left(-\frac{(x'+\xi)^2+y'^2}{4\varkappa t}\right)+$$

$$\left.+ Ei\left(-\frac{(x'-\xi)^2+y'^2}{4\varkappa t}\right)\right]d\xi,$$

where $x' = x\cos\alpha - y\sin\alpha$ and $y' = x\sin\alpha + y\cos\alpha$.

A comparative analysis (Fig. 4) shows that the pressure drop along the fractures increases substantially with increasing filtration resistance.

Let us consider the distribution of the inflow into the reservoir with a uniform pressure distribution along the fractures , $P_f = P_w$, in the absence of filtration resistance ($k_f \to \infty$). An analysis of the solution of the inverse problem of the outflow distribution at a given pressure shows that when the opening angle between fractures increases, the pressure gradients in the near wellbore zone of the reservoir decrease and the local outflow of liquid decreases, as shown in Fig. 5. And at the remote end part of the fracture , the reverse effect is observed – the flow density increases due to the decrease in interference between the fractures.

When the opening angle tends to 0°, the pressure in the well near the wellbore is equalized and the injection density is correspondingly reduced – two fractures begin to work as one and the outflow from the central part increases.

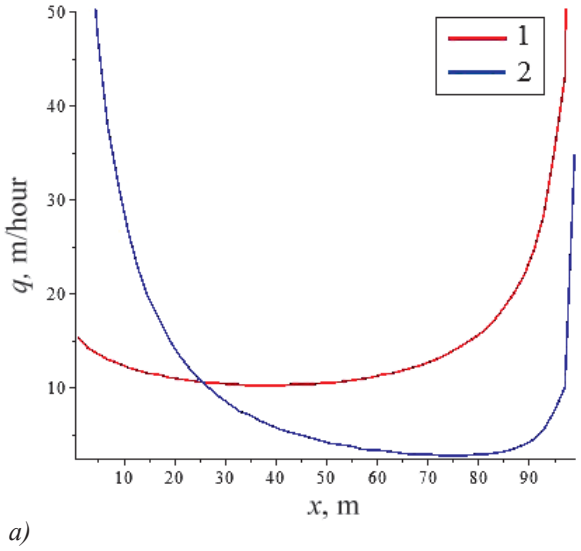

a)

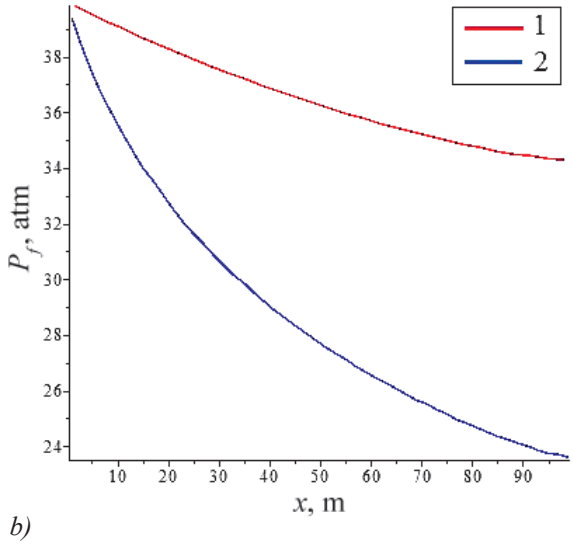

b)

Fig. 3. The distribution of flows to the fracture (a) and the pressure along the fracture (b) in the vicinity of the well at a mutually perpendicular arrangement of fractures and different permeabilities: 1 – $k_f = 5\cdot10^4$ mD and 2 – $k_f = 10^4$ mD.

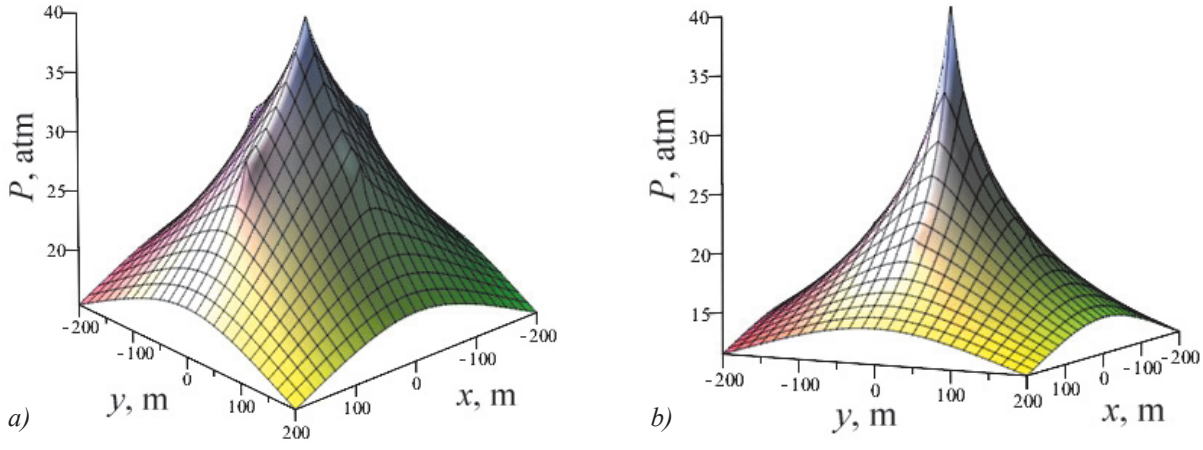

Fig. 4. Perturbation of reservoir pressure in the vicinity of the well with mutually perpendicular arrangement of fractures with permeability: (a) – $k_f = 5 \cdot 10^4$ mD ($kx_f / (k_f \delta_f) \sim 1$) and (b) – $k_f = 10^4$ mD ($kx_f / (k_f \delta_f) \sim 5$)

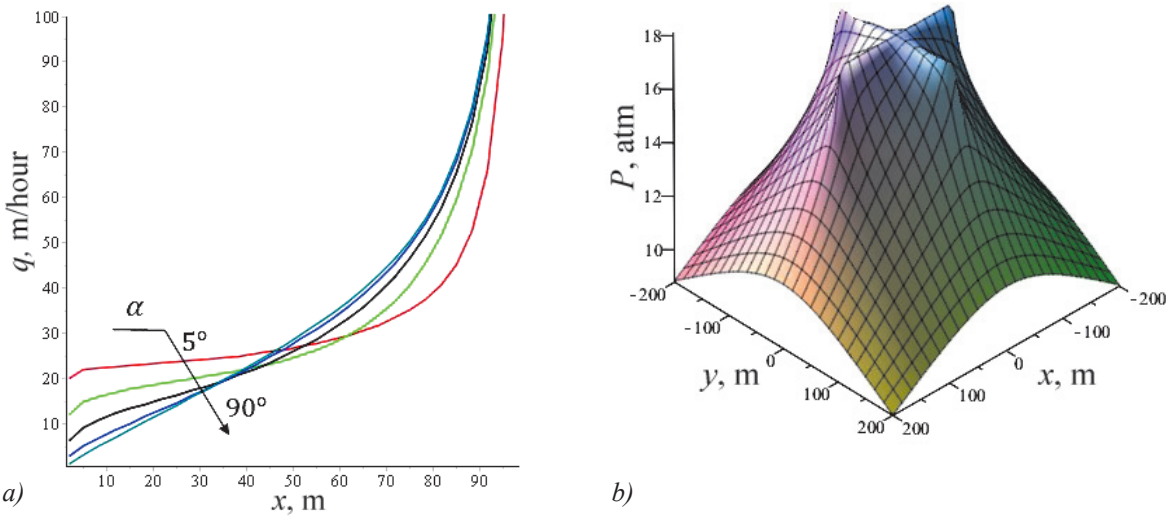

Fig. 5. Distribution of the inflow along the primary fracture (a) at a constant depression of 40 atm at different opening angles and perturbation of the reservoir pressure (b) in the vicinity of the well with mutually perpendicular arrangement of the fractures

Well productivity and pseudoskin factor

Summarizing the traditional concept of the skin factor (Economides et al., 2002; Morozov, 2016), we define the pseudoskin factor of the well with intersecting fractures of the finite permeability for a given depression. From the relation (8) for $x = 0$ it follows immediately:

$$P_w = -\frac{\mu Q(t)}{4hx_f}\left[\int_0^{x_f} \frac{2\overline{q}(\xi)}{\pi k} ln\left(\frac{\xi}{\sqrt{2.2458\varkappa t}}\right) d\xi\right] =$$

$$= -\frac{\mu Q(t)}{2\pi khx_f}\left\{\int_0^{x_f} \overline{q}(\xi)\left[ln\left(\frac{\xi}{r_w}\right) - ln\left(\sqrt{\frac{2.2458\varkappa t}{r_w^2}}\right)\right] d\xi\right\},$$

where r_w is the radius of the well. As a result, the productivity of the well will be given by the formula:

$$\frac{Q}{P_w} = \frac{2\pi hk}{\mu} \frac{1}{S + ln\left(\sqrt{\frac{2.2458\varkappa t}{r_w^2}}\right)}, \qquad (9)$$

where pseudoskin factor is:

$$S = -\frac{1}{x_f}\int_0^{x_f} \overline{q}(\xi)\, ln\left(\frac{\xi}{r_w}\right) d\xi.$$

In the particular case of a single fracture of infinite conductivity ($\overline{q} = 1$) the pseudoskin factor in (9) is equal to $S = -ln(x_f/e)$. In addition, according to the estimates obtained in (Charnyy, 1963), on the basis of the method of successive change of stationary states, the expression $\sqrt{2.2458\varkappa t}$ can be considered as the radius of the mobile current circular feed loop r_e. As a result, the above relation (9) can be rewritten in the equivalent form:

$$P_w = \frac{\mu Q}{2\pi kh}\, ln\left(\frac{r_e}{x_f/e}\right),$$

which coincides with the solution (Raghavan, Joshi, 1993).

Calculation results of pseudoskin factor (9), shown in Fig. 6, show that the minimum pseudoskin factor and the maximum injection (inflow) volume increase is achieved with the perpendicular arrangement of fractures and essentially depends on their resistance to filtration.

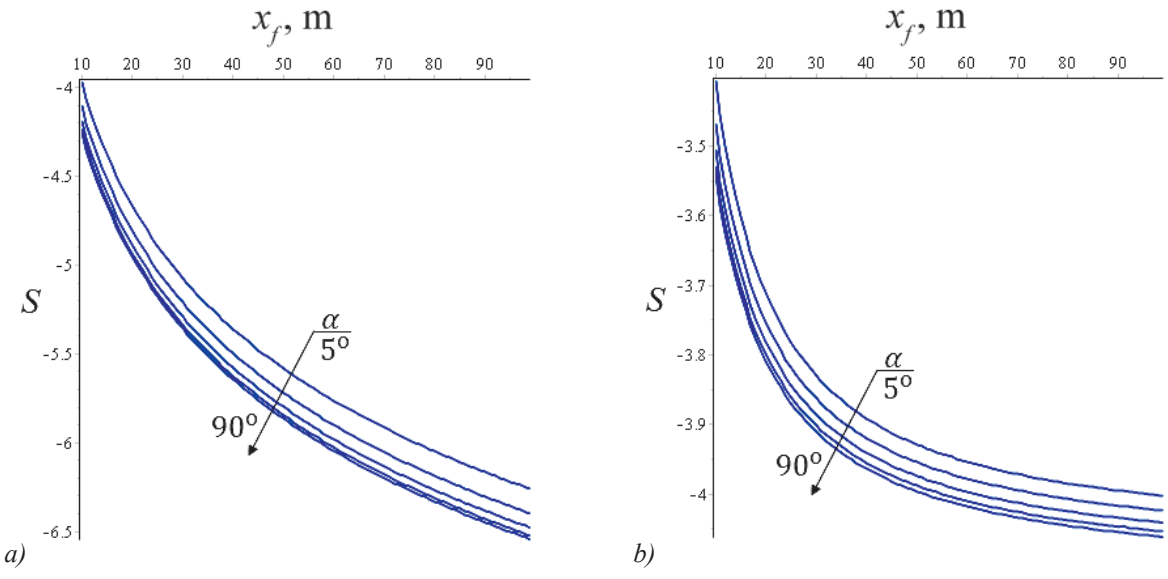

Fig. 6. Pseudoskin factor at a given bottomhole pressure P_w with permeability (a) $k_f = 10^6$ mD ($kx_f/(k_f\delta_f) \sim 0{,}05$) and (b) $k_f = 10^4$ mD ($kx_f/(k_f\delta_f) \sim 5$)

Repeated hydraulic fracturing allows to increase the pseudoskin factor at high fracture permeability up to 5-10%, as shown in Fig. 6a. Efficiency of re-fracturing according to Fig. 6b increases to 10-20% in the case of small fractures permeability, which is in agreement with the numerical solutions obtained in (Lihtarev, Pestrikov, 2010).

Conclusion

As is known, hydraulic fracturing of the reservoir is a complex, energy-intensive and expensive technological process for intensifying field development. Every year, this technology is increasingly used in the operation of both producing and injection wells. However, the consequences of applying repeated fracturing are not always positive, which makes the task of assessing its effectiveness urgent.

In the study of the hydrodynamic regime of a well with intersecting fractures penetrating a homogeneous reservoir, it is shown that under unchanged conditions of well operation (steady pressure at the bottom P_w or constant flow rate Q), a quasi-stationary operation mode of the well with a constant injection profile (inflow) in fractures is established. The distribution of the inflow along the fracture essentially depends on its relative filtration resistance, $kx_f/(k_f\delta_f)$. At the same time, as the opening angle is increased, the pressure gradients in the near wellbore zone of the reservoir decrease and the local outflow (inflow) of the liquid decreases. At the remote end part of the fractures , the reverse effect is observed – the flux density increases due to the decrease in interference between the fractures. The maximum total increase in inflow into the reservoir is achieved with a perpendicular arrangement of the fractures .

Repeated hydraulic fracturing of the productive formation allows to increase the pseudoskine factor at a high permeability ($k_f \sim 10^6$ mD, $kx_f/(k_f\delta_f) \sim 0{,}05$) fractures up to 5-10%. The effectiveness of re-fracturing increases to 10-20% in the case of small permeability ($k_f \sim 10^4$ mD, $kx_f/(k_f\delta_f) \sim 5$).

Further research continuation can be aimed at solving both more general problems of unsteady filtration and inverse problems: justifying the methods of hydrodynamic exploration of wells in order to determine the opening angle between two hydraulic fracturing fractures and other hydrodynamic characteristics of the fracture system.

Acknowledgements

The author expresses gratitude to the scientific adviser, Professor A.N. Salamatin for valuable advice in the planning and implementation of research and recommendations on the formatting of work. The author thanks Professor G.T. Bulgakova for choosing the topic and area of research and expresses gratitude to the reviewer for valuable comments and suggestions that contributed to the improvement of this article.

References

Abramowitz M., Stegun A. (1979). Handbook of Mathematical Functions. Moscow: Nauka, pp. 58-59. (In Russ.)

Carslaw H.S, Jaeger J.C. (1964). Conduction of Heat in Solids. Moscow: Nauka, pp. 251-259. (In Russ.)

Charnyy I. A. (1963). Underground hydro gas dynamics. Moscow: Gostoptekhizdat, pp. 250-313. (In Russ.)

Cinco-Ley H., Samaniego V.F., Domínguez A.N. (1978). Transient pressure behavior for a well with a finite-conductivity vertical fracture. *SPE Journal,* 18(4), pp. 253-264.

Economides M., Oligney R., Valkó P. (2002). Unified fracture design: bridging the gap between theory and practice. Alvin, Texas: Orsa Press, 25 p.

Lihtarev A. V., Pestrikov A. V. (2010). Opredelenie kojefficienta produktivnosti skvazhiny, peresechennou dvumua treshhinami gidrorazryva plasta raznogo azimuta, na osnove matematicheskogo modelirovaniua [Determination of the production efficiency of a well crossed by two induced hydraulic fractures of a different azimuth, based on mathematical modeling]. *Nauchno-tehnicheskiy vestnik OAO "NK" Rosneft'"*, pp. 12-14. (In Russ.)

Meehan D. N., Horne R.N., Ramey H.J. (1989). Interference testing of finite conductivity hydraulically fractured wells. *SPE Annual Technical Conference and Exhibition. Society of Petroleum Engineers,* pp. 137-152.

Morozov P.E. (2016). Psevdoskin-faktor i optimal'naya provodimost' vertikal'noy treshhiny gidavlicheskogo razryva plasta [Pseudoskine factor and optimal conductivity of vertical induced hydraulic fracture]. *Mezhd. nauchno-prakt. konf.: Innovacii v razvedke i razrabotke neftyanyh i gazovyh mestorozhdeniy* [Proc. Sci. and Pract. Conf.: Innovations in explorationa and development of oil and gas fields], Kazan, pp. 53-56. (In Russ.)

Prats M. (1961). Effect of vertical fractures on reservoir behavior-incompressible fluid case. *SPE Journal*, 1(02), pp. 105-118.

Raghavan R., Joshi S.D. (1993). Productivity of multiple drainholes or fractured horizontal wells. *SPE Form. Eval.,* 8(01), pp. 11-16.

Tikhonov A. N., Samarskii A. A. (1999). Equations of Mathematical Physics. Moscow: MSU, pp. 477-485. (In Russ.)

About the Author

Yulia I. Yakhina – Junior Software Engineer, Engineering-Analytical Group, Department of Scientific Research, Termosim LLC

59/1 Magistralnaya str., Kazan, 420108, Russian Federation

E-mail: vib-210@mail.ru

Manuscript received 29 January 2018;
Accepted 28 April 2018;
Published 30 June 2018

ORIGINAL RESEARCH ARTICLE
DOI: https://doi.org/10.18599/grs.2018.2.115-121

Expanding the experience of using non-stationary waterflooding technology with changing direction of the filtration flow in the example of the Northern Buzachi field

E.M. Almukhametova
Branch of Ufa State Petroleum Technical University in Oktyabrsky, Ufa, Russian Federation
E-mail: elikaza@mail.ru

Abstract. The last few years, work has been carried out to study the effectiveness of non-stationary exposure in the highly viscous oil field Northern Buzachi (Republic of Kazakhstan). It has been proved that this technology is quite effective in the development of highly viscous oil reservoirs, however, in order to constantly maintain high technological effect, a constant modification of this technology is required, since it has a characteristic feature of rapid «aging». Further search for the conditions of effective application of non-stationary exposure on highly-viscous oil deposits can be carried out in two directions: the implementation of non-stationary exposure in new areas with other reservoir parameters and the change in the parameters of non-stationary exposure technology (including combining with other technologies) in areas where this technology is already in use. Both approaches are used on the Northern Buzachi field. Thus, the positive experience of using non-stationary waterflooding in combination with changing direction of the filtration flow in the section of the seventh block of the Northern Buzachi field allowed us to recommend new sites for the implementation of this technology. With the participation of the author of this work, a non-stationary waterflooding program was developed and implemented on the site of the sixth block (south) of the first operational facility.

Keywords: hydrodynamic connection, carbonate, terrigenous reservoirs, erosion incisions, oil recovery coefficient, indicator studies, fluorescein, filtration current lines

Recommended citation: Almukhametova E.M. (2018). Expanding the experience of using non-stationary waterflooding technology with changing direction of the filtration flow in the example of the Northern Buzachi field. *Georesursy = Georesources,* 20(2), pp. 115-121. DOI: https://doi.org/10.18599/grs.2018.2.115-121

In order to maintain a constant high technological effect from the use of non-stationary technology in the Northern Buzachi (Republic of Kazakhstan) high-viscosity oil field, it is rationally to combine it with other technologies (Ogandzhanyants, 1969; Zhang et al., 2010; Zhdanov et al., 1996).

Let us consider the experience of using the technology of non-stationary exposure in combination with the MDFF (modifying directions of filtration flows) technology in the section of the sixth block (the southern part of the first operational facility).

The main geological and physical characteristics of the first operational site of the Northern Buzachi field (the Jurassic horizons Yu_1 and Yu_2) are presented in Table 1. The main distinguishing features of the geological structure of the deposit are high average permeability of the reservoir, high layered heterogeneity of the permeability field, high viscosity of the reservoir oil.

The structure of oil reserves of Jurassic deposits in the area of the NE (non-stationary exposure) site (Fig. 1) of the sixth block, Northern Buzachi field is shown in Fig. 2. Structuring of the reserves is carried out according to the following main indicators: permeability, layered heterogeneity, zonal heterogeneity of the reservoir, reservoir type, clay index. The intervals of the change in indices, dividing the investigated values into groups, were determined on the basis of the statistical distributions of the parameters of the reservoir properties. During the analysis of the geological structure features of oil deposits in the Northern Buzachi horizons (Nauchno-tekhnicheskoe soprovozhdenie razrabotki mestorozhdeniya Severnye Buzachi, 2014), it was established that the main parameters determining possible complications in the field development are the presence of extensive contact water-oil zones, high layer heterogeneity of permeability properties of the reservoir, zone heterogeneity of permeability. Therefore, the study of oil reserves distribution by these parameters is of particular interest (Almukhametova, 2016).

Parameters	I object
Average depth of occurrence, m	470
Gas and oil contact, m	428-436
Type of deposit	bedded roof fault-bounded
Type of reservoir	terrigenously-porous
Average total thickness, m	47.6
Average net oil thickness, m	20.8
Average net gas thickness, m	4.6
Average porosity, un.fr.	0.34
Average permeability, mkm^2	2.43
Initial oil saturation coefficient, un.fr.	0.73
Sandiness coefficient, un.fr.	0.42
Compartmentalization coefficient, un.fr.	5.9
Initial reservoir temperature, ^{0}C	29.7
Initial reservoir pressure, MPa	5.8
Viscosity of oil in reservoir conditions, mPa*s	380
Density of oil in reservoir conditions, t/m^3	0.92
Formation volume factor, un.fr.	1.029
Initial (current) saturation pressure, MPa	3.97 (2.29)
Initial (current) gas content, m^3/t	11.8 (7.39)
Viscosity of water in reservoir conditions, mPa*s	1.05
Density of water in reservoir conditions, t/m^3	1.04

Table 1. Basic geological and physical characteristics of the first operational facility of the Northern Buzachi field

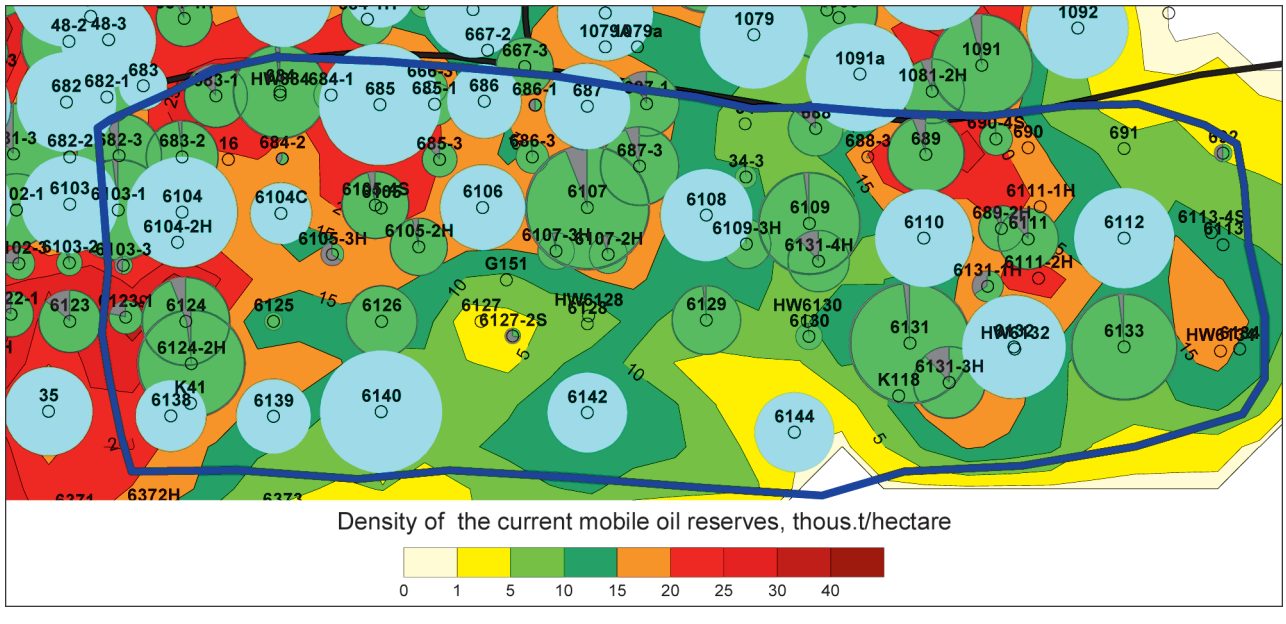

Fig. 1. The map fragment of the current mobile oil reserves of the first operational facility. The area of the non-stationary flooding of Block No. 6. The blue line indicates the contour of the NE site.

Figure 2a shows that for reservoirs of the Jurassic sediments, more than 71% of the oil reserves of the site are concentrated in reservoirs with a high and ultra-high average permeability in the section. In low-permeability zones there is an insignificant share of reserves (2%). The site is fairly homogeneous in permeability along lateral. The overwhelming share of oil reserves (70%) is located in the reservoirs with a small zone heterogeneity of the permeability field (Fig. 2b). A wide spread of average permeability values is accompanied by high (and even super high) values of layered heterogeneity of permeability properties of the reservoir. A significant part of the geological reserves of oil is located in the reservoirs, the permeability of which differ by tens and hundreds of times (55%). 44% of all geologic oil reserves of the facility are concentrated in relatively homogeneous reservoirs (Fig. 2c). The distribution of oil reserves according to the clay index of the reservoir shows that a significant part (43%) of the oil reserves is located in clay reservoirs (more than 20%) (Fig. 2d). This fact brings to the forefront the problem of changing the reservoir properties when it is flooded (Almukhametova, 2016).

Calculations show that when the ultimate water cut is reached, up to 26.2% of all geological reserves and 25.1% of all the mobile oil reserves of the Jurassic deposits of the site remain in the undeveloped reservoir intervals (Almukhametova, 2016). Therefore, the use of

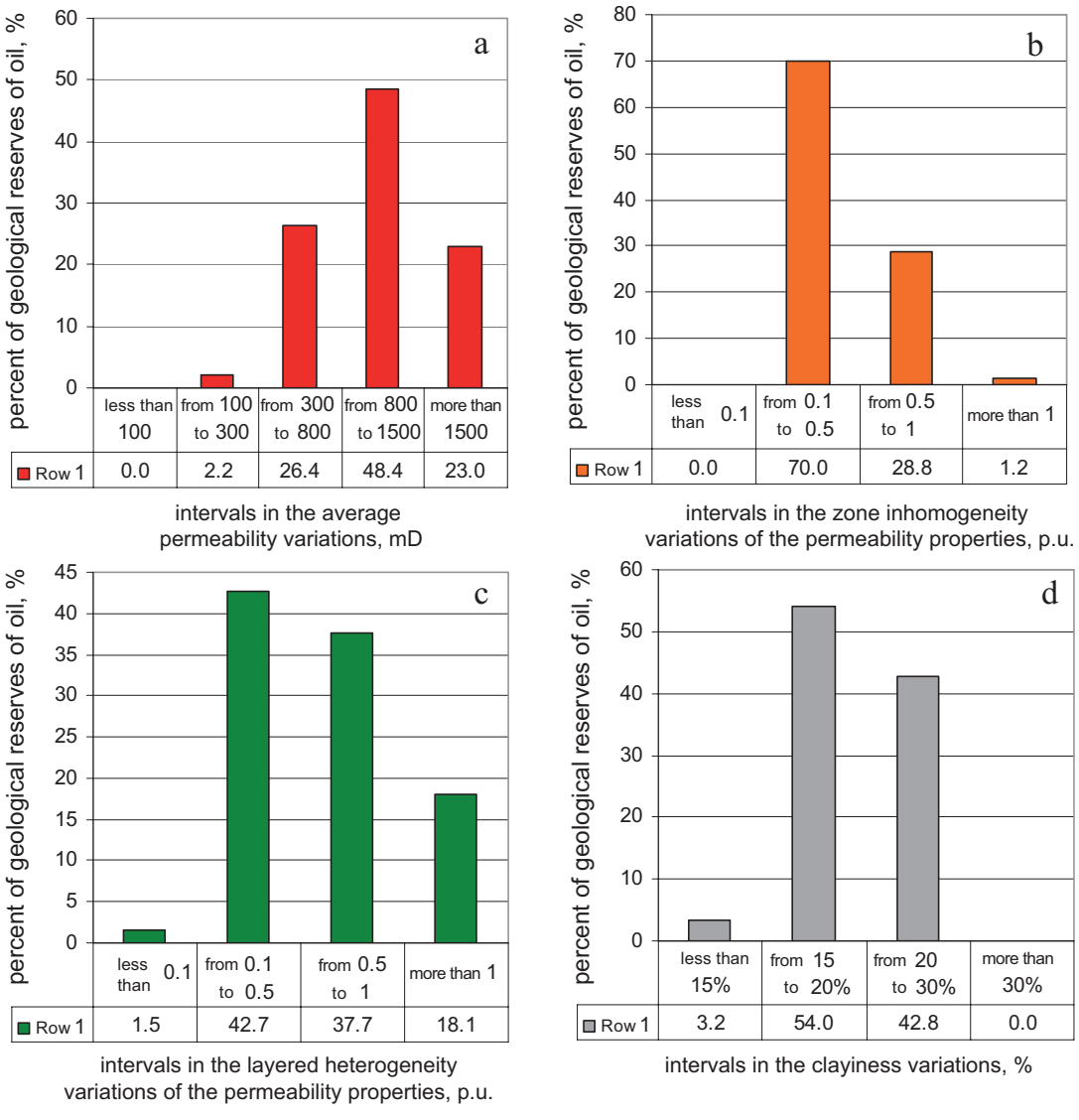

Fig. 2. Distribution of the initial geological reserves of oil in the Jurassic deposits in the area of the NE section of the sixth block along the intervals in the average permeability variations of the reservoir (a), the zone inhomogeneity of the permeability properties of the reservoir (b), layered heterogeneity of the permeability properties of the reservoir (c), clayiness (d) (according to the data (Almukhametova, 2016)).

technologies allowing to connect to active drainage the oil reserves concentrated in the low permeable layers of the reservoir is extremely relevant for the development of the sixth block of the Northern Buzachi field.

Let us consider the dynamics of technological indicators of site development. Figure 3 shows the dynamics of the average monthly production rate and watercut of production in recent years. It can be seen that in recent years (up to 04.2014 –the beginning of the application of NE), the dynamics of the average monthly oil production is characterized by significant fluctuations in its magnitude, which is due to geological and technical measures being carried out at the site. The watercut of the production is slowly increasing. The current compensation for liquid withdrawals by water injection as of 04.2013 was 87%, accumulated compensation – 65%.

Analysis of the production of oil reserves from the first production facility of the NE section of the sixth block shows that as of 01.03.2014 the current oil recovery factor was 0.114 unit shares.

At the same time, the current water cut in the whole area (Jurassic) is 90.8%, the extraction from approved initial recoverable reserves is 35%.

In April 2014, the application of NE technology in combination with the technology of changing the direction of the filtration flow was started at the site. According to the program for the introduction of non-stationary waterflooding in the section 13, exposing injection wells were divided into the northern and southern rows (Scientific and technical support for the development of the Northern Buzachi field, 2014). The northern row includes wells Nos. 685, 6104, 6104C, 6106, 6108, 6110, 6112, the southern row – 6132, 6138, 6139, 6140, 6142, 6144. Groups of injection wells operate in antiphase, i.e. when the wells of the northern row are pumping, the injection wells of the southern row are idle, and vice versa.

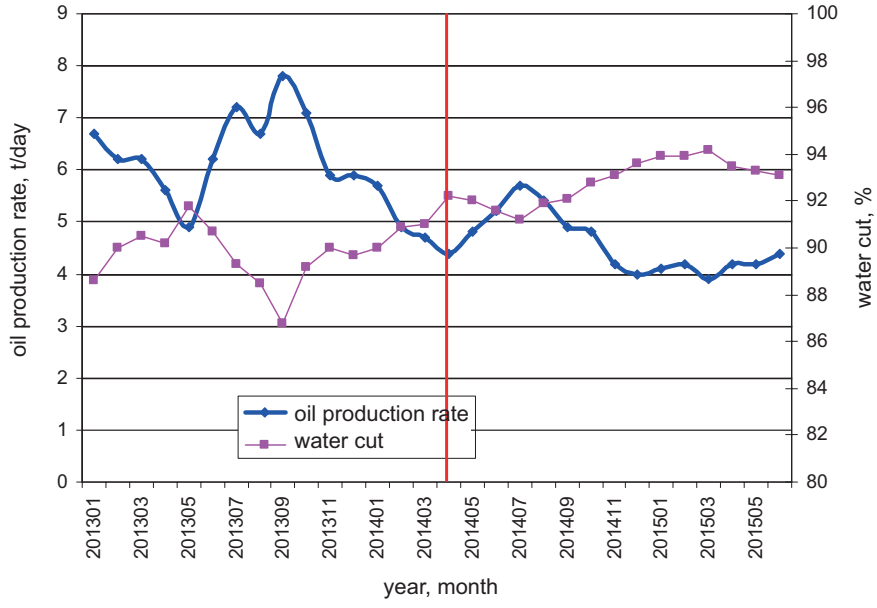

Fig. 3. Dynamics of the average monthly oil production and water cut of the southern section of the sixth block (section NE) in recent years. The first operational site of the Northern Buzachi field

The duration of the half-life of the operation/shutdown groups of the injection wells was determined from the hydrodynamic studies of the injection wells (the pressure drop curve method). Based on the piezoconductivity values obtained and the average distances between the injection and production wells, the mean time of propagation of the pressure change was determined, which was taken as the half-cycle duration. The duration of half-periods of operation/shutdown of injection wells in this area was 6 days.

According to the historical data of the operation of injection wells, the possibility of increasing their injectivity was established, and the operating modes of the water supply system of the reservoir pressure maintenance system of the section were determined during periodic operation of groups of injection wells (Vladimirov, Veliev, Almukhametova, 2014). Due to the fact that all injection wells of the site are supplied with water from a group of water intake wells, regulation of the volumes of injected water during non-stationary flooding was not difficult.

In addition, regimes of non-stationary water flooding were developed in the summer and winter periods of the year. In summer, non-stationary water flooding was applied with the shutdown of groups of injection wells, in winter – with periodic restriction of water injection into groups of wells. In order to avoid complications in the work of reservoir pressure maintenance wells in the winter, the minimum values of the injectivity were established for injection wells, at which the water did not freeze in the water ducts. These injectivity values were taken as the lower threshold for the values of the daily water injection at NE in winter.

The non-stationary water flooding in the area under consideration was started from the stop of the injection wells of the northern row by 5 days. Later, the duration of the half-period varied from 5 to 7 days (Fig. 4). Symmetric cycles with the downtime of injection wells equal to the time of their operation were used.

All 45 production wells were considered as reacting production wells.

By the beginning of the implementation of non-stationary waterflooding technology (04.2014), the dynamics of indicators was characterized by a decrease in oil production with increasing water cut in production. At the beginning of the NE, the average monthly water cut was 92.2%, the average monthly oil production decreased to 4.4 tons per day with a flow rate of 56 tons per day. Average monthly injectivity was 120 m^3/day.

Let us consider the change in technological indicators as a result of applying the technology of non-stationary impact. Figure 3 shows that the beginning of non-stationary waterflooding with the use of technology to change the direction of filtration flows is accompanied

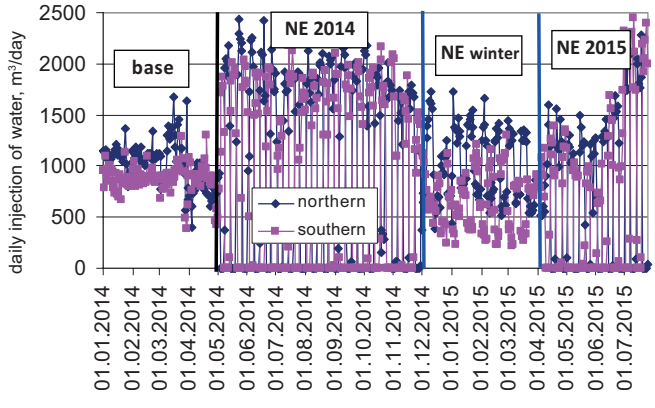

Fig. 4. Cyclical switching on and switching off of series of injection wells in the southern section of the sixth block (the first operational facility). Dynamics of daily injection of injection wells

by an increase in the average oil production rate and a decrease in water cut of the products. However, starting from August 2014, there is a tendency to increase watercut production and reduce oil production. It would seem that the effect of using the technology is over. However, as the comparison of the rate of decline in oil production shows, during the non-stationary waterflooding period 08.2014-12.2014 the rate of decline in oil production is less intensive.

The non-stationary waterflooding on the site in question was carried out continuously during 2014-2015. In winter, the periodicity of the exposure was carried out by limiting the injection along the rows of injection wells (Vladimirov et al., 2014; Khalimov et al., 2014). When switching to the winter regime of non-stationary flooding technology with a change in the direction of the filtration flow, stabilization of oil production and water cut is observed (Vladimirov et al., 2016). With the onset of non-stationary injection in 2015 with shutdown of the series of injection wells, there was a slight decrease in water cut and an increase in oil production.

Thus, non-stationary water flooding at the site allows reducing the rate of decline in oil production and the growth of water-cut production.

Calculation of the efficiency of the applied NE technology was carried out on the basis of displacement characteristics. During the base period, the period of stationary injection on the site was taken. The results of calculating the technological efficiency of NE in combination with the MDFF are presented in Table 2. It should be noted that the magnitude of the effect differs greatly for different displacement characteristics from 3.076 to 10.343 thousand tons. The final value of the effect from the technology of non-stationary water flooding is taken as the average value obtained for the five best displacement characteristics. Evaluation of the effect as of 01.07.2015 showed that the effect of using the technology of non-stationary water flooding amounted to 7.230 tons of additional oil produced.

Let us note some features of the NE use in this area. The first – there are wells of the main and fill-in stocks on the site. The wells of the fill-in stock were drilled at a time when some of the production wells of the main stock were already working with a sufficiently high water cut of the production. In this case, the wells of the fill-in stock were located at smaller distances from the injection wells than the wells of the main stock. Therefore, the problem arises of estimating the technological effect of NE + MDFF by categories of wells.

As a result of the effectiveness analysis of the applied technology of non-stationary exposure on the wells of the main and fill-in stocks, it was found that the maximum specific effect falls on the wells of the fill-in stock (Table 3, Fig. 5a). In general, for

Characteristics of displacement	Technological effect size, t	Duration of effect, month	Theil Index, relat. un.
Qo(1/Ql)	10343	14	3.12E-04
lgQw/Qo(lgQw)	3076	6	3.28E-04
Qo(1/SQR(Ql)	10257	14	3.72E-04
Ql/Qo(Qw)	7213	14	4.06E-04
Qo(lgQw)	5260	14	4.30E-04
Average for the three best	7230	12.4	

Table 2. The technological effect of the application of NE + MDFF on the section of the 6th block (south) of the first operational facility in 2014-2015 (Almukhametova, 2016)

the analyzed period, the specific effect on the wells of the main stock was 325 tons/ well (23 tons / (well month)), the fill-in stock – 563 tons/well (40 tons / (well month)) (Almukhametova, 2016). Thus, the difference in efficiency of the non-stationary waterflooding on the wells of the fill-in and main stocks is significant. The higher effect of NE + MDFF on the wells of the fill-in stock is due to two reasons: the first is the higher amplitude of non-stationary exposure (the well is closer to the source of exposure), the second is less the degree of high-permeability channel production (shorter work time), which increases the efficiency of changing the direction of filtration flows.

The second feature is the use by the subsoil user at the NE site of changes in the operating modes of production wells (optimization). In this case, optimization of operating modes of production wells was mainly aimed at increasing liquid flow rates. In the period of non-stationary flooding, optimization of operating modes of production wells in more than 58% of the well stock of the site was carried out at the site.

Evaluation of the effect of the joint application of optimization technology and non-stationary waterflooding showed that the specific effect was 1.5 times lower in wells where the complex effect (NE + optimization) was applied in comparison with the wells that were located only in the zone of non-stationary water flooding (Table 4, Fig. 5b).

Decrease in the efficiency of NE + MDFF technology in wells with optimization is associated with a sharp increase in water cut in these wells and an increase in liquid production (disproportionate to the change in phase fractions in the flow). On the displacement characteristics, this measure is reflected as a deterioration in the quality of oil displacement, although in some cases there was an increase in daily oil sampling with increasing water cut.

Conclusions

The North Buzachi high-viscosity oil field has become a testing ground for the application of non-stationary water flooding technology. It is well known that waterflooding on deposits of high-viscosity oil is of low efficiency because of the high difference in mobility

Fund	Main	Fill-in	Total
Number of wells, pcs	11	22	33
Cumulative effect, t	3572	12384	15956
Specific effect, t/well	324.7	562.9	483.5

Table 3. Distribution of the effect of NE on the wells of the main and fill-in stocks

Type of geological and technical measures	Cumulative effect, t	Number of wells, pcs	Specific effect, t/well	Percent of failed wells in a group, un.fr.
optimization+ NE	8380	21	399.0	0.24
NE	7576	12	631.3	0.08

Table 4. Distribution of the effect of NE + MDFF on wells with the use of optimization and without it

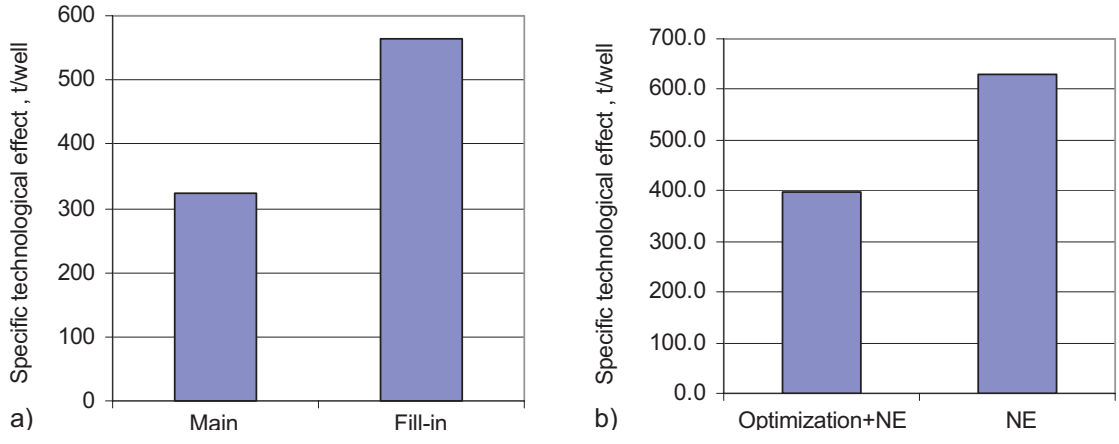

Fig. 5. Distribution of the effect of NE + MDFF on the wells of the main and fill-in stocks (a), along the wells with the use of optimization and without it (b)

of fluids. However, non-stationary water flooding increases the efficiency of the current development system even with a high difference in viscosity of oil and water.

The results presented in the paper showed that the expansion of non-stationary waterflooding to new sections of the field, characterized by different reservoir properties, demonstrated a significant effectiveness of NE. At the same time, it should be noted that the technology of NE on deposits of high-viscosity oil has the property of rapid aging, i.e. their technological efficiency is rapidly decreasing. Therefore, along with the expansion of the use of NE in new areas of the field, it is necessary to constantly modify the applied NE technology. This direction has good prospects for increasing the effectiveness of non-stationary exposure.

The development of NE technology at the Northern Buzachi field has passed a number of stages. Originally cyclic waterflooding was used, which showed a significant technological effect. At the next stage (at the present time), cyclic waterflooding was combined with the technology of changing the direction of the filtration streams. In the future, cyclic waterflooding in conjunction with the MDFF will be combined with the periodic operation of high-yield high-water-producing production wells.

The application of NE + MDFF in the NE section of the sixth block (south) showed the following features. Fill-in wells that have large mobile reserves in the drainage zone than the wells of the main stock are more responsive to the technology of changing the direction of the filtration flow and the cyclic action. The average specific effect of NE for fill-in wells is 1.7 times higher than for wells in the main stock.

The second feature is the fact that the subsoil user has massively used optimization of the operating modes of production wells (mainly the increase in liquid rates). The application of this type of geological and technical measures significantly affected the efficiency of non-stationary water flooding in the area under consideration. Wells with the use of optimization have an average of 1.5 times less specific effect.

References

Khalimov R.N., Tazetdinov I.R., Korepanov D.I., Al'mukhametova E.M., Khalimov I.N., Gabdrakhmanov N.Kh., Petrova L.V., Nugaev R.Ya., Khazipov R.Kh. (2014). Issledovanie nagnetatel'nykh skvazhin s povyshennymi ust'evymi davleniyami vsledstvie vysokikh plastovykh davleniy avtonomnymi priborami metodom termometrii [Study of injection wells with high wellhead pressure and high reservoir pressure by autonomous equipment based on thermometry method]. *Problemy sbora, podgotovki i transporta nefti i nefteproduktov* [Problems of gathering, treatment and transportation of oil and oil products], 4(98), pp. 98-107. (In Russ.)

Nauchno-tekhnicheskoe soprovozhdenie razrabotki mestorozhdeniya Severnye Buzachi (2014). [Scientific and technical support for the development of the Northern Buzachi Oil Field (Contract No. SC12/113/00/S)]. Moscow, ZAO «Konkord», 369 p. (In Russ.)

Obosnovanie programmy geologicheskikh issledovaniy flyuidov. Informatsionnyy otchet o NIR po dogovoru «Nauchno-tekhnicheskoe soprovozhdenie razrabotki mestorozhdeniya Severnye Buzachi» (2013). [Feasibility of the Program of fluids geological studies. Research report on contract «Scientific and technical support for the development of the Northern Buzachi Oil Field» (Contract No. SC13/242/00/S)]. Moscow, ZAO «Konkord», 71 p. (In Russ.)

Ogandzhanyants V.G. (1969). Teoriya i praktika dobychi nefti pri tsiklicheskom zavodnenii [Theory and practice of oil production in cyclic waterflooding]. *Itogi nauki i tekhniki, ser. «Gornoe delo»* [Results of science and technology, ser. «Mining»]. Moscow, pp. 39-79. (In Russ.)

Vladimirov I.V., Al'mukhametova E.M., Varisova R.R. (2014). Vliyanie izmeneniya rezhima raboty dobyvayushchey skvazhiny na effektivnost' vyrabotki zapasov nefti. Teoriya [Effect of changing the producing well operation mode on the efficiency of developing oil reserves. Theory]. *Problemy sbora, podgotovki i transporta nefti i nefteproduktov* [Problems of gathering, treatment and transportation of oil and oil products], 2(96), pp. 15-16. (In Russ.)

Vladimirov I.V., Varisova R.R., Al'mukhametova E.M. (2016). Izmenenie rezhima raboty dobyvayushchey skvazhiny kak variant optimizatsii kollektora dvoynoy pronitsaemosti [Changing the mode of production wells as an option to optimize collector dual permeability]. *Neftegazovoe delo = Petroleum Engineering*, 14(4), pp. 40-44. (In Russ.)

Vladimirov I.V., Veliev E.M., Al'mukhametova E.M., Abilkhairov D.T. (2014). Primenenie nestatsionarnogo zavodneniya na zalezhakh vysokovyazkoy nefti s kollektorom dvoynoy pronitsaemosti. Teoriya [Application of non-stationary flooding for extra-viscous oil from the collector with dual permeability. Theory] *Problemy sbora, podgotovki i transporta nefti i nefteproduktov* [Problems of gathering, treatment and transportation of oil and oil products], 4, pp. 16-25. (In Russ.)

Vladimirov I.V., Veliev E.M., Al'mukhametova E.M. (2014). Opredelenie optimal'nykh periodov raboty/prostoya nagnetatel'nykh skvazhin pri nestatsionarnom zavodnenii zalezhey vysokovyazkoy nefti s kollektorom dvoynoy pronitsaemosti [Determination of optimal periods of operation/downtime of injection wells in the non-stationary flooding of high viscosity oil reservoirs with a double permeability collector]. *Energoeffektivnost'. Problemy i resheniya: materialy XIV mezhd. nauch.-prakt. konf.* [Power Efficiency. Problems and Solutions: Proc. XIV Int. Scientific and Practical Conf.], pp. 56-57. (In Russ.)

Zhang H., Bai B. (2010). Preformed Particle Gel Transport through Open Fractures and its Effect on Water Flow. SPE 129908, 16(2), pp. 388-400.

Zhdanov S.A., Miyan A.V., Surguchev L.M., Castanier L.M., Hanssen J.E. (1996). Application of Foam for Gas and Water Shut-off: Review of Field Experience. *European Petroleum Congress*, Milan, Italy, pp. 377-388.

About the Author

Elvira M. Almukhametova – PhD (Engineering), Associate Professor, Department of Exploration and Development of Oil and Gas Fields

Branch of Ufa State Petroleum Technical University in Oktyabrsky

54a Devonsky str., Oktyabrsky, 452607, Russian Federation

E-mail: elikaza@mail.ru

Manuscript received 9 February 2018;
Accepted 18 May 2018; Published 30 June 2018

ORIGINAL RESEARCH ARTICLE

DOI: https://doi.org/10.18599/grs.2018.2.122-132

Heat flow asymmetry on the mid-oceanic ridges of Northern and Southern Earth hemispheres

M.D. Khutorskoy[*], *E.A. Teveleva*
Geological Institute of the Russian Academy of Sciences, Moscow, Russian Federation

Abstract. A statistical analysis of heat flow (HF) distribution along nine geotravers crossing the mid-oceanic ridges in the Atlantic, Pacific and Indian oceans is carried out. A significant asymmetry in HF distribution is established – its mean values differ on opposite sides of the ridges axis. In the Earth southern hemisphere geotraverses, their western flank has a higher HF mean, and in the northern hemisphere geotraverses there is the eastern flank. Various tectonic factors that lead to such a distribution are taken into account, but the universal cause of this regularity is suggested to be the effect of the Coriolis force, which deflects the ascending magma flow in divergent zones, when the planet rotates, respectively, to the west – in the southern and to the east – in the northern hemispheres.

Keywords: heat flow, geotraverses, statistic, asymmetry, mid-oceanic ridge, Coriolis force

Recommended citation: Khutorskoy M.D., Teveleva E.A. (2018). Heat flow asymmetry on the mid-oceanic ridges of Northern and Southern Earth hemispheres. *Georesursy = Georesources*, 20(2), pp. 122-132. DOI: https://doi.org/10.18599/grs.2018.2.122-132

Detailed heat flow studies within the slopes of the mid-oceanic ridges and adjacent abyssal basins have shown that its distribution is not symmetric everywhere relative to the ridge axis in the same-type zones, but is subject to a complex redistribution mechanism that depends on many geological causes associated with tectonics and features of the structure of the lithosphere of these zones.

The presence of the geothermal asymmetry of the mid-ocean ridges (MOR) slopes, adjacent abyssal basins and passive parts of the transform faults in the Atlantic, Indian and Pacific Oceans was justified and confirmed on the basis of statistical processing of data from the global heat flow database along the geotraverses, Crossing MOR and covering the above structural elements of the oceanic crust (Podgornykh, Khutorskoy, 1998; Podgornykh, Khutorskoy, 1999; Khutorskoy, Teveleva, 2016; Khutorskoy, Polyak, 2017; Khutorskoy, et al., 2017). It is important to note that the MOR asymmetry is observed not only in the thermal field, but also in other geophysical fields: magnetic (Glebovsky et al., 1986) and gravity (Budanov et al., 1997), and also in the crust structure (Naryshkin, Pogrebitsky, 1986, Pushcharovsky et al., 1995).

The nature of this phenomenon was repeatedly discussed, and various geological and geophysical models were proposed to explain the existing asymmetry. Some researchers note the existence of different oceanic plates spreading rates on different sides of the ridges axis (Naryshkin, Pogrebitsky, 1986; Pushcharovsky et al., 1995; Schrader, 2001), others believe that the geodynamic processes in the adjacent plates differ, and on one of them the compression regime, which replaced the initial tension situation, creates overthrust structures characteristic for compression (Budanov et al., 1997; Pushcharovsky et al., 1995).

We previously proposed to consider the influence of the Coriolis force (Khutorskoy, Teveleva, 2018), which acts on any mass, moves along the radius of the rotating Earth and diverts this mass from the orthogonal trajectory, respectively, to the west in the southern hemisphere and to the east – in the northern hemisphere. An upward flow of magma in the divergent zones of the middle ridges can be considered as such a "mass". The deviation of this flow from a trajectory orthogonal to the planet's surface determines the observed geothermal asymmetry.

The purpose of this paper is a comparative analysis of the heat flow distribution along geotraverse crossing MOR in the southern and northern hemispheres of the planet. Naturally, we consider those MOR intersections, which are most representative of heat flow measurements. The compilation of measured heat flow values is reflected in global databases (Jessop et al., 1976; Pollack et al., 1992; Podgornykh, Khutorskoy, 1997; Hasterok, 2010).

To establish the fact of geothermal asymmetry

[*] *Corresponding author: Mikhail D. Khutorskoy*
E-mail: mkhutorskoy@ginras.ru

on the MOR slopes, we compared heat flow data for the same type of elements along the long profiles (geotraverses) crossing the ridges in the World Ocean: the Mid-Atlantic ridge, the East Pacific Rise and the West Indian Ridge (Fig. 1). Statistical sampling for each of these geotraverses is quite representative (Table 1) for comparative analysis.

The proof of the possible geothermal asymmetry of structural morphological elements along geotraverses is based on a statistical comparison of empirical data related to different its parts, in our case, to its western and eastern strike.

To verify of the statistically significant difference in the mean heat flow values, the parametric Cramer-Welch criterion (T) was used in the samples, the value of which is found from the formula (Gmurman, 2015):

$$T = \frac{\sqrt{mn}\cdot(\bar{x}-\bar{y})}{\sqrt{ns_x^2 + ms_y^2}},$$

where $\bar{x}, s_x^2, n$ and $\bar{y}, s_y^2, m$, respectively, sample means, variances, and the amount of data from two comparative samples.

If $T < \varphi(1-\frac{\alpha}{2})$, where $\varphi(1-\frac{\alpha}{2})$ is the inverse of the normal distribution function from the significance level α, where α = 1 – P, P is the confidence probability, then the hypothesis of homogeneity of the mean heat flow values, i.e. the existence of asymmetry is not confirmed.

No. geotraverse	No. 1 Angola-Brazil		No. 2 -31° s.l.	
west/east	west	east	west	east
Average value of heat flow	62	39	91	61
Standard deviation	25	21	94	62
Number of measurements	16	18	6	27
Value of Cramer-Welch criterion	3		0,99	
Confidence probability	99%		70%	

Table 1. Statistical characteristics of geotraverse in the southern hemisphere of the Atlantic Ocean

If $T \geq \varphi(1-\frac{\alpha}{2})$, then the hypothesis is accepted that the average values for the considered feature are non-uniform, and the asymmetry is confirmed. With a significance level α = 0.05 (at P = 95%), the critical value of the Cramer-Welch criterion is T = 1.96. Therefore, if the value of the criterion does not exceed this value, then it is necessary to accept the hypothesis of homogeneity of the sample data by the mean value. If the value of the criterion is greater than or equal to the critical value, then the samples by the mean value are recognized as different.

Southern hemisphere of the Earth

In the southern hemisphere, we analyzed the heay flow distribution along five geotraverses: 1) Angola-Brazil geotraverse (12 °S), 2) geotraverse along 31 °S – in the

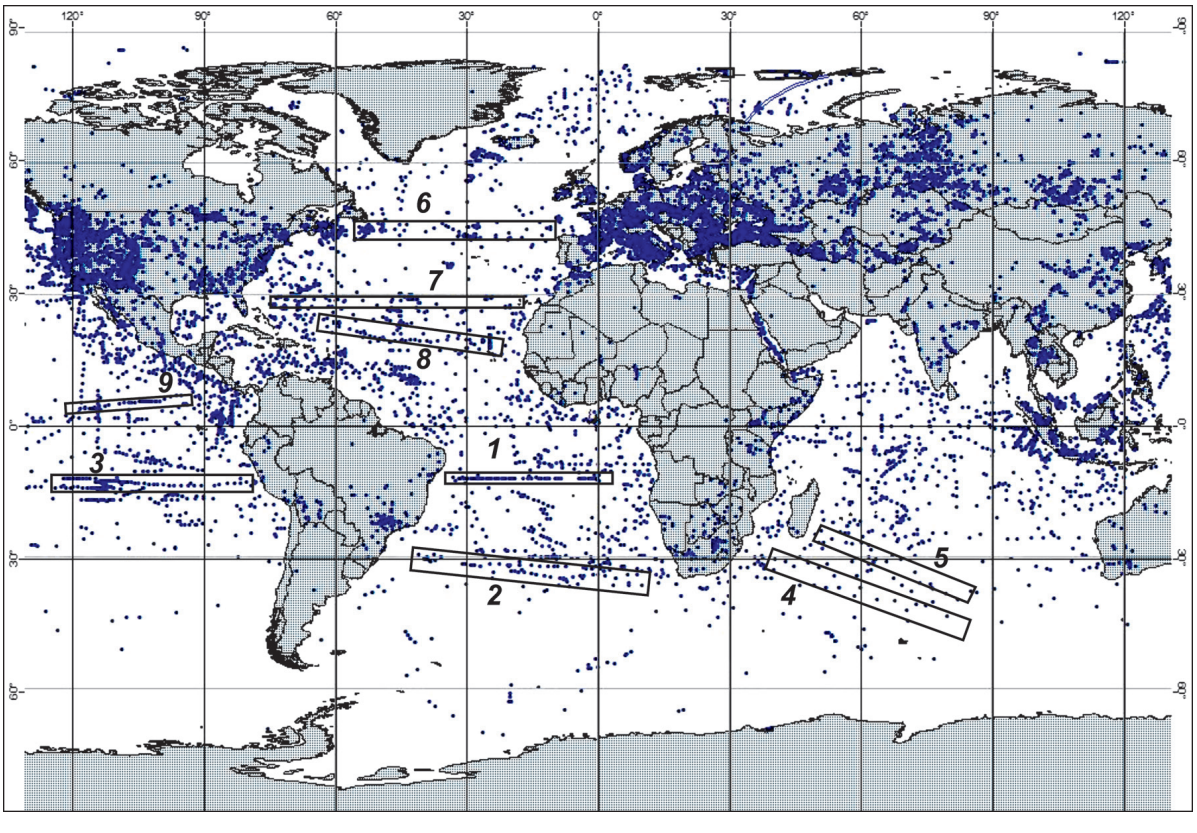

Fig. 1. The scheme of the location of the measurement points of the heat flow and the investigated geotraverses in the World Ocean (see the text for the numbers)

Atlantic Ocean; 3) geotraverse 15 °S – in the Pacific Ocean, as well as geotraverse in the Indian Ocean: 4) the southern part of the Crozet-Mozambique Basin and 5) the northern part of the Crozet-Madagascar (Fig. 1).

Atlantic Ocean

Most of the geothermal data for the Angolo-Brazilian geotraverse (No.1) was obtained during many years of expeditionary geological and geophysical research by VNIIOceangeology (Podgornykh, Khutorskoy, 1998; Popova et al., 1984; Pogrebitsky et al., 1990; Mashchenkov, Pogrebitskii, 1995).

Within the Angola-Brazil geotraverse, detailed heat flow measurements, gravitational and magnetic fields, the bottom relief, and a large volume of seismic surveys were carried out.

The bottom morphostructure along the geotraverse conform to the traditional transoceanic structures scheme (Naryshkin, Pogrebitsky, 1986). In the central part of the geotraverse there is a mid-Atlantic uplift, on both sides of which abyssal plates lie (the Angolan and Brazilian basins) and the marginal-continental flexures (African and South American continental slopes with foothills) interfaced with plates (Fig. 2). The listed first-order structures are complicated by a system of subordinate and superimposed morphostructures: mosaic-cellular and linear-ridge uplifts, plateaus, troughs, volcanic buildings of central type are distinguished. Despite the smooth interface of structures in general, longitudinal zones relative to the middle ridge of the zone are contacted by faults. Based on the landscape characteristics (size, amplitude, orientation), the asymmetry of the wings of the median uplift is noted: in the formation of the basalt bed, the tectonic -magmatic activity was most intensively manifested in the western "Brazilian" wing (Pogrebitsky et al., 1990).

The structure of the magnetic field of the western and eastern flanks of the uplift is also asymmetric. The anomalies of the western flank are characterized by a relatively high intensity (up to 150 nT) and a more consistent linearity. They are well identified up to the 33rd anomaly inclusive. Anomalies of the eastern flank are characterized by smoothed (up to 100 nT) fragmentarily linear field with alternating signs, and the correlation is quite arbitrary here (Mashchenkov, Pogrebitskii, 1995). Asymmetry in the structure of the anomalous magnetic field of the western and eastern flanks of the middle elevation is also established on the geomagnetic cross-section: the surface of the lower edges of magnetized bodies on the western flank does not deeper than 12 km, and in the east reaches 20 km from the ocean surface.

According to the data of CDP, there are structural seams buried beneath the sedimentary cover. On the seismic section, they are expressed in the form of a powerful reflector that passes through the entire crust and displaces the Moho surface. Although these seams are not expressed either in the bottom relief or in the gravitational field, in the structural plan they also give grounds for assuming the asymmetry of the

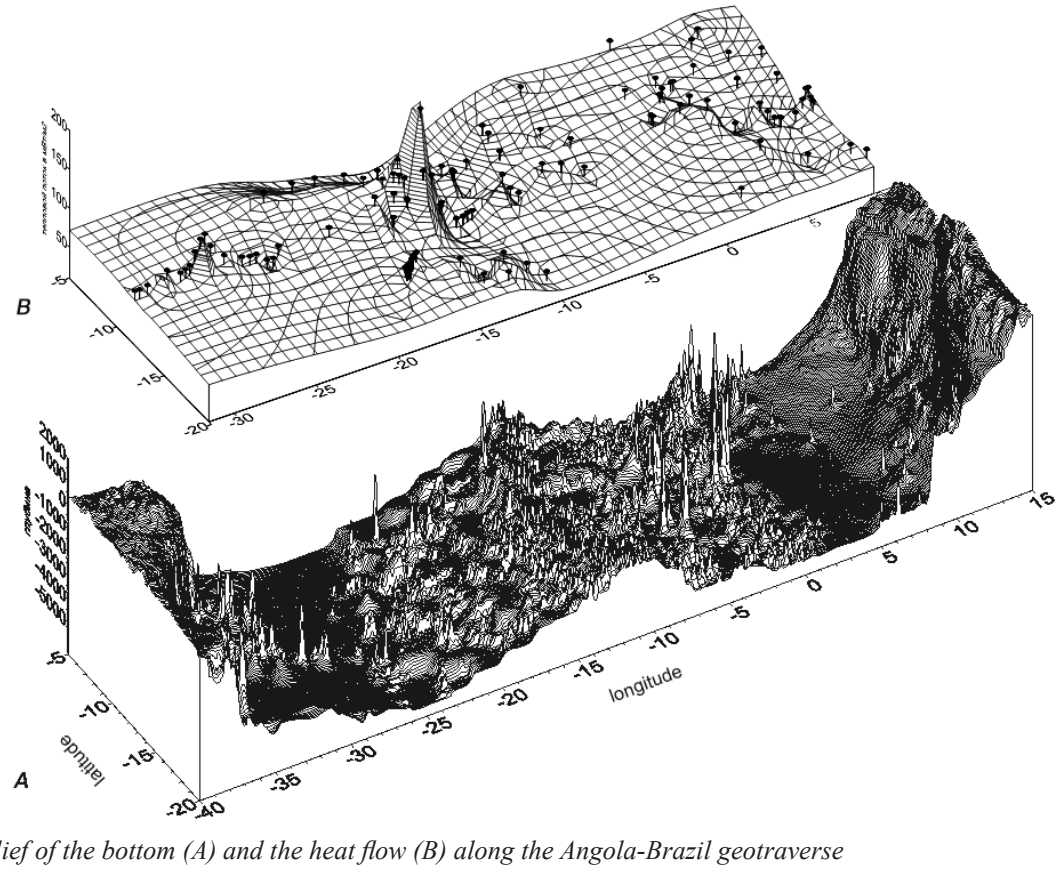

Fig. 2. The relief of the bottom (A) and the heat flow (B) along the Angola-Brazil geotraverse

underlying tectonic processes. On the Angolan seam, the oceanic lithosphere is advancing on the surface of the paleocontinental slope toward the continent, and on the Brazilian slope listric slipping off is observed.

The observed asymmetry in the deep structure of the slopes and abyssal basins along the geotraverse, as well as in the magnetic field, is naturally related to the difference in the energy of the geodynamic processes, which can be judged from the analysis of geothermal data. They showed, at statistical processing and calculation of the Cramer-Whelch criterion, a significant difference in heat flow on different sides of Mid-Atlantic Ridge. Thus, the average heat flow to the west of the Mid-Atlantic Ridge is 62 mW/m^2, and to the east 39 mW/m^2 (Table 1).

Discussing the reasons for the geothermal asymmetry of the ridge, we can agree in the first approximation with the authors of the report (Pogrebitsky et al., 1990, p. 21), who explain it "... by the absence of a single mechanism for the formation of the oceanic lithosphere", but the result obtained by us suggest the presence of additional deep thermal sources, which caused an increase in heat flow on the western flank of the ridge in the geotraverse zone.

We can assume either the presence of different lithosphere thicknesses from the western and eastern sides of the ridge (in this case, differences in the background heat flow values will remain in the stationary geothermal field), or the action of non-stationary and later geodynamic processes that altered the thermal structure of the already formed oceanic lithosphere.

The first of our assumptions does not agree with the independent geophysical results obtained in the study of geotraverse, and also with estimates of the lithosphere thicknesses from the bottom bathymetry data (Mashchenkov et al., 1998). The second assumption is more real, because structural heterogeneity and the presence of superimposed tectonic processes in the formed lithosphere is confirmed by magnetometry and seismic profiling data.

Geotraverse along 31 °S stretches from the Cape basin in the east to the Plateau Rio-Grande in the west of the Atlantic Ocean. In the geotraverse strip[1], there are 6 measurements to the west of the Mid-Atlantic Ridge and 27 measurements to the east. Applying the same method of data comparison, we calculated that the average heat flow west of Mid-Atlantic Ridge is 91 mW/m^2, and to the east 61 mW/m^2, i.e. came to a similar result: the western flank of the Mid-Atlantic Ridge on the geotraverses of the southern hemisphere in the Atlantic has a higher heat flow (Table 1).

As was announced above, we will discuss more general and universal models for explaining the observed asymmetry of heat flow after characterizing all geotraverses.

Pacific Ocean

In the southern hemisphere of the Pacific Ocean, we examined one geotraverse crossing the East Pacific Rise at 15 °S. The East Pacific Rise represents one of the main links of the global chain of mid-oceanic ridges. In the southeastern Pacific it serves as a boundary between the Pacific plate in the west and the plates of the Antarctic, Chilean, Nazca and Cocos in the east. Morphologically, the uplift is expressed in the form of a wide (1000-1200 km) swell with gentle slopes dissected into large and small blocks, among which submarine volcanic mountains or volcanic arrays are elevated. Parallel to the main axis of the East Pacific Rise, sometimes there are clay-volcanic uplifts of relatively small extent. The crest of the East Pacific Rise is located at a depth of 2-3 km, and only a few individual volcanoes rise to less than 2 km. The highest point of the ridge in this part of the ocean is Easter Island, located in the zone of its connection with the latitude-volcanic Sala y Gomez ridge.

The peculiarity of the East Pacific Rise, which distinguishes it from other middle ridges, is the absence of a longitudinal rift valley and its ridge framing, which is explained by the high rate of spreading (up to 16 cm/year), at which abundant masses of magmatic material arriving at the surface completely fill rift valley (Naryshkin, Pogrebitsky, 1986; Menard, 1966).

Sedimentary layer on the rise is quite thin, and in a number of places and generally absent. The second layer, represented mainly by basalts, has a thickness of 1 km, and the "basalt layer", which, judging by the results of dredging on the Heizen fault in the 24th cruise of the Academik Kurchatov R/V, consists of amphibolite shales, 6-3.7 km, which is almost 2 km less than the thickness of this layer outside the East Pacific Rise. G. Menard in his works called the East Pacific Rise as a meganticlinal uplift of the oceanic crust, in which the layers gradually become thinner as they approach the crust (Gainanov, 1980).

Throughout the course of the East Pacific Rise, it is dissected by numerous transform faults, over which its blocks are sometimes displaced over considerable distances. For example, the displacement of the East Pacific Rise axis in the Heisen and Tharp faults of the Eltanin transform system between 53 and 57 °S reaches 15 ° in longitude, i.e. more than 1500 km. The nature of the displacements varies along the strike of the East Pacific Rise: to the south of the parallel 40 °S the right-hand displacements predominate, between 40 ° and 20 ° S – left-sided, and northern of 20 °S, right up to the junction with the latitudinal Galapagos uplift, again right-sided ones predominate.

Many researchers also note similar features in the geophysical fields of the southern part of the mid-Atlantic ridge and the East Pacific Rise in the southeastern Pacific

[1] *The sampling of the heat flow data included all measurements located in a stripe ± 2° from the geotraverse axis.*

(Kuo, Forsyth, 1988). This similarity is expressed in identical anomalies of the total geomagnetic field vector and gravitational anomalies in the free air reduction.

American and Canadian scientists obtained the main volume of geothermal measurements in this part of the Pacific Ocean. Nevertheless, about 50 heat flow measurements were carried out by Russian scientists, including the authors of this work, during the 14th cruise of the "Dmitry Mendeleyev" R/V and the 24th cruise of the "Akademik Kurchatov" R/V (Popova et al., 1984).

Geotraverse area 15 °S is characterized by the highest geothermal knowledge from all considered objects. A total of 7260 heat flow measurements were analyzed here, of which 3740 are located western of the East Pacific Rise axis, and 3520 are to the east. The calculation of the statistical difference in the samples showed that at this intersection of the East Pacific Rise there is a significant asymmetry of the heat flow: its mean value to west of the ridge is 88 mW/m^2, and to the east 72 mW/m^2 (Table 2).

Indian Ocean

In this paper, we analyzed heat flow distribution on the flanks of the South-West Indian Ridge (Fig. 1). It is morphologically divided into the West-Indian ridge and the African-Antarctic ridge, the connection of which occurs in the zone of the Prince Edward transform fault at 37 °E (Fig. 3). The ridges are characterized by an intensely subdivided relief with a height difference of up to 4 km. They are intersected by numerous transform faults, displacing the modern spreading axis sometimes for tens of miles (Schrader, 2001).

South-West Indian Ridge refers to slowly spreading ridges (Hosford, 2001). The spreading rate here, on the average, does not exceed 14 km/million years (1.4 cm/year)[2], and the accretion of the crust on both sides of the ridge axis is sharply asymmetric. So, on the "Antarctic" side it is 8.5 km/million years, and on the "African" side it is 5.5 km/million years (Cannat et al., 1999). Along the strike of South-West Indian Ridge,

No. geotraverse	No. 3 -15°s.l.	
west/east	west	east
Average value of heat flow	88	72
Standard deviation	61	59
Number of measurements	3745	3520
Value of Cramer-Welch criterion	2,84	
Confidence probability	99%	

Table 2. Statistical characteristics of geotraverse in the southern hemisphere of the Pacific Ocean

[2] *For comparison, the average spreading rate is 2.5 cm/year on the Mid-Atlantic ridge.*

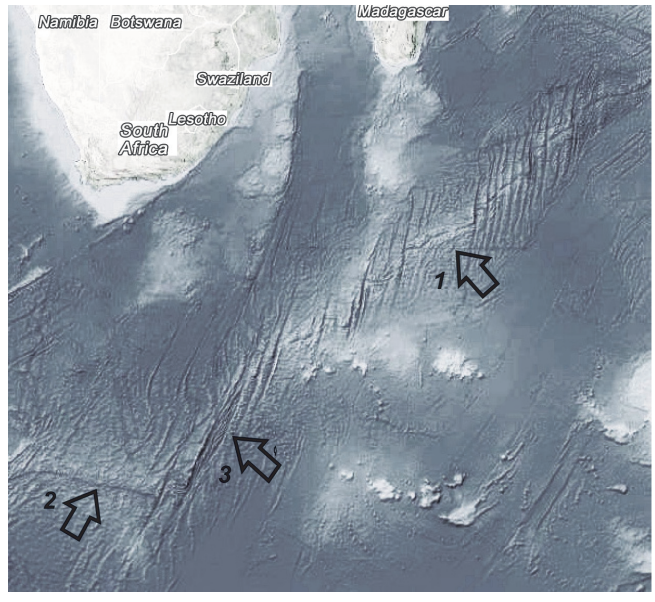

Fig. 3. Morphological scheme of the South-West Indian Ridge. The arrows show: 1 – West Indian ridge; 2 – the African-Antarctic ridge; 3 – the transform fault of Prince Edward.

structural asymmetry is also observed. The parts of the ridge lying west of the Andrew Bayne transform fault (30 °E) and east of the Malville transform fault (61 °E) are characterized by an abnormally deep axial valley, oblique spreading, a small central magnetic anomaly and unstable morphological manifestation at the bottom of transform faults passive parts (Patriat et al., 1997; Cannat et al., 1999).

Such properties of the peripheral parts of South-West Indian Ridge allow us to assume that they have a relatively "cold" mantle, a strong and thick lithosphere and limited magma reserves. On the contrary, the central part of South-West Indian Ridge, between 30 and 61 °E, is characterized by superficially manifested transformations in the relief, orthogonal spreading and a pronounced central magnetic anomaly (Patriat et al., 1997). Within this part of South-West Indian Ridge, between the transform faults of Atlantis II (56 °45'E) and Navar (58 °40'E), lies a segment which, judging by the spreading rate, can be compared with most segments Mid-Atlantic ridge.

Thus, South-West Indian Ridge is characterized by structural and morphological asymmetry along and across its strike.

In the southwestern part of the ocean, since the late 60s of the 20th century, expeditions to American, French and Japanese research vessels have been carried out repeatedly, including heat flow measurements (Anderson et al., 1977; Anderson et al., 1979, Courtney, Recq, 1986, Hyndman et al., 1987). The compilation of the measured heat flow values is reflected in global databases (Jessop et al., 1976; Pollack et al., 1992; Podgornykh, Khutorskoy, 1997; Hasterok, 2010). Figure 4 shows all known points of measurement in this part of the Indian Ocean.

To establish the fact of geothermal asymmetry on the flanks of West Indian Ridge, we compared the samples of heat flow data along two long geotraverses crossing the ridge (Fig. 4). Statistical sampling for each of these geotraverses is quite representative (Table 3) for comparative analysis.

Thus, in the southwestern part of the Indian Ocean, we note the presence not only of a structural but also a geothermal asymmetry of the West Indian Ridge relative to its axis. The western slope and the adjacent abyssal basin are characterized by a higher heat flow than the eastern part of the West Indian Ridge in the strip of both geotraverses.

Summing up the statistical analysis of the asymmetry of the MOR of the southern hemisphere, we note that for all crossings of ridges in the three oceans of the Earth, the western flank has a higher heat flow than the eastern one.

Northern hemisphere of the Earth

In the northern hemisphere four geotraverses were considered: 6) geotraverse 45 °N, 7) Canary-Bahamian geotraverse (28 °N), 8) geotraverse 19 °N, – in the Atlantic and 9) geotravers 10 °N in the Pacific Ocean.

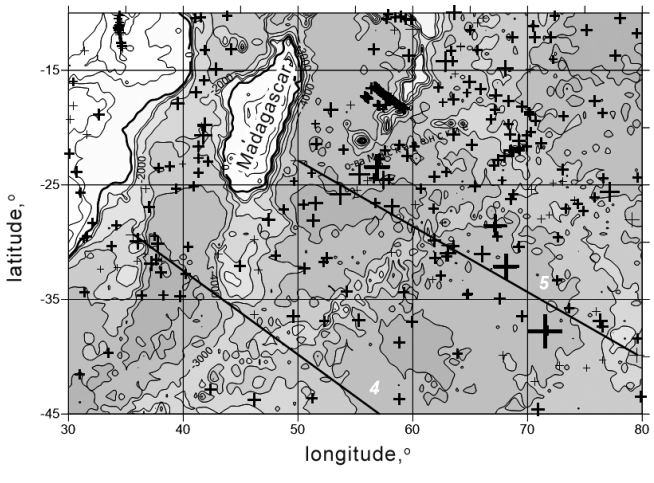

Fig. 4. Bathymetric map of the southwestern part of the Indian Ocean (cross-section of isobaths – 1000 m) and location of points of heat flow measurement (crosses). The size of crosses is proportional to the amount of heat flow. 4-5 – geotraverse, along which statistical processing of geothermal data was carried out.

No. geotraverse	No. 5		No. 4	
West or East of West Indian Ridge axis	W.	E.	W.	E.
Average value of heat flow	76	48	124	77
Standard deviation	59	30	79	40
Number of measurements	65	28	12	48
Value of Cramer-Welch criterion	2,38		2,9	
Confidence probability	99%		99%	

Table 3. Statistical characteristics for the values of the heat flow (mW/m²) according to geotraverses No. 5 and No. 4

Atlantic Ocean

Geotraverse 45 °N extends from the Bay of Biscay in the east to the Newfoundland depression in the west, crossing the Mid-Atlantic Ridge by 28 °W. The area has been thoroughly studied by all geological and geophysical methods. Suffice it to say that only measurements of the heat flow here are more than 250 (Fig. 5). The range of the heat flow is very wide. The minimum value is 25 mW/m², and the maximum value is 180 mW/m². Note that the Mid-Atlantic Ridge in this region is not characterized by the most extreme values, which is usually associated with a decrease in the conduction heat flow due to heat and mass transfer in the rift valley of the ridge.

The maximum heat flow values refer to the eastern slope of the Mid-Atlantic Ridge in the region of the 8-10th magnetic anomalies. Further to the east, in the Bay of Biscay, heat flow decreases somewhat, but, nevertheless, remains elevated compared to the Newfoundland depression. A comparison of heat flow samples to the west and east of the Mid-Atlantic Ridge axis showed that the sample in the east has a statistically significant excess of the average values above the sample in the west (Table 4).

The position of the Canary-Bahamian geotraverse (23-29 °N) is chosen so that it intersects only one divergent plate boundary (Mid-Atlantic Ridge) (Fig. 6), which functioned throughout the history of the Atlantic expansion. The geotraverse strip covers the region most representative for the processes of accretion and evolution of the oceanic crust in a slow spreading environment, as located between the most distant from each other Atlantic transform faults – Kane and Atlantis (Mashchenkov, Pogrebitskii, 1995).

According to the seismic results, two earth's crust types are distinguished in the geotraverse area, with a certain wave field structure and velocity characteristics, the normal and anomalous crust. Normal crust is characterized by the presence of three seismic complexes: the first seismic complex, which, in accordance with the features of the wave field, is compared with the pillow-lavas and basalt flows in the ophiolite sections; the second – (acoustically transparent horizon) is interpreted

No. geotraverse	No. 6 (45°n.l.)	
west/east	west	east
Average value of heat flow	69	84
Standard deviation	57	43
Number of measurements	95	200
Value of Cramer-Welch criterion	2,6	
Confidence probability	99%	

Table 4. Statistical characteristics for the values of the heat flow (mW/m²) according to geotraverses No. 6

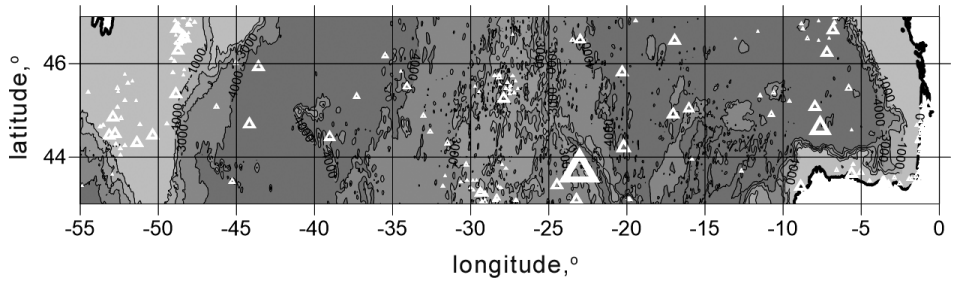

Fig. 5. The relief of the bottom and the points of measurement of the heat flow (triangles) in the region of geotraverse 45 ° N. The size of the triangles is proportional to the value of the heat flow

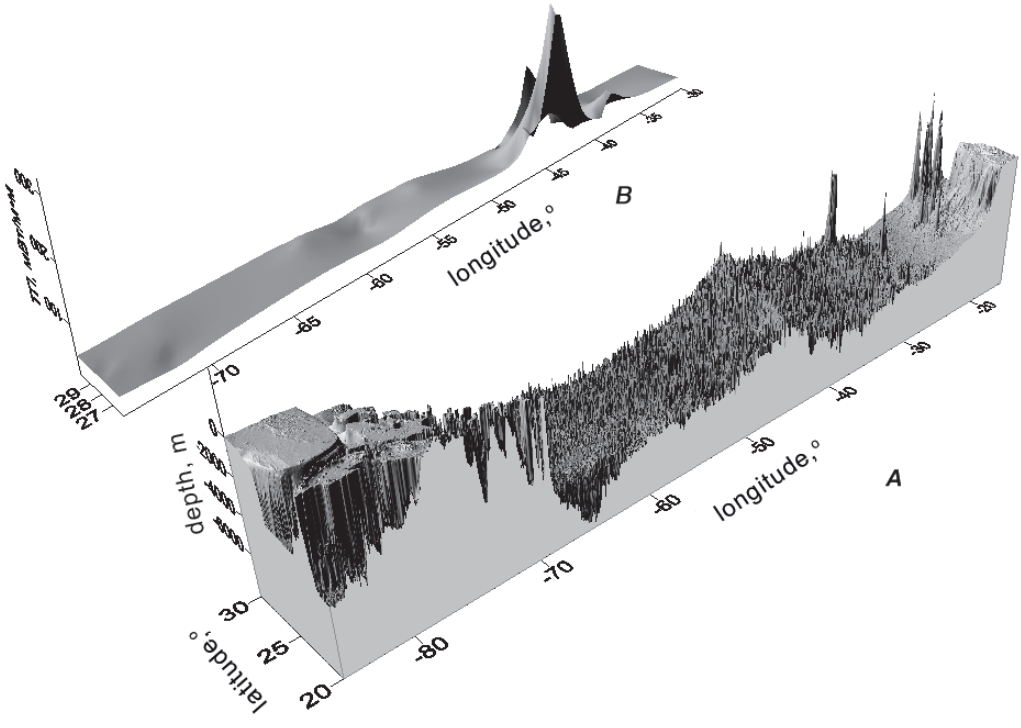

Fig. 6. Block diagrams of the bottom relief (A) and heat flow (B) along geotraverse No. 7 (Canaro-Bahamian)

as a complex of parallel dikes; the third seismic complex, due to the presence of dynamically expressed reflecting areas and inclined reflectors, corresponds to the lower parts gabbroids of the typical ophiolites section. On most temporary sections of the seismic reflection survey, the Moho section is highlighted, marking the transition from "layered" to "nonlayered" recording. On the seismic reflection profiles in the Canary-Bahamian geotraverse band, there are also areas where the wave fields have anomalous features: saturation with diffraction axes or reflecting the boundaries of a complex structure (inclined and "spike-shaped" reflectors).

Manifestations of asymmetry on the geotraverse were noted in the analysis of the "root dependence" of the relief on the slopes of the Mid-Atlantic Ridge (Mashchenkov et al., 1998), the gravitational free air anomalies (Gaynanov, 1980; Kuo, Forsyth, 1988) and heat flow (Podgornykh, Khutorskoy, 1999). However, a statistical comparison of the geothermal characteristics of the same morphological elements along the Canary-Bahamian geotraverse revealed their heterogeneity. For example, a comparison of heat flow statistics in abyssal basins showed that in the Canary Basin in the geotraverse strip, heat flow is statistically significantly higher than in the southern part of the North American (Bahamian) basin. At the same time, a comparison of heat-flow distribution on the slopes of Mid-Atlantic Ridge did not reveal a significant difference from the east and west sides of the ridge axis.

The emergence of a new, much more representative database on heat flow (Hasterok et al., http://heatflow.org/data) made it possible to significantly increase the analyzed sample in the Canary-Bahamian geotraverse. If earlier in the geotraverse strip we analyzed 42 measurements, in the last base we included 70 measurements for the same coordinates.

Table 5 shows the results of statistical processing of heat flow samples in the western and eastern the geotraverse periphery. Calculations showed that, despite a slight excess of the average heat flow east of Mid-Atlantic Ridge, this difference is statistically insignificant, i.e. there is no reason to consider the existence of a geothermal asymmetry on this geotraverse. A possible interpretation of this result will be given below.

Canary-Bahamian geotraverse No. 7		
west/east	west	east
Average value of heat flow	58	61
Standard deviation	48	39
Number of measurements	50	20
Value of Cramer-Welch criterion	0,27	
Confidence probability	<20% (no significant difference)	

Table 5. Statistical characteristics for the values of the heat flow (mW/m²) according to geotraverse No. 7

Fig. 7 shows the relief of the bottom in the geotraverse area of 19 °N (No. 8). This earth's crust block is almost unaffected by transform displacements and can be considered as a tectonotype of the symmetrical arrangement of the ocean floor morphological elements: slopes of Mid-Atlantic Ridge and adjacent abyssal basins.

However, a comparison of heat flow samples generated from measurements on different sides of the Mid-Atlantic Ridge axis showed a statistically significant difference – the eastern flank of the geotraverse has a higher average heat flow (Table 6).

Pacific Ocean

In the Pacific, only one geotraverse in the northern hemisphere satisfies the condition of sufficient geothermal study. This geotraverse is No. 9, crossing the EPR at 10 °N. More than 5000 heat flow measurements were obtained along this geotraverse by efforts of mainly American researchers (McKenzie, Sclater, 1969; Parsons, Sclater, 1977; Von Herzen, Uyeda, 1963). The overwhelming number of measurements lies in the range of 65-100 mW/m². Only about 20 points are characterized by hurricane values of 250-260 mW/m², gravitating towards the axis of the East Pacific Rise. Statistical analysis showed a slight but significant difference in heat flow of the East Pacific Rise flanks: the eastern flank has a higher average value than the western flank (Table 7).

The discussion of the results

A comparison of geothermal data for geotraverse flanks crossing all the MORs in the Worls oceans revealed a statistically significant asymmetry of heat flow that varies in direction in the southern and northern the Earth hemispheres: in the southern hemisphere, higher heat flow characterises the western flanks of geotraverses, and in the north – the eastern flanks. Of the nine geotraverses studied, only one of them (Canary-Bahamian) shows a statistically insignificant heat flow difference on the oppositt sides of Mid-Atlantic Ridge.

The explanation of this phenomenon requires not only the correction of the basic principles of the ocean bottom spreading paradigm, but also the more global, planetary causes of asymmetry in the fast and slowly spreading ridges. There are at least two possible causes that complicate the symmetrical divergence mechanism. They include differing age of tectonic plates blocks on opposite sides of the axis of the ridge and/or the imposition of secondary processes on primary spreading, which proceed with the release or energy absorption. Among such processes, we can point to the expansion of the crust in the accretion zone and in adjacent abyssal basins, which is accompanied by the formation of listric faults, as well as the formation of shaded blocks shielding the deep heat flow. With these tectonic processes, the complex redistribution of convective flows in the oceanic lithosphere upper part,

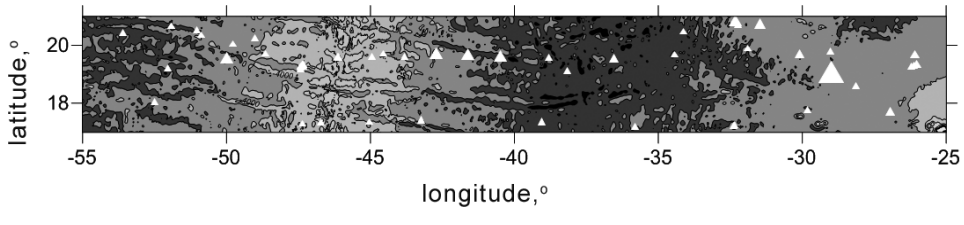

Fig. 7. Relief and position of measurement points of heat flow (triangles) along the geotraverse 19 °N (the size of the triangles is proportional to the value of the heat flow)

No. geotraverse	No. 8 19° n.l.	
west/east	west	east
Average value of heat flow	74	93
Standard deviation	51	100
Number of measurements	22	30
Value of Cramer-Welch criterion	1,34	
Confidence probability	82%	

Table 6. Statistical characteristics for the values of the heat flow (mW/m²) according to the geotraverse of 19 °N. (No. 8)

No. geotraverse	No. 9 10°n.l.	
west/east	west	east
Average value of heat flow	69	74
Standard deviation	53	56
Number of measurements	2829	3160
Value of Cramer-Welch criterion	1,49	
Confidence probability	87%	

Table. 7. Statistical characteristics for the values of the heat flow (mW/m²) according to geotraverse 10 °N in the Pacific Ocean (No. 9)

which is fixed in the geothermal field by the presence of anomalously high and anomalously low (and even zero) heat flow values, is inextricably linked.

The existing methodology for the age of the second layer of the oceanic crust calculating according to geothermal data (eg, (Sorokhtin, 1974)) is based on the assumption of equal spreading speed on both sides of the oceanic ridges axis. Based on this, formula is derived that allows us to calculate the age of the bottom (t) from the measurements of the heat flow (q):

$$q = \lambda \cdot T_a / \sqrt{\pi a t},$$

where λ is the lithosphere thermal conductivity; T_a is the temperature of the asthenosphere; a is the thermal diffusivity, as well as the derivative of the other formula for estimating lithosphere thickness (H_L):

$$H_L = (T_s/T_a)\sqrt{\pi a t},$$

where T_s is the solidus temperature of the mantle substance. The presence of geothermal asymmetry greatly complicates the application of these formulas and suggests another, more complex model for quantitative estimates of the oceanic lithosphere parameters. Previous studies of the oceanic crust age correlation with respect to magnetic anomalies and heat flow magnitude have not established a significant correlation (Budanov et al., 1997).

The idea of the geothermal asymmetry existence makes it possible to explain the reason for the correlation absence. These factors undoubtedly need to be taken into account when analyzing the geothermal field of the oceanic crust, but they do not explain the different "direction of asymmetry" in the northern and southern hemispheres. Above we mentioned the influence of the Coriolis force, which invariably manifests itself on a rotating Earth.

On any material point of the Earth (m), due to its counterclockwise rotation with angular velocity (ω), the Coriolis force $F_k = 2m \cdot v \cdot \omega \cdot \sin\varphi$ will act, which in the southern hemisphere will shift the mass to the left relative to the radius (Fig. 8), and in the north, respectively, to the right. In the divergent zones, such a mass is magma rising from the asthenospheric mantle reservoir at a velocity v, ensuring spreading of the ocean plates. However, we do not observe a connection between the rise of the magma rate (v) nor the magnitude of the average heat flow, nor with the degree of asymmetry of its mean values on different sides of MOR. This follows from a comparative analysis of data on geotraverses in a rapidly spreading East Pacific Rise and in slow spreading Mid-Atlantic Ridge and West Indian Ridge. Under the action of the Coriolis force directed perpendicularly to the trajectory of the rise of the magma, the velocity vector becomes not orthogonal to the bottom surface, but shifted to the west. The mass m will move from point A to point B (Fig. 8).

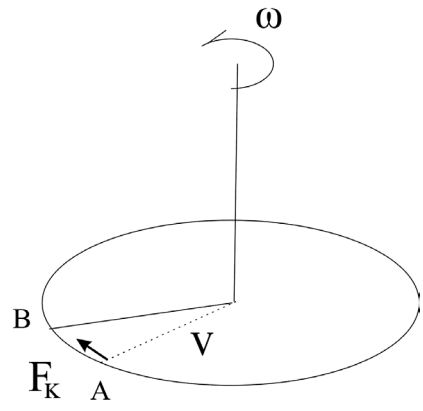

Fig. 8. The action of the Coriolis force (explanations in the text)

The amplitude of the displacement of the magmatic stream will be greater at high latitudes (φ) than when approaching the equator. Under the action of the same force, the material point in the northern hemisphere will deviate to the east relative to the trajectory orthogonal to the surface of the planet.

Geotraverses No.No. 1-5 are located in the southern hemisphere, therefore the flow of rising magma invariably deviates to the west, which explains the observed asymmetry in the World Ocean.

For geotraverses No.No. 6-9 located in the northern hemisphere, the eastern flank of the geotraverse turns out to be more "warm", which can also be unambiguously associated with the influence of the Coriolis force. Here the exception is the Canary-Bahamian geotraverse (No. 7), in which the difference in average heat flows on the flanks was statistically insignificant. Apparently, the newest tectonic activity manifested in the Bahamian basin (Mashchenkov et al., 1997) increases the overall heat flow background on the western flank geotraverse flank.

Thus, we confirmed with the help of statistical analysis that in geotraverses of the southern hemisphere of the Earth, crossing the mid-oceanic ridges, their western flank has a higher mean arithmetic heat flow, and in the geotraverses of the northern hemisphere it is the eastern flank. The influence of the Coriolis force can be considered as the universal cause of this pattern, which, when the planet rotates, tilts the ascending stream of magma and other products of eruptions in divergent zones, respectively, to the west – in the southern hemisphere, and to the east – in the northern hemisphere.

Acknowledgements

The work was carried out with financial support of the state budget theme No. 0135-2015-0021 and the Program of Presidium of the Russian Academy of Sciences No. 49.

References

Anderson, R.N., Langseth M.G., Hobart M.A. (1979). Geothermal convection through oceanic crust and sediments in the Indian Ocean. *Science*, 204, pp. 828-832. DOI: 10.1126/science.204.4395.828

Anderson, R.N., Langseth M.G., Sclater J.G. (1977). The mechanisms of heat transfer through the floor on the Indian Ocean. *J. Geophys. Res.*, 82, pp. 3391-3409.

Budanov V.G., Ermakov B.V., Podgornykh L.V. (1997). Geophysical asymmetry of the wings of mid-Atlantic ridge (MAR): gravity, magnetic fields, heat flow. European Geophysical Society, Annales Geophysical, part I, Society Symposia, Solid Earth Geophysics & Natural Hazards, Supplement I to Volume 15, SE27 Tectonic evolution and thermal structure at mid-ocean ridges, p.161.

Cannat M., Rommevaux-Jestin C., Sauter D., Deplus C., Mendel V. (1999). Formation of the axial relief at the very slow spreading Southwest Indian Ridge (49° to 69°E). *J. Geophys. Res*., 104, pp. 22825-22843.

Courtney, R.C., Recq M., (1986). Anomalous heat flow near the Crozet Plateau and mantle convection. *Earth Planet. Sci. Lett*., 79, pp. 373-384. DOI: https://doi.org/10.1016/0012-821X(86)90193-7

Gainanov A.G. (1980). Gravimetricheskie issledovaniya zemnoi kory okeanov [Gravimetric studies of the Earth's crust of the oceans]. Moscow: Moscow State University, 240 p. (In Russ.)

Glebovskii V.Yu., Kaminskii V.D., Osipov V.A. (1986). Struktura anomal'nogo magnitnogo polya ot sredinnogo khrebta do Angol'skogo shel'fa [Structure of an anomalous magnetic field from the middle ridge to the Angolan shelf]. *Litosfera Angol'skoi kotloviny i vostochnogo sklona Yuzhno-Atlanticheskogo khrebta* [The lithosphere of the Angolan basin and the eastern slope of the South Atlantic Ridge]. Leningrad, pp. 70-80. (In Russ.)

Gmurman V.E. (2005). Teoriya veroyatnostei i matematicheskaya statistika [Theory of Probability and Mathematical Statistics]. Moscow: Vysshaya shkola Publ., pp. 327-349. (In Russ.)

Gorodnitskii A.M. (1985). Stroenie okeanicheskoi litosfery i formirovanie podvodnykh gor [The structure of the oceanic lithosphere and the formation of seamounts]. Moscow: Nauka Publ., 166 p. (In Russ.)

Hasterok D. (2010). Thermal Regime of the Continental and Oceanic Lithosphere. *Ph.D. Dissertation*, University of Utah, 156 p.

Hasterok et al. http://heatflow.org/data

Hosford A. (2001). Crustal accretion and Evolution at slow and ultra-slow spreading mid-ocean ridges. *Doct. Dissertation*, Massachusetts Institute of Technology, 254 p. http://hdl.handle.net/1721.1/58441

Hyndman R.D., Langseth M.G., Von Herzen R.P. (1987). Deep Sea Drilling project geothermal measurements: a review. *Rev. Geophys*., 25(8), pp. 1563-1582. DOI: https://doi.org/10.1029/RG025i008p01563

Jessop, A.M., Hobart M.A., Sclater J.G. (1976). The world heat flow collection – 1975. Geothermal Series 5, Energy, Mines and Resources, Earth Physics Branch, Ottawa, Canada.

Khutorskoy M.D., Polyak B.G. (2017). Teplovoi potok v transformnykh razlomakh Severnoi Atlantiki i Yugo-Vostochnoi Patsifiki [Heat flow in the transform faults of the North Atlantic and South-Eastern Pacific]. *Geotektonika = Geotectonics*, 2, pp. 55-66. (In Russ.)

Khutorskoy M.D., Teveleva E.A. (2016). Teplovoi potok v abissal'nykh kotlovinakh Patsifiki i Atlantiki [Heat flow in the abyssal basins of Pacific and Atlantic]. *Monitoring. Nauka i tekhnologii = Monitoring. Science and technology*, 4(29), pp. 20-27. (In Russ.)

Khutorskoy M.D., Teveleva E.A. (2018). O geotermicheskoi asimmetrii yugo-zapadnogo Indiiskogo khrebta [On the geothermal asymmetry of the southwestern Indian ridge]. *Monitoring. Nauka i tekhnologii = Monitoring. Science and technology*, 1. pp. 6-16. (In Russ.)

Khutorskoy M.D., Teveleva E.A., Podgornykh L.V. (2017). Geotermicheskaya asimmetriya transformnykh razlomov ekvatorial'noi chasti Atlanticheskogo okeana [Geothermal asymmetry of transform faults in the equatorial part of the Atlantic Ocean]. *Doklady akademii nauk = Proc. of the Academy of Sciences*, 475(3), pp. 325-328. (In Russ.)

Kuo B.-Y., Forsyth D.W. (1988). Gravity anomalies of the ridge transform system in the South Atlantic between 31 and 34,5°S. Upvelling centers and variation in crustal thickness. *Mar. Geophys. Res.*, 10, pp. 205-232. DOI: https://doi.org/10.1007/BF00310065

Mashchenkov S.P., Pogrebitskii Yu.E. (1995). Simmetriya i asimmetriya SAKh po materialam kompleksnykh geofizicheskikh issledovanii na atlanticheskikh geotraversakh [Symmetry and asymmetry of the MAR on the basis of data from complex geophysical studies on Atlantic geotraverses]. *Geologiya i mineral'nye resursy Mirovogo okeana* [Geology and mineral resources of the World Ocean]. St. Petersburg: VNIIOkeanologiya Publ., pp. 64-79. (In Russ.)

Mashchenkov S.P., Pogrebitsky Yu.E., Astafurova E.G. et al. (1998). Glubinnoe stroenie i evolyutsiya litosfery Tsentral'noi Atlantiki (rezul'taty issledovanii na Kanaro-Bagamskom geotraverse) [Deep structure and evolution of the lithosphere of the Central Atlantic (research results on the Canary-Bahamian geotraverse)]. St. Petersburg: VNIIOkeanologiya Publ., 290 p. (In Russ.)

McKenzie D.P., Sclater J.G. (1969). Heat flow in the eastern Pacific and sea-floor spreading. *Bulletin of Volcanology*, 33, pp. 101-118.

Menard H.W. (1966). Fracture zones and offsets of the East-Pacific rise. *J. Geophys. Res.*, 71(2), pp. 682-685. DOI: https://doi.org/10.1029/JZ071i002p00682

Naryshkin G.D., Pogrebitsky Yu.E. (1986). Morfostruktura dna Yugo-Vostochnoi Atlantiki [Morphostructure of the bottom of the South-East Atlantic]. *Litosfera Angol'skoi kotloviny i vostochnogo sklona Yuzhno-Atlanticheskogo khrebta* [The lithosphere of the Angolan basin and the eastern slope of the South Atlantic Ridge], Leningrad, pp. 10-23. (In Russ.)

Parsons B., Sclater I.C., (1977). An analysis of the variation of ocean floor bathymetry and heat flow with age. *J. Geophys. Res*., 82(5), pp. 883-890.

Patriat P., Sauter D., Munschy M., Parson L. (1997). A survey of the Southwest Indian Ridge axis between Atlantis II Fracture zone and the Indian Ocean Triple Junction : Regional setting and large-scale segmentation. *Mar. Geophys. Res*., 19, pp. 457-480. DOI: https://doi.org/10.1023/A:1004312623534

Pogrebitsky Yu.E., Goryachev Yu.V., Osipov V.A., Trukhalev A.I. (1990). Stroenie okeanicheskoi litosfery po rezul'tatam issledovanii na Angolo-Brazil'skom geotraverze [The structure of the oceanic lithosphere from the results of studies on the Angola-Brazil geotraverse]. *Sov.geologiya = Soviet Geology*, 3, pp. 8-22. (In Russ.)

Podgornykh L.V., Khutorskoy M.D. (1997). Planetarnyi teplovoi potok [Planetary heat flow]. A map of scale 1: 30 000 000 and an explanatory note to it. Moscow-St. Petersburg, Orgservis LTD, 65 p. (In Russ.)

Podgornykh L.V., Khutorskoy M.D. (1998). Asimmetriya raspredeleniya teplovogo potoka vdol' Angolo-Brazil'skogo geotraversa (Yuzhnaya Atlantika) [Asymmetry of heat flow distribution along the Angola-Brazil geotraverse (South Atlantic)]. *Doklady RAN = Proc.of the Russian Academy of Sciences*, 355(4), pp. 212-215. (In Russ.)

Podgornykh L.V., Khutorskoy M.D. (1999). Geotermicheskaya asimmetriya sredinnykh khrebtov Mirovogo okeana [Geothermal asymmetry of the medial ridges of the World Ocean]. *Geotektonika = Geotectonics*, 3, pp. 21-42. (In Russ.)

Pollack, H.N., Hurter S.J., Johnston J.R. (1992). Global heat flow data set. World Data Center A for Solid Earth Geophysics. NOAA E/GCI, 325 Broadway, Boulder, CO 80303, USA.

Popova A.K., Smirnov Ya.B., Khutorskoy M.D. (1984). Geotermicheskoe pole transformnykh razlomov. Glubinnye razlomy okeanskogo dna [Geothermal field of transform faults. Deep faults in the ocean floor]. Moscow: Nauka Publ., pp.78-87. (In Russ.)

Pushcharovsky Yu.M., Peive A.A., Raznitsin Yu.N., Bazilevskaya E.S. (1995). Razlomnye zony Tsentral'noi Atlantiki [Fault zones of the Central Atlantic]. *Tr. GIN RAN* [Proc. of the Geological Institute of the Russian Academy of Sciences], 495, Moscow: GEOS Publ., 163 p. (In Russ.)

Shreider A.A. (2001). Geomagnitnye issledovaniya Indiiskogo okeana [Geomagnetic studies of the Indian Ocean]. Moscow: Nauka Publ., 320 p. (In Russ.)

Sorokhtin O.G. (1974). Global'naya evolyutsiya Zemli [Global evolution of the Earth]. Moscow: Nauka Publ., 184 p. (In Russ.)

Von Herzen R.P., Uyeda S. (1963). Heat flow through the eastern Pacific ocean floor. *J. Geophys. Res*., 68(14), pp. 4219-4250. DOI: https://doi.org/10.1029/JZ068i014p04219

About the Authors

Mikhail D. Khutorskoy – DSc (Geology and Mineralogy), Professor, Head of the Heat and Mass Transfer Laboratory

Geological Institute of the Russian Academy of Sciences

7 Pyzhevsky lane, Moscow, 119017, Russain Federation

E-mail: mkhutorskoy@ginras.ru

Elena A. Teveleva – PhD (Physics and Mathematics), Senior Researcher, Laboratory of the Heat and Mass Transfer

Geological Institute of the Russian Academy of Sciences

7 Pyzhevsky lane, Moscow, 119017, Russain Federation

Manuscript received 1 April 2018;
Accepted 2 June 2018;
Published 30 June 2018